Microdosimetric measurements and some applications in radiobiology and radiation protection

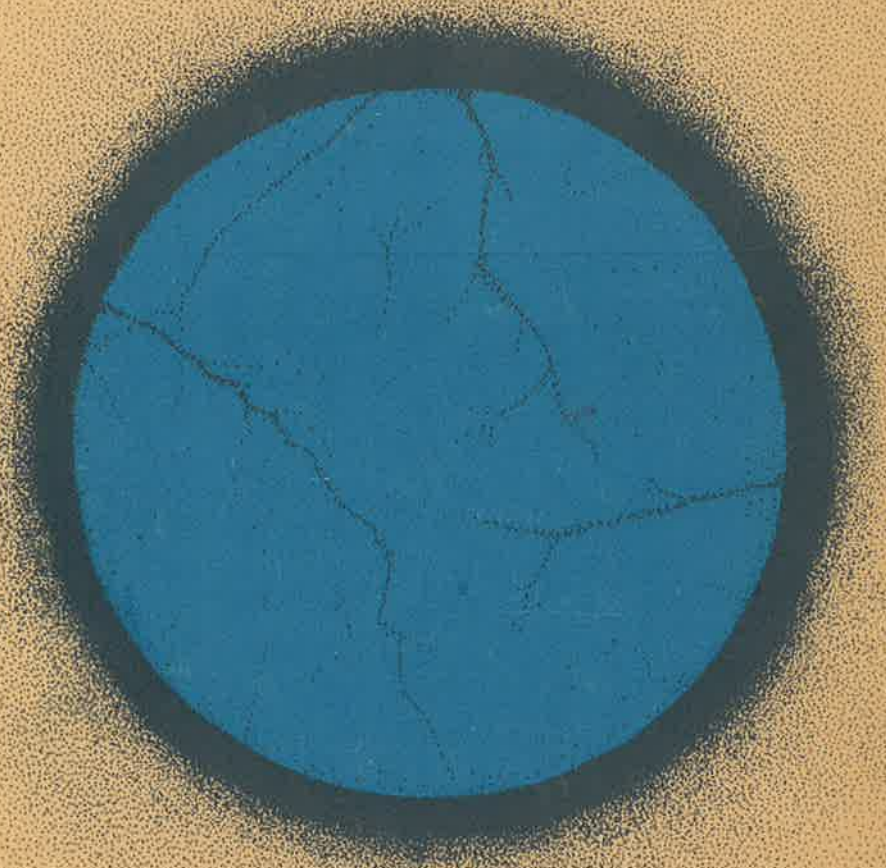

B. Hogeweg

MICRODOSIMETRIC MEASUREMENTS AND SOME APPLICATIONS IN RADIOBIOLOGY AND RADIATION PROTECTION

The work described in this thesis has been performed at the Radiobiological Institute TNO, Rijswijk, The Netherlands.

This thesis is available as a publication of the Radiobiological Institute of the Organization for Health Research TNO, 151 Lange Kleiweg, Rijswijk, The Netherlands.

Cover design by Mr. J. Ph. de Kler.

STELLINGEN

I

Het verdient aanbeveling om, bij vergelijking van biologische resultaten verkregen met neutronen van verschillende bundels, naast dosis en neutronenenergie tevens verdelingen van lineale energie in beschouwing te nemen.

Dit proefschrift (hoofdstuk VII)

II

Ten onrechte is door Bichsel bij de berekening van de strooiingsparameter, welke toegepast wordt om Vavilov-verdelingen te karakteriseren, de invloed van het effectief atoomnummer der invallende deeltjes verwaarloosd; de opgegeven waarden voor alfadeeltjes zijn derhalve een factor vier te laag.

H. Bichsel, Charged-particle interactions, Radiation Dosimetry, Vol I, 1968.

III

Aangezien de energie-afgifteverdeling door neutronen in een gasholte afhankelijk is van de grootte en van de vorm van deze holte, verdient het aanbeveling om bij internationale neutronendosimetrie-vergelijkingen van één type ionisatievat gebruik te maken.

IV

De invoering van SI-eenheden in de radiologie zal de bestaande verwarring tussen eenheden voor exposie en geabsorbeerde dosis slechts kunnen verminderen.

V

Bij de evaluatie van r.b.e. als functie van neutronenenergie zijn door Kellerer et al. resultaten, verkregen met mono-energetische en poly-energetische neutronen, zonder onderscheid bij de analyse gebruikt. Daarbij zijn ten onrechte voor poly-energetische bundels versnellingsspanningen, van de voor de reactie gebruikte deeltjes, als neutronenenergie opgegeven. Een duidelijke reactie-notatie zou als karakteristiek voor het spectrum tenminste moeten worden vermeld.

A. M. Kellerer et al., Rad. Res. **65**, 172–186 (1976)

VI

Het door Fowler et al. toegepaste scoringssysteem, voor het aanduiden van biologische effecten door getallen, moet beschouwd worden als een verkorte schrijfwijze, maar laat de veelal gebruikte quantitatieve analysemethodes niet toe.

J. F. Fowler et al., Int. J. Rad. Biol. 9, 241–252 (1965)

VII

Bij de bepaling van de verdubbelingstijd van haemopoëtische, pluripotente, kolonievormende cellen in de milt van bestraalde en gereconstitueerde muizen, wordt zonder voldoende redenen de bijdrage van migratie verwaarloosd.

VIII

Tegen de achtergrond van het feit dat overheid en maatschappij veelal gebruik maken van adviezen, welke worden ingewonnen bij deskundigen van onderzoekinstellingen als Universiteit en TNO en welke door deze adviseurs veelal à titre personnel worden gegeven op basis van hun in functie verkregen deskundigheid, is het verwijt aan deze instellingen van een slecht maatschappijgericht functioneren niet terecht.

Wetenschap en Samenleving, mei 1977
NRC-Handelsblad, 2 november 1977

IX

In het kader van de grondstoffeneconomie zouden wetenschappelijke publikaties, mede gezien hun veelal tijdelijke betekenis, in meerdere mate op herwinningspapier moeten worden uitgegeven.

X

Zonder „Don Quichotterie" te willen bedrijven, lijkt een waarschuwing tegen het enthousiasme voor windmolens als alternatieve energiebron zeker op zijn plaats; de hiervoor in ontwikkeling zijnde molens zullen, mede gezien de benodigde aantallen, het landschap niet verrijken.

XI

Bij het opstellen van plannen voor verkeerslichten zou meer aandacht gegeven dienen te worden aan het verkeersregelende dan aan het verkeersstoppende aspect.

Amsterdam, 1 maart 1978 B. Hogeweg

MICRODOSIMETRIC MEASUREMENTS AND SOME APPLICATIONS IN RADIOBIOLOGY AND RADIATION PROTECTION

ACADEMISCH PROEFSCHRIFT

TER VERKRIJGING VAN DE GRAAD VAN
DOCTOR IN DE WISKUNDE EN NATUURWETENSCHAPPEN
AAN DE UNIVERSITEIT VAN AMSTERDAM,
OP GEZAG VAN DE RECTOR MAGNIFICUS, DR. G. DEN BOEF,
HOOGLERAAR IN DE FACULTEIT DER WISKUNDE EN
NATUURWETENSCHAPPEN,
IN HET OPENBAAR TE VERDEDIGEN IN DE AULA DER UNIVERSITEIT
(TIJDELIJK IN DE LUTHERSE KERK, INGANG SINGEL 411, HOEK SPUI)
OP WOENSDAG 1 MAART 1978 DES NAMIDDAGS TE 3 UUR PRECIES

DOOR

BERNARD HOGEWEG

GEBOREN TE AMSTERDAM

W. D. MEINEMA B.V. - DELFT

Promotor: Prof. Dr. G. W. Barendsen

Co-referent: Prof. Dr. F. A. Muller

Aan Mia

aan Dirk Jan en Maarten

CONTENTS

De natuur is het bewonderenswaardigst
in de kleinste dingen.

CHAPTER I

INTRODUCTION

I-1 Significance of microdosimetric parameters for radiation biology

Effects induced in biological systems, organisms, tissues, cells or DNA molecules by exposure to ionizing radiation are the consequence of discrete energy transfer events. The energy transferred to the medium is deposited along the tracks of charged particles which are either initially present in the incident beam or are generated through interaction of the incident beam with the medium. The different interaction mechanisms for various types of radiation are illustrated in figure I-1.

In directly ionizing interactions of charged particles (e.g., electrons, protons, etc.) with matter, the energy is lost in a large number of relatively small increments via the Coulomb forces causing ionizations and exitations of the molecules. Consequently, the energy deposited is mainly concentrated along the tracks of the particles which are gradually slowed down. Because of this type of interaction mechanism, the length of the track for a charged particle is restricted to a finite range.

Indirectly produced ionizations arise from uncharged particles (e.g., neutrons) and from electromagnetic radiation (x-rays and gamma rays) through the production of charged directly ionizing particles by various processes. In general, a greater variation in energy transfer modes is possible which result in these, so-called, secondary charged particles. The energy deposition pattern for each of the secondary particles formed is equal to the pattern resulting from a directly ionizing particle of identical charge and energy. Traversals of neutral particles or photons over relatively long distances without interactions are quite possible; consequently, the tracks of the secondary particles are randomly generated within the medium. Another consequence of this long free-path length for indirectly ionizing radiation is that the beam will be attenuated exponentially, in contrast to the finite range for directly ionizing radiation.

Because of the variety in possible interaction mechanisms and because of the discontinuous nature of the energy transfers, the spatial distributions of energy deposition for the various types of ionizing radiations will show great differences. Therefore, the distributions of the energy deposition depend on the dimensions of the domain considered. For these reasons, specific stochastic quantities (energy imparted, specific energy and lineal energy) for

the physical description of the irradiation conditions have been adopted by the International Commission on Radiation Units and Measurements [ICRU, 1971]. Important nonstochastic quantities that can be derived from

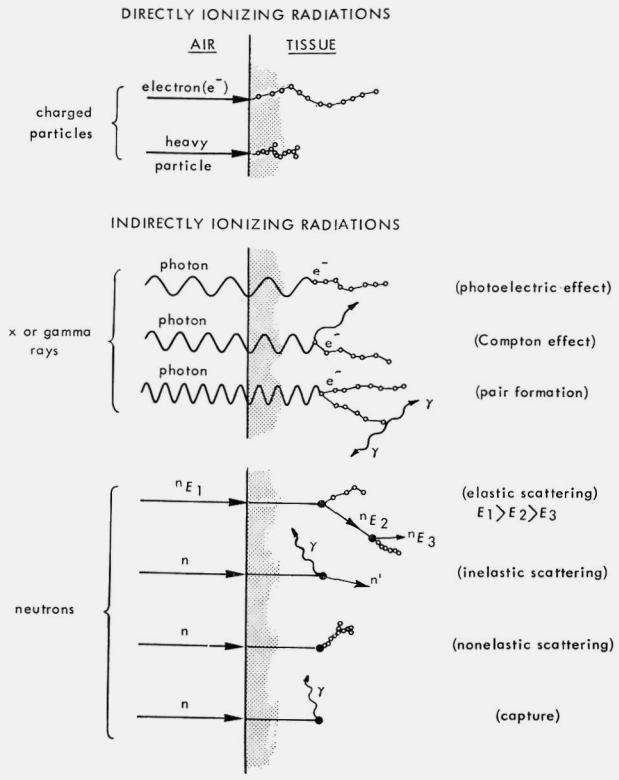

Fig. I-1. Schematic presentation of interaction mechanisms for various ionizing radiations. *Directly ionizing radiations* (electrons and heavy charged particles) interact with the electrons of the tissue elements causing ionizations and excitations. The ionization density per unit track length and the range depend on the mass and energy of the particle (see figure II-2).
By the interaction of *indirectly ionizing x or gamma rays*, electrons of various energies are produced in photoelectric, Compton and pair formation processes. The energy of these directly ionizing secondary electrons is transferred to the medium by the production of ionizations and excitations.
Charged particles, gamma radiations and neutrons of lower energy are produced via elastic scattering, inelastic scattering, nonelastic scattering and capture processes of the indirectly ionizing *neutrons* with the nuclei of the tissue elements. These secondarily produced radiations transfer their energy to the medium by their characteristic processses.

the stochastic quantities and provide a less detailed description of the energy deposition pattern are linear energy transfer (l.e.t.), a measure of the average energy transferred per unit track length, and the absorbed dose, a measure of the average energy transfer per mass unit. The techniques for measurements and calculations of the stochastic quantities and the evaluation of the dependence of their frequency distributions on the size of the volumes considered constitute the subject of microdosimetry.

Results obtained from studies of microdosimetric phenomena are of great importance for the elucidation of the mechanisms of action in radiobiology. Differences in relative biological effectiveness (r.b.e.) for equal doses of different types of radiation and in oxygen enhancement ratio (o.e.r.) have been observed [Barendsen, 1968]. The differences in effectiveness can be related to the diversities in energy deposition patterns mentioned. In general, biological effects are produced less effectively by ionizing particles with a low l.e.t. than by radiations with a high l.e.t., while the dependence of the effectiveness on various factors, e.g., the presence of oxygen, and the repair of damage is smaller for radiations having high l.e.t. values.

A number of hypotheses have been advanced for the interpretation of the dependance of the r.b.e. on the l.e.t. These studies are of interest not only because of their fundamental aspects in relation to the action of radiation on living organisms, but also because of practical applications. They can be of practical importance, for instance, with regard to the extrapolation of the r.b.e. at very low doses or dose rates and the related assessment of quality factors for radiation protection purposes. Moreover, worthwhile information on the risk to patients inherent in irradiations of tumors can be deduced from measured or calculated energy deposition distributions in collimated neutron beams.

Differences in effectiveness for induction of damage in a number of biological systems irradiated with x-rays and neutrons have been interpreted in terms of microdosimetric quantities in a "dual radiation action" model [Kellerer and Rossi, 1971, 1972]. An important result of this interpretation is that interaction distances for the radiation sensitive sites in the order of 0.2–2 μm of unit density tissue have been calculated. Unsatisfying from the physical point of view is the fact that the model developed is principally based on experimental results derived with x-rays and neutrons, which have rather complex energy deposition patterns.

Complicating factors with respect to biological and physical aspects are reduced if directly ionizing particles are used under conditions where monolayers of cultured cells are traversed by selected short portions of the particle

tracks, since the distributions of dose in l.e.t. are relatively narrow under these conditions. Such experiments are commonly referred to as "track segment experiments". Data on cell reproductive death as a function of dose under these irradiation conditions have been obtained for various cell lines [Barendsen et al., 1960; Barendsen and Walter, 1964; Todd, 1967; Skarsgard et al., 1967].

Data on microdosimetric distributions of energy deposition for directly ionizing particles provide a useful basis for the interpretation of these dose-effect relationships.

I-2 Scope of this thesis

In this thesis, measured and theoretical energy deposition distributions will be presented and then related to the data on the clonogenic capacity of cultured cells as derived from track-segment experiments. Interpretation of these relationships will be based on the hypothesis that, for damage to the clonogenic capacity of mammalian cells, a certain minimum amount of energy deposited within a small critical volume is required. From the interpretation of these track segment results, a size for the critical distance of about 100 nm of unit density tissue is derived, which is in strong contrast to the dimension resulting from the dual radiation action model. These differences in the derived interaction distance are most likely the result of differences in the mechanism of action between spatially condensed energy depositions which occur in the passage of directly ionizing heavy particles and the spatially scattered depositions for indirect ionizing radiation. In the latter situation, a combination of distributed events can give rise to an identical biological endpoint.

After the discussion of fundamental radiobiological aspects, the energy deposition spectra for collimated and uncollimated neutron beams will be discussed in comparison with the measured neutron energy spectra and with r.b.e. values derived from cell survival curves obtained for these neutrons.

In chapter II, some microdosimetric concepts and theoretical local energy distributions are defined and discussed. For the measurement of microdosimetric quantities, the proportional counter is at present the best suited detector.

Small volumes of tissue can be simulated simply by reduction of the gas pressure in the counter. The high gas gain of the counter permits the measurement of relatively small numbers of ionizations, corresponding to small amounts of absorbed energy. The principle and construction of the pro-

portional counters and the related electronic system used for the measurements will be described in chapter III.

From the theoretical discussion in chapter II, it will become evident that the most simple distributions of local energy deposition are obtained for heavy charged particles crossing the sensitive site over a short length of their path. Increasing complexity is encountered for spectra of heavy particles produced by the indirect interactions of neutrons. Chapter IV gives a description of the sources and their energy distributions which were used for the measurement of the various event size distributions.

In chapter V, measured gas gain values and resolution of the detector will be presented. The consequential limitation in the use of a proportional counter as a l.e.t. counter for small volume sizes imposed by these characteristics will be discussed.

Measured energy deposition distributions for alpha particles and protons of different energies will be presented and discussed in relation to theoretical distributions in chapter VI. These event size distributions will be related to published biological data on damage to mammalian cells obtained in track segment experiments.

Chapter VII is concerned with the measurements of event size distributions at various simulated diameters of tissue volumes for neutrons of different energies. Conclusions will be drawn from these measured spectra of collimated beams with respect to therapeutical applications.

CHAPTER II

FUNDAMENTAL ASPECTS OF ENERGY DEPOSITION

II-1 Significance of ionizations versus excitations

Radiation passing through a medium will generally cause the transfer of different amounts of energy to particles. Due to the complexity of the interaction processes, the size spectrum and spatial distribution of the energy depositions are dependent on properties of the beam as well as on the interacting medium. Energy deposited in the irradiated medium will ultimately give rise to some measurable effects with a wide range of possibilities and frequencies. Because of their applications to the studies reported in this thesis, only interaction mechanisms of electromagnetic radiations (x-rays and gamma rays), neutrons and charged particles with tissue or tissue-equivalent media for restricted energy ranges will be considered.

Transfer of energy from ionizing radiation to tissue is mainly a result of Coulomb and other interactions which result in the formation of ions and, to a lesser degree, in the production of excitations. Energy transfers in the form of excitations are less important from the biological point of view and will therefore be neglected.

The relatively small importance of excitations for biological effects can be deduced from the results obtained for irradiations with u.v. light, which deposits its energy predominantly via the formation of excitations. It is generally accepted that the inactivation of cells by irradiation, as measured by the impairment of reproductive capacity, is the effect of damage induced in the DNA [Hutchinson, 1966; Okada, 1970]. Maximal inactivation of DNA by u.v. light of different wavelengths has been obtained for u.v. light with a wavelength of about 250 nm [Lea, 1962]. Westra [1971] has demonstrated that the efficacy for cell inactivation by irradiation with u.v. light of a wavelength of 253 nm is about a factor of 50–100 less than for irradiation with 250 kV x-rays. The low efficiency of u.v. light for biological effects has been discussed in more detail by Dertinger and Jung [1969] using different examples of biological systems.

II-2 Quantities and units

It is the aim of dosimetry to quantitatively describe the magnitude and

spatial distribution of absorbed energy and thereby to open possibilities to relate measured effects to these characteristics.

In order to deal with the problems of radiation measurements and standardization, the International Commission on Radiation Units (ICRU) was established in 1925 at the First International Congress of Radiology. At first, only problems in relation to radiology were studied, but the field of interest was later extended to related disciplines such as radiobiology, health physics and radiation physics. Quantities and units were initially developed according to nonstochastic principles. Starting in the early sixties, it was realized that statistical fluctuations in energy deposition are of great importance for the explanation of the observed differences in biological effectiveness of various types of radiation. Consequently, in 1971, the ICRU established a set of quantities which account for these stochastic characteristics of the radiation, from which the nonstochastic quantities can be derived by averaging methods.

According to the ICRU [1971], the stochastic quantity energy imparted, ε, by ionizing radiation to matter in a volume element is:

$$\varepsilon = \Sigma\varepsilon_{in} - \Sigma\varepsilon_{ex} + \Sigma Q$$

where $\Sigma\varepsilon_{in}$ and $\Sigma\varepsilon_{ex}$ are sums of the energies (excluding rest energies) of all those directly and indirectly ionizing particles which have, respectively, entered and left the volume element; ΣQ is the sum of all the energies released minus the sum of all energies expended in any transformations of nuclei and elementary particles which have occurred within the volume.

Since it is subject to random fluctuations arising from the discrete nature of absorption processes, the energy imparted is a stochastic quantity. For very small volumes the imparted energy results from traversals of the individual charged particles, the number of which decreases with decreasing sizes. In fact, if the volume is small enough, it can even occur that no particle traverses the volume of interest. Evidently, the relative fluctuations become larger with decreasing volume sizes. With identical reasoning, it will be clear that fluctuations in energy imparted also become larger in situations where the fluence of charged particles becomes smaller.

Effects arising from ionizing radiation will depend, however, not only on the energy imparted, but also on the density distribution of this energy.

A quantity specifying this density is the specific energy or specific energy imparted, z, which is the quotient of ε by m, where ε is the energy imparted by ionizing radiation within a volume element of mass, m. It follows that z

is defined for finite domains only and, since z varies discontinuously in space and time, it is impossible to discuss it in terms of its rate of change.

A value for z in a given volume cannot be predicted; any particular value, however, is determined by a probability distribution. The dispersion of the distribution function increases with decreasing volume size, as demonstrated in figure II-1, due to the decreasing mass and the mentioned increase in fluctuations of the energy imparted.

The probability, P, that the specific energy, z, is equal to or less than z can be given by the value of the distribution function, $F(z)$

$$F(z) = P(z' \leqslant z)$$

The probability density, $f(z)$, is the derivative of $F(z)$ with respect to z

$$f(z) = \frac{\mathrm{d}F(z)}{\mathrm{d}z}$$

The specific energy for a volume element may be the result of one or more

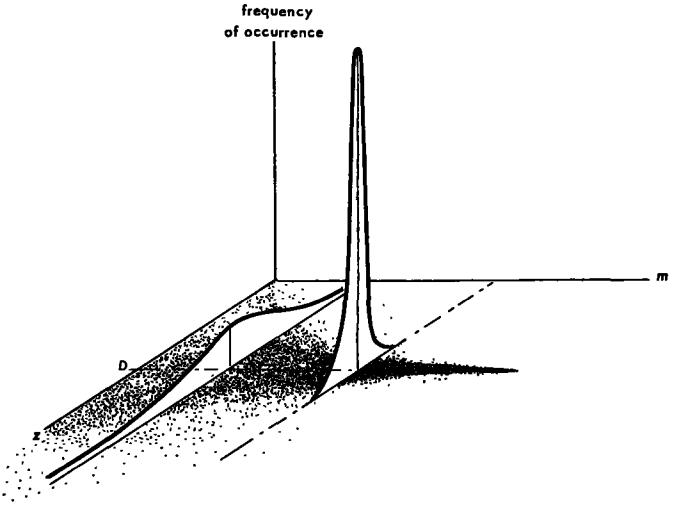

Fig. II-1. Values for the specific energy, z, as can be measured for indirectly ionizing radiation in volumes of different mass, m.
As indicated, a plot of the frequency of occurrence as a function of z for a defined volume size will represent the energy deposition distribution for that volume. For volumes of increasing size, the points are increasingly concentrated around the value of the absorbed dose, D.

events. The distribution function of the specific energy deposited in one single event, $F_1(z)$, is given by the conditional probability that a specific energy, z', equal to or less than z is deposited in one event:

$$F_1(z) = P(z' \leqslant z | \nu = 1)$$

where ν represents the number of deposition events. Analogous to the definition for $f(z)$, the probability density, $f_1(z)$, is defined as the derivative of $F_1(z)$ with respect to z.

The special unit of specific energy is the gray [Lidén, 1975]

$$1 \text{ Gy} = 1 \text{ J kg}^{-1}$$

It can be proved that the nonstochastic quantity absorbed dose, D, is the limit of the mean specific energy, $\bar{z}$, as the mass tends to zero.

The stochastic quantity lineal energy, y, is the quotient of ε by $\bar{d}$, where ε is the energy imparted to the matter in a volume during an energy deposition event and $\bar{d}$ is the mean chord length of the volume of interest:

$$y = \frac{\varepsilon}{\bar{d}}$$

The distribution function, $F(y)$, is given by the probability that y' is equal to or less than y:

$$F(y) = P(y' \leqslant y)$$

and the probability density, $f(y)$, is the derivative of $F(y)$ with respect to y. Since, by definition, only single energy deposition events are involved, the distribution of y is independent of absorbed dose and absorbed dose rate.

The related nonstochastic quantity is the linear energy transfer (l.e.t.) or restricted linear collision stopping power, L_Δ. According to the definition of the ICRU [1970], the linear energy transfer of charged particles in a medium is the quotient of $\mathrm{d}E$ by $\mathrm{d}l$, where $\mathrm{d}l$ is the distance traversed by the particle and $\mathrm{d}E$ is the mean energy loss due to collisions with energy transfers less than some specified value, Δ.

Although this definition specifies an energy cut-off and not a range cut-off, the energy losses are sometimes called "energy locally imparted". The symbol L_∞ is used when all possible energy transfers are included and the subscript ∞ does not mean that infinitely large energy transfers are possible.

The l.e.t. is the quantity previously used to express the quality of a given type of radiation. Limitations in the use of the l.e.t. are discussed in detail in the ICRU report dealing with linear energy transfer [1970].

It is evident from the definitions that the distribution functions of the defined quantities are determined by the different interaction mechanisms for the various types of radiation. This will be discussed briefly in the following section.

II-3 Interaction mechanisms of charged particles

As mentioned in the introduction, ionizing radiations can be subdivided into two categories on the basis of their characteristics, namely, directly and indirectly ionizing radiation. Directly ionizing interactions arise along the paths of charged particles in Coulomb interactions with the electrons or nuclei of the medium. The relative importance of the various energy transfer processes is dependent on the rest mass and velocity of the incident charged particles.

On the basis of their mass, charged particles can be classified into electrons with small rest mass and the heavy charged particles.

In passing through matter, electrons lose energy by various processes such as collisions with nuclei and electrons, excitation of atoms and by radiation production. The relative importance of the contribution of scatter as an energy loss process increases with decreasing energy, as follows from the Rutherford formula [Rutherford et al., 1951]. In these collisions, the electrons generally lose relatively large amounts of energy and undergo considerable changes in their direction of motion because of their small rest mass. Consequently, energy straggling and path length straggling will be large for electrons [Bichsel, 1968; Starodubtsev and Romanov, 1965]. Radiation or "Bremsstrahlung" is produced by the deceleration of electrons in the Coulomb field of the nuclei of the interacting medium. For media with atoms of low atomic number and at electron energies of $< 5\ mc^2$, the energy lost in this Bremsstrahlung production is negligibly small in comparison to energy lost by collision processes [Heitler, 1944]. Therefore, in tissue and tissue-equivalent materials, energy is lost by medium energy electrons primarily through collisions and to a smaller extent in excitation processes; more detailed descriptions of these processes are given in the literature [Birkhoff, 1958; McGinnies, 1959; Kim, 1975].

Heavy charged particles whose mass exceeds the electron mass by a large factor impart part of their energy to matter in the following processes:

a. inelastic collisions with the electrons, resulting in excitation or ionization. This type of energy loss is designated ionization loss;
b. elastic collisions with the nuclei, whereby part of the energy is transferred to the recoil atoms. The total kinetic energy of the colliding particles remains unchanged;
c. inelastic collisions with the nuclei, leading to the excitation of nuclear levels or to nuclear reactions.

The maximum energy transfer, E_{max}, from a moving particle with mass, m_1, and energy, E, to a stationary particle with mass, m_2, results from an elastic so-called head-on collision and is equal to:

$$E_{max} = \frac{4m_1 m_2}{(m_1 + m_2)^2} E \tag{II-1}$$

Thus, the maximum energy transferable in a head-on collision between particles of equal mass, for example a neutron and a proton, is equal to the energy of the colliding particle.

For charged particles with mass, m, and energies, E ,in the range between $10^{-4}mc^2$ and 1 mc^2, the slowing down is mainly caused by the inelastic collisions with the electrons. In this range, the mean total energy loss per unit path length, dE/dx, through these inelastic collisions is equal to the sum of losses in close and distant collisions and can be expressed by the corrected Bethe-Bloch formula [Fano, 1963]:

$$\frac{dE}{dx} = \frac{4\pi e^4 z^2}{m_e v^2} NZ \left\{ \ln\left[\frac{2m_e v^2}{I}\right] - \ln(1-\beta^2) - \beta^2 - \frac{C}{Z} - \frac{\delta}{2} \right\} \tag{II-2}$$

where:
e = electron charge = 1.6021×10^{-19}C
m_e = electron mass = 9.1091×10^{-28}g
z = atomic number of the interacting particle
Z = atomic number of the interacting medium
v = particle velocity
c = velocity of light in vacuum = 2.9979×10^{10}cm sec^{-1}
$\beta = v/c$
N = Loschmidt's constant = 2.68719×10^{19}atoms cm^{-3}
I = mean excitation energy
C/Z = shell correction term
δ = correction term for the polarization effect

Except at very high energies, the correction term for the density effect, δ, is negligible in biological materials [Kim, 1973].

The mean excitation energy, I, is the logarithmic mean over the excitation energies, E_i, weighted according to the corresponding oscillator strengths, f_i, and is defined by:

$$\ln I = \Sigma_i f_i \ln E_i \tag{II-3}$$

Determination of the value of I from its definition presents serious difficulties, since the oscillator strengths, f_i, are generally not well known. In practice, the value determined empirically from the particle stopping power data is the mean adjusted excitation energy, I_{adj}. Since the polarization term vanishes for intermediate particle energies, these stopping power measurements provide the value of $\ln I + C/Z$. The relationship between these mean excitation energies I_{adj} and I is given by the equation:

$$\ln I_{adj} = \ln I + \frac{C}{Z} \tag{II-4}$$

Values of I_{adj} for several elements are given by Turner [1964], while, for $Z \gg 13$, an empirical relation between I_{adj} and Z has been proposed by Sternheimer [Berger and Seltzer, 1964].

The value of the charge of the positive ion is not constant. Due to charge pick-up and loss during traversal through the medium, the average value of the charge will be reduced. Consequently, in calculations of the stopping power, the charge of the particle, z, has to be replaced by an average effective charge, z_{eff}, which can be calculated according to empirical formulas as given by Williamson and Boujot [Oldenburg and Booz, 1972] and by Srivastava and Mukherji [1976].

Charged particles with low energies will lose energy in elastic collisions with the whole atom as well as in inelastic collisions with the electrons. The relative contribution of energy loss in elastic collisions increases with decreasing energy. Lindhard and Scharff proposed means to determine the energy losses for this region of energies by a semiempirical method. This method was used by Oldenburg and Booz [1972] to calculate the values of mass stopping power and range for a series of recoil nuclei produced by neutrons in tissue and tissue-equivalent materials. Stopping power values for protons and alpha particles derived from this tabulation are presented in figure II-2.

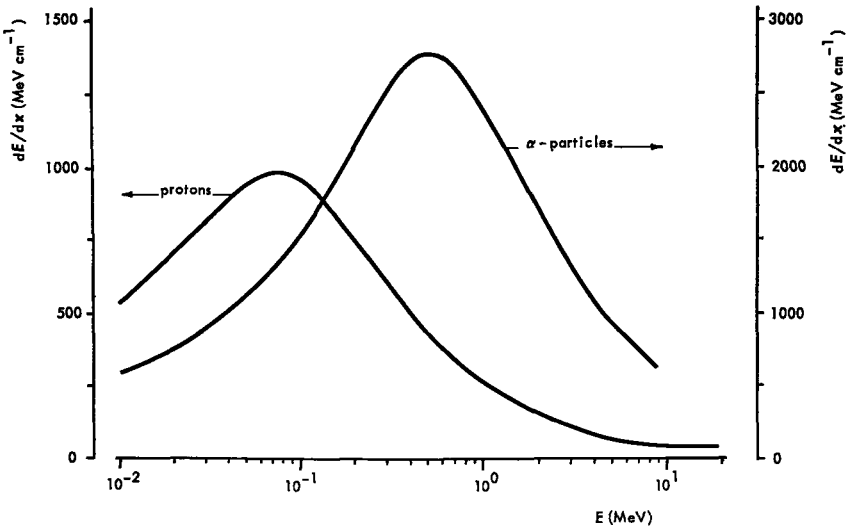

Fig. II-2. Stopping power, dE/dx, values as a function of energy, E, for protons and alpha particles in tissue.

The mean energy loss per unit path length of particles traversing a medium consisting of compounds and mixtures can be determined by the assumption that the contributions of the various constituents are additive as defined in the Bragg-Kleeman rule [1905]. The validity of this rule has been tested by many investigators. For alpha particles, only small deviations from this additivity rule, which were in the range of the experimental errors, have been reported [Williamson and Watt, 1972; Baglin and Ziegler, 1974].

Interactions of charged particles with nuclei of the stopping medium are mostly of an elastic nature; however, some interactions may lead to nuclear excitation or to nuclear reactions. At the nonrelativistic energies, attenuation of charged particle beams due to inelastic nuclear interactions is relatively insignificant. There are, however, a number of nuclear reactions of charged particles in nontissue-equivalent materials which are of special interest for the production of mono-energetic neutrons. These reactions will be discussed in chapter IV.

II-4 Fluctuations in energy loss by heavy charged particles in thin absorbers

Although mammalian cells are rather large (with diameters of 5–20 μm), subcellular structures and macromolecules of interest in the initiation of

radiation damage are much smaller, with dimensions in the order of 10^{-2} μm or less. Since the collisions of heavy charged particles are discrete and occur at random along their path, statistical fluctuations in the amount of energy transferred per collision must be expected. Related to this phenomenon of energy straggling is the variation in the range of particles of equal initial energy. However, this problem will not be discussed in detail as it is considered to be outside the scope of this thesis. Because of the association with the model for radiation damage to the clonogenic capacity of cultured cells, a more extensive review of the problem of energy straggling will be given. This model will be discussed in chapter VI.

A first approach to the theory of energy loss fluctuations was given by Flamm [1914] and by Bohr [1915]. On the basis of the assumption that the number of collisions is large, Bohr arrived at a Gaussian distribution function. This assumption is only valid, however, for thick absorbers.

A more rigorous treatment was introduced by Landau [1944] for very thin absorbers. The distribution function, $f(\Delta,s)\mathrm{d}\Delta$, for the probability that a charged particle traversing a path length, s, will lose an amount of energy between Δ and $\Delta+\mathrm{d}\Delta$, was given by him in the form of the kinetic equation:

$$\frac{\partial f(s,\Delta)}{\partial s} = \int_0^\infty \omega(\varepsilon) f(s,\Delta-\varepsilon)\,\mathrm{d}\varepsilon - f(s,\Delta)\int_0^\infty \omega(\varepsilon)\,\mathrm{d}\varepsilon \qquad \text{(II-5)}$$

where the energy loss, $\Delta = E-E_0$, occurring in the path length, s, is small compared to the initial energy, E_0, and therefore the probability, $\omega(\varepsilon)$, of energy loss per unit length can assumed to be independent of the final energy.

Application of the Laplace transformation with respect to the variable Δ will produce the transformed distribution function:

$$\varphi(s,\mathrm{p}) = \int_0^\infty f(s,\Delta)\mathrm{e}^{-\mathrm{p}\Delta}\,\mathrm{d}\Delta \qquad \text{(II-6)}$$

and, from the inversion theorem, it follows that:

$$f(s,\Delta) = \frac{1}{2\pi\mathrm{i}}\int_{\mathrm{c}-\mathrm{i}\infty}^{\mathrm{c}+\mathrm{i}\infty} \mathrm{e}^{\mathrm{p}\Delta}\varphi(s,\mathrm{p})\,\mathrm{dp} \qquad \text{(II-7)}$$

Substituting the Laplace form (II-6) for $\varphi(s,\mathrm{p})$ in equation (II-5) and applying Heaviside's shifting theorem, it follows that:

$$\frac{\partial \varphi(s,\mathrm{p})}{\partial s} = -\varphi(s,\mathrm{p}) \int_0^\infty \omega(\varepsilon)(1-\mathrm{e}^{-\mathrm{p}\varepsilon})\,\mathrm{d}\varepsilon \tag{II-8}$$

Integration of this equation yields:

$$\varphi(s,\mathrm{p}) = \varphi(0,\mathrm{p}) \exp\left[-s \int_0^\infty \omega(\varepsilon)(1-\mathrm{e}^{-\mathrm{p}\varepsilon})\,\mathrm{d}\varepsilon\right] \tag{II-9}$$

For the initial condition of zero path length, the probability density function, f(0,Δ), is a delta function and consequently the transformed function, φ(0,p), is equal to 1. Substitution of the equation for the transformed distribution (II-9) in the inverse Laplace transform (II-7) under the forementioned condition at zero path length yields:

$$f(s,\Delta) = \frac{1}{2\pi \mathrm{i}} \int_{\mathrm{c}-\mathrm{i}\infty}^{\mathrm{c}+\mathrm{i}\infty} \exp\left[\mathrm{p}\Delta - s \int_0^\infty \omega(\varepsilon)(1-\mathrm{e}^{-\mathrm{p}\varepsilon})\,\mathrm{d}\varepsilon\right] \mathrm{dp} \tag{II-10}$$

This is the general expression for the distribution function which, in principle, can be evaluated when the collision spectrum, $\omega(\varepsilon)$, is known. A number of attempts to solve this general equation have been reported over the years, each based on different postulates for the collision spectrum. Only a few will be discussed in nonchronological order.

It was suggested by Blunck and Leisegang [1950] to write the expression for the distribution function in terms of moments of the collision spectrum, defined as:

$$\overline{\varepsilon^n} = \int_{\varepsilon_{\min}}^{\varepsilon_{\max}} \varepsilon^n \omega(\varepsilon)\,\mathrm{d}\varepsilon \tag{II-11}$$

which results in an expression for the distribution function:

$$f(s,\Delta) = \frac{1}{2\pi \mathrm{i}} \int_{\mathrm{c}-\mathrm{i}\infty}^{\mathrm{c}+\mathrm{i}\infty} \exp\left[\mathrm{p}\Delta - s g(\mathrm{p})\right] \mathrm{dp} \tag{II-12}$$

where

$$g(\mathrm{p}) = \int_0^\infty \omega(\varepsilon)(1-\mathrm{e}^{-\mathrm{p}\varepsilon})\,\mathrm{d}\varepsilon = -\sum_{n=1}^{\infty} \frac{\overline{\varepsilon^n}(-\mathrm{p})^n}{n!}$$

In his attempt to solve the general equation of the distribution function, Landau assumed the following conditions for the collision spectrum:

$p\varepsilon_{max} \gg 1$ and $p\varepsilon_0 \ll 1$, where ε_{max} is the maximum energy transferred during a single collision and ε_0 is a characteristic energy of the order of the mean electron binding energy. This latter assumption means, in terms of moments of the expansion serie as given by equation (II-12), that the contributions of moments with $n > 1$ resulting from resonances in the collision spectrum were neglected.

As is evident from the formulation in equation (II-5), the upper limit of integration used by Landau extends to $\varepsilon = \infty$, thereby accounting for the possibility of energy losses larger than ε_{max}.

Using the nonrelativistic expression for the collision spectrum:

$$\omega(\varepsilon) = \frac{2\pi e^4 z^2 NZ}{m_e v^2} \left(\frac{d\varepsilon}{\varepsilon^2}\right) \tag{II-13}$$

he arrived at an expression for the energy loss distribution:

$$f(s, \Delta)\, d\Delta = \xi^{-1} \varphi(\lambda_L)\, d\lambda_L$$

where

$$\xi = \frac{u}{p} = \frac{2\pi e^4 z^2 NZ}{m_e v^2} s \tag{II-14}$$

$$\varphi(\lambda_L) = \frac{1}{2\pi i} \int_{c-i\infty}^{c+i\infty} \exp[u \ln u + \lambda_L u]\, du$$

and

$$\lambda_L \equiv \left\{\Delta - \xi\left[\ln\left[\frac{\xi 2 m_e v^2}{I^2(1-\beta^2)}\right] - \beta^2 + 1 - \gamma\right]\right\} \xi^{-1}$$

with $\gamma = 0.577216\ldots$, Euler's constant.

The function $\varphi(\lambda_L)$ has been calculated numerically [Börsch-Supan, 1961] for a wide range of λ_L.

It can be proved that the condition $p\varepsilon_{max} \gg 1$ results in $\varkappa = \xi/\varepsilon_{max} \ll 1$, which is valid for small values of path lengths, s.

Vavilov [1957], in his attempt to find the solution for the distribution function, and to circumvent the restrictions of the validity of the Landau solution to very thin path lengths, used an approximation of the kinetic equation. He derived this approximation by restricting the integral limits of the general form and derived the equation:

$$\frac{\partial f(s,\Delta)}{\partial s} = \int_0^b \omega(\varepsilon) f(s,\Delta-\varepsilon)\,\mathrm{d}\varepsilon - f(s,\Delta)\int_0^{\varepsilon_{max}} \omega(\varepsilon)\,\mathrm{d}\varepsilon \qquad \text{(II-5a)}$$

He further assumed that the collision spectrum $\omega(\varepsilon) = 0$ for $\varepsilon > \varepsilon_{max}$, where ε_{max} is the maximum energy transferred in a single collision, $b = \Delta$ for $\Delta < \varepsilon_{max}$ and $b = \varepsilon_{max}$ for $\Delta > \varepsilon_{max}$.

Using the relativistic formulation for the collision spectrum of heavy charged particles

$$\omega(\varepsilon) = \frac{\xi}{s\varepsilon^2}\left(1-\beta^2\frac{\varepsilon}{\varepsilon_{max}}\right) \qquad \text{(II-15)}$$

where

$$\varepsilon_{max} = \frac{2m_e c^2\beta^2}{(1-\beta^2)}$$

thereby neglecting distant collisions, applying for the mean energy loss the formula:

$$\bar{\Delta} = \xi\left[\ln\frac{2m_e c^2\beta^2\varepsilon_{max}}{(1-\beta^2)I^2} - 2\beta^2\right] \qquad \text{(II-16)}$$

and introducing in an identical manner as Landau a dimensionless parameter:

$$\lambda_v = \frac{\Delta-\bar{\Delta}}{\varepsilon_{max}} - \varkappa(1+\beta^2-\gamma) \qquad \text{(II-17)}$$

Vavilov arrived at the solution for the distribution as given by:

$$f(\Delta,s)\,\mathrm{d}\Delta = \frac{1}{\xi}\varphi_v(\lambda_v,\varkappa,\beta^2)\,\mathrm{d}\lambda_v$$

where

$$\varphi_v(\lambda_v,\varkappa,\beta^2) = \frac{\varkappa}{\pi}\mathrm{e}^{\varkappa(1+\beta^2\gamma)}\int_0^\infty \mathrm{e}^{\varkappa f_1}\cos(y\lambda_v+\varkappa f_2)\,\mathrm{d}y$$

$$f_1 = \beta^2(\ln y - \mathrm{Ci}(y)) - \cos y - y\,\mathrm{Si}(y)$$

$$f_2 = y(\ln y - \mathrm{Ci}(y)) + \sin y + \beta^2\,\mathrm{Si}(y)$$

$$\mathrm{Si}(y) = \int_0^y \frac{\sin u}{u}\,\mathrm{d}u$$

$$\mathrm{Ci}(y) = \int_0^y \frac{\cos u}{u}\,\mathrm{d}u \qquad \text{(II-18)}$$

For the condition of $\varkappa = 0$, the Vavilov distribution function reduces to the Landau distribution and, when $\varkappa \gg 10$, the function becomes approximately Gaussian. A comprehensive tabulation of these Vavilov distributions in terms of the parameters $\varkappa$ and β^2 is given by Seltzer and Berger [1964]. Vavilov distributions for $\beta = 0$ and $\varkappa = 0.01$, 0.1, 1 and 10 obtained from this tabulation are presented in figure II-3. These curves clearly demonstrate the increasing width and skewness with decreasing $\varkappa$, corresponding to decreasing path length.

In his treatise on the energy loss fluctuations, Vavilov disregarded, as did Landau, the effect of electron binding by ignoring moments with $n > 1$ (see equation II-12). A correction regarding this electron binding was introduced by Blunck and Leisegang [1950], using moments up to the second order. In his review, Fano [1963] showed how this Blunck-Leisegang correction can be applied to the rigorous Vavilov solution. If we denote the uncorrected Vavilov distribution as $f_v(\Delta, s)$, then the corrected distribution is given by:

$$f(\Delta, s) = \frac{1}{\xi b \sqrt{\pi}} \int_{-\infty}^{\infty} f_v(\Delta - u, s) \exp\left[-(u^2/\xi^2 b^2)\right] du \qquad \text{(II-19)}$$

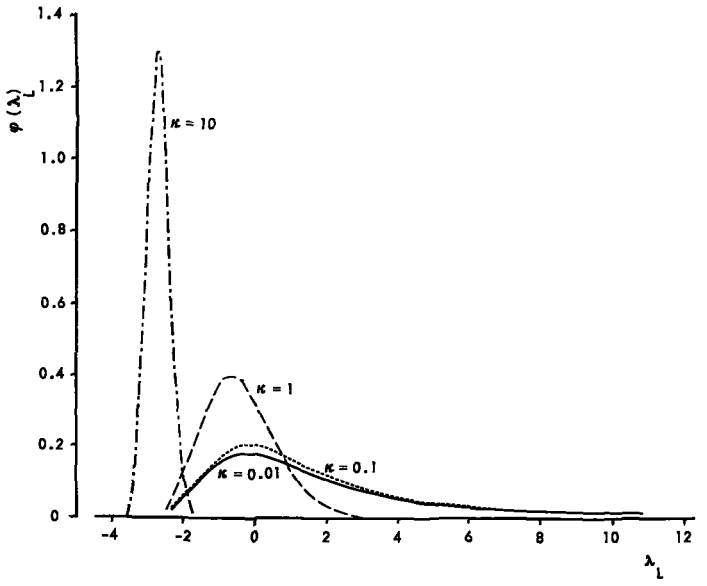

Fig. II-3. Vavilov distributions, $\varphi(\lambda_L)$, as a function of the Landau parameter, λ_L, for $\beta = 0$; $\varkappa = 0.01$, 0.1, 1 and 10. For the definitions of λ_L and $\varkappa$ see text.

where the parameter, b, according to Blunck and Westphal [1951] is given by:

$$b^2 \cong \frac{\bar{A}Z^{\ddagger}}{\xi} \times 20\text{eV}$$

Shulek et al. [1967] used a method similar to the one used by Blunck-Leisegang to calculate the correction of the shell structure and arrived at a distribution function analogous to the Vavilov distribution, differing only in the appearance of an additional term. This additional term introduces broadening and shift of the uncorrected distribution curve. According to the theory developed by Blunck and co-workers for $b^2 \leqslant 3$, the fluctuations in energy loss are described by a Landau-Vavilov distribution and, if $b^2 > 3$, by the Blunck-Leisegang corrected distribution.

Generally, the measured ionization loss distributions for very small path lengths disagree with theoretical distributions. This applies to Vavilov distributions as well as Blunck-Leisegang corrected ones. The first type gives an underestimation of the effect of straggling, while the latter overestimates straggling. It has been demonstrated by Chechin and Ermilova [1976] that this is due to restrictions in the order of moments from the power series (II-12) used for the solution of the differential equation (II-5). Restrictions to a first order moment will underestimate the width of the distribution curve, while a restriction to a second order will generally overestimate the effect.

On the basis of an harmonic oscillator model, Chechin and Ermilova arrived at a probability density function:

$$f(\Delta, s) = \sum_{n=0}^{\infty} \delta(\Delta - nI) C_n \qquad \text{(II-20)}$$

where n is the number of particle collisions with atoms; I is the mean excitation energy of the medium and C_n is determined from a generating function, $\phi(z)$, by the equations:

$$C_n = \frac{1}{n!} \frac{\mathrm{d}^n}{\mathrm{d}z^n} \phi(z)\Big|_{z=0} \qquad \text{(II-21)}$$

and

$$\phi(z) = \exp\left\{\frac{(z-1)\xi \ln[a/(1-z)]}{I}\right\}$$

where

$$\ln a = \ln\left[\frac{2m_e v^2}{I(1-\beta^2)}\right] - \beta^2 + 1 - \gamma - \delta$$

The discrete distribution, $\varphi_n(\lambda_n)$, which is equivalent to the Landau function, $\varphi(\lambda_L)$, with parameter, $\lambda_n = nI/\xi - \ln(a\xi/I)$, has been calculated and plotted by Chechin and Ermilova for various values of ξ/I at $\ln a = 10.7$. This value corresponds to energy values for protons and alpha particles of 1000 and 4000 MeV, respectively, which are beyond the energy range considered in this thesis. It can be concluded from the calculations of these authors that the fluctuation curve, $\varphi_n(\lambda_n)$, approaches the Landau-Vavilov curves when $\xi/I \gg 10$. For tissue, this corresponds to values for ξ of 700 eV and larger, values which will be achieved with energy loss distributions of 5 MeV alpha particles in layers with thickness larger than 70 nm. Consequently, Vavilov distributions provide reasonable approaches for the energy loss distributions in the region of interest.

Due to the finite thickness of the absorber, the energy actually deposited in the absorber is different from that discussed on the basis of theoretical principles, because the formulation refers to energy locally lost and not to energy locally deposited. High energy knock-on electrons having energies with ranges in excess of the absorber thickness will escape from the absorber and deposit their energy partly or totally outside the region of interest. A mathematical approach to loss by electron escape is given by Badhwar [1973] and Adams et al. [1975], introducing the energy limit, $b = \varepsilon_d$, in the kinetic equation (II-5A), where ε_d is determined from the practical range of the absorber. The effect of escaping electrons on the shape of the distribution curve is that the distribution curve becomes more Gaussian, since the skewness is reduced by cutting the high-energy tail from the Landau-Vavilov distributions.

The loss of escaping electrons from the region of interest, on the other hand, can be compensated for by electrons produced in preceeding layers. Laulainen and Bichsel [1972] demonstrated that this "wall effect" effectively compensates for the loss due to escaping δ-rays even for relatively high energy of the interacting particle.

As demonstrated by Vavilov and can be explained by the central limit theory of statistics, the shape of the energy loss distribution for absorbers of medium thickness will approach the Gaussian pattern. For thick absorbers where the energy lost in the absorbers amounts to the initial energy, the distribution is, moreover, influenced by the energy dependence of the collision probability. Distributions of large and extremely large energy losses up

to 50 percent of the initial energy have been discussed and calculated by Tschalär [1968, 1968a]. These large energy losses are not relevant to the subjects to be discussed later and will, therefore, not be more thoroughly reviewed.

II-5 Interaction mechanisms of indirectly ionizing radiation

Indirectly ionizing interactions arise from uncharged particles (e.g., photons and neutrons) via the production of charged directly ionizing particles in various processes. Due to the absence of attractive Coulomb forces, indirectly ionizing radiations can travel over relatively long distances without interactions with atoms of the medium. The deposition of energy is consequently widely distributed in space and the attenuation of the beam with depth is, apart from secondary effects, exponential.

Photons, x-rays and gamma rays in the energy region of 0.01 to 100 MeV interact with tissue by the photoelectric effect, Compton effect and pair production. The relative importance of each of these interaction mechanisms compared to the others depends on the photon energy. For low photon energies, the process of photoelectric absorption is dominant, while electron pair production starts only for photon energies larger than 1.02 MeV.

In the photoelectric effect, the low energy photon interacts by direct collision with one of the shell electrons.

Compton interaction from photons in the intermediate energy range of about 0.05 to 10 MeV occurs with the free or loosely bound electrons. The primary energy of the photon is distributed according to conservation laws for momentum and energy over the electrons set in motion and over a scattered photon with reduced energy. Energy distributions of Compton recoil electrons for various incident photon energies are given by Johns et al. [1952].

For energies in excess of 1.02 MeV (i.e. two times the equivalent of the electron rest mass energy), a photon can interact with the nucleus. In so doing, the photon is totally absorbed and an electron-positron pair is emitted. The positron will be annihilated with an electron and the energy will appear in the form of two annihilation quanta.

In summary, it can be concluded that, in the processes mentioned for photons, they all interact with the tissue medium through the creation of electrons, generally with wide distributions in energy; the electrons will be stopped in ionizing collisions.

Interaction of neutrons with the nuclei of the tissue constituents generally

occurs via elastic scattering, inelastic scattering, nonelastic scattering, capture and spallation. A review of the most important interaction processes with the main tissue components which are relevant for fast neutrons with energies in the range of 0.5 to 15 MeV will be presented here.

The relative importance of the different interaction modes is dependent on neutron energy and the elemental composition of the medium. According to an ICRU report [1964], the assumption for "normal" tissue composition in elements of H, C, N, O and "others" in percent by weight is 10.2, 12.3, 3.5, 72.9 and 1.2, respectively. The elemental composition of "normal" tissue in comparison to some tissue-equivalent materials and commercial plastics are presented in table III-1. Great differences in composition have been reported for various organs compared to "normal" tissue by Kim [1974] and the values for "normal" tissue should not be taken as too strict.

In the inelastic scatter process, neutrons undergo capture and reemission. The scattering nucleus may be left in an excited state; if so, it will decay to its ground state within a short interval of time, emitting one or more gamma rays. These reactions are possible only when the neutron energy is greater than a certain threshold energy. The energy transferred, E_{rec}, to a recoil nucleus left in an excited state with mean energy $\overline{E^*}$ above the ground state is given by the formula [Bach and Caswell, 1968]:

$$E_{rec}(\theta_{cm}) = \frac{2AE_n}{(A+1)^2} - \frac{\overline{E^*}}{(A+1)} - \frac{2AE_n}{(A+1)^2}\left[1 - \frac{(A+1)\overline{E^*}}{AE_n}\right]^{\frac{1}{2}} \cos\theta_{cm} \qquad \text{(II-22)}$$

where A is the mass of the recoiling nucleus relative to that of the neutron and θ_{cm} is the angle of the scattering of the neutron in the center of mass system. The initial spectrum, $N(E_{rec})$, of recoils per unit incident neutron fluence can be determined from the differential cross section, $(d\sigma/d\Omega)_{E_{rec}}$, by the relation [Caswell and Coyne, 1972]:

$$N(E_{rec}) = \pi n_i \frac{(A+1)^2}{A\left(1 + \frac{(A+1)\overline{E^*}}{AE_n}\right)^{\frac{1}{2}}} \left(\frac{d\sigma}{d\Omega}\right)_{E_{rec}} \qquad \text{(II-23)}$$

and where n_i is the number of atoms of the i th kind per gram.

Important inelastic reactions in tissue are those with carbon, nitrogen and oxygen.

The kinetic energy transferred from a neutron to a nucleus in an elastic

collision can be treated mathematically as a special case of inelastic collision for $\widetilde{E^*} \equiv 0$. The energy transfer is maximal for large scattering angles ($\theta_{cm} = -\pi$) and equal to $[4A/(A+1)^2]E_n$. For instance, the maximum energy of a proton, a carbon, a nitrogen or an oxygen recoil resulting from a collision of 15 MeV neutrons is 15, 4.3, 3.8 and 3.3 MeV, respectively.

Energy transfer in nonelastic collision or capture occurs via mutations of the nucleus with neutrons of energy exceeding a threshold determined by the reaction. The mutated nucleus will decay with the emittance of a heavy charged particle and/or gamma ray and a recoil nucleus, visualized for two-body reactions as:

$$n + T \rightarrow l + R$$

were n is the neutron, T is the target nucleus, l is the lighter emitted particle and R is the heavier recoil nucleus.

Of particular importance are (n,p) reactions with ^{14}N and ^{16}O, (n,d) reactions with ^{14}N and ^{16}O and (n,α) reactions with ^{12}C and ^{16}O. Only scarce data are available on the various nuclear reactions with regard to excited states and cross sections [Caswell and Coyne, 1972; ICRU, 1977].

II-6 Energy loss distributions of neutrons

From the initial energy density spectra of secondaries as a result of the most important reactions for 0.6 and 14 MeV neutrons, Caswell and Coyne [1974] calculated the equilibrium density distributions of secondary particles for tissue. In these equilibrium spectra, the recoil protons are particularly dominant, especially in the region of high energy recoils.

Although hydrogen atoms constitute only about ten percent of the tissue composition, it can be concluded that an important part of the energy is deposited via the recoil proton process. Illustrative of this fact is that, for neutrons in the energy range of 0.2 to 15 MeV, about 80 percent of the absorbed dose is due to protons.

The energy deposition distributions from neutrons are composed of distributions associated with the various particles generated in the interactions of these neutrons with the medium. Therefore, theoretical energy deposition distributions can be obtained from a mathematical folding procedure of the energy density spectra of the various recoil particles with the appropriate energy loss distributions of these various charged particles and their track length distributions.

This method was used by Caswell and Coyne [1974] in the calculation of the energy deposition distributions in tissue and Shonka plastic (a tissue-equivalent material) for neutrons of 0.22, 0.55, 2 and 14 MeV energy in 1 μm spheres. Although they ignored the effect of straggling in the density distribution, good fits were obtained for this dimension. Booz and Coppola [1974] calculated energy deposition distributions for neutron energies in the range of 50 keV to 6 MeV for an effective diameter of 1 μm, using a Monte Carlo program ENSPERE [Oldenburg and Booz, 1971, 1972]. Applying a symmetrical straggling distribution as a first order approximation, Coppola et al. [1974] demonstrated that, for small diameters, the effect of straggling will be important.

These computer approaches emphasize the complexity of energy deposition distributions by neutrons and the reliance on measured distributions to improve the programs.

CHAPTER III

TECHNIQUE FOR THE MEASUREMENT *OF SPECIFIC ENERGY*

III-1 Requirements for the detector, a basis for the choice

As explained in chapter II, all of the quantities in microdosimetry are defined in terms of the actual energy deposition in microscopically small volumes with dimensions of 10 μm or less. The experimental determination of these quantities requires, therefore, a device which can provide sensitivity to detect small amounts of energy; in addition, it should have a small detection volume, which can simulate at least a tissue or tissue-equivalent volume of some ten nanometers in diameter.

An insight into the required sensitivity of the detector can be obtained from the following argumentation. The deposition of energy by ionizing radiation will be manifested by the creation of one or more ion pairs in the detector volume. These ion pairs will induce an electric signal of small amplitude at the output terminals of the detector. For instance, one ion pair will induce a total charge of 1.6×10^{-19}C at the output terminals and this will result in a voltage pulse of about 1.6×10^{-8}V for a detector having a capacity of 10 pF. Additional amplification of the signal before processing is therefore required. However, this additional electronic amplification will inherently add extra noise sources from the various electronic components. The root mean square value of this noise referred to the input for a practical low noise preamplifier is equivalent to a few hundred electrons and, since the ultimate lower level for the measurements is determined by the amount of energy deposition required for the creation of a few ion pairs, it will be obvious that additional amplification in the detector itself is necessary. Srdoc [1968] demonstrated, as a rule of thumb, that, for the measurement of an energy deposition distribution of ^{60}Co gamma radiation, a detector amplification of about fifty times the input noise of the amplifier is required.

The most sensitive detector at least partly fulfilling this requirement is the gas-filled proportional counter. This type of counter belongs to the group of the gas-filled detectors. Other detectors of this group are the ionization chamber and the Geiger-Müller counter. The additional gain obtained in the proportional counter is free from noise, but it is not without variation and consequently some loss in resolution will be caused.

In a homogenous detector in which the cavity material differs from the

wall material in density only, according to Fano's theorem [1954], the flux density spectrum and the spectrum of ionizing particles are the same for cavity and wall. This property offers the possibility to determine energy deposition and other dosimetric quantities in solid media via the measurement of these dosimetric quantities in gases. In order to measure the important dosimetric quantities in tissue, the wall and gas filling of the counter have to be of tissue-equivalent composition. This tissue equivalency can be approximated by a compound material which is similar to tissue in elemental composition (chapter II).

The determination of the main dosimetric quantity "energy imparted" with a proportional counter requires knowledge of the relation between energy deposited and number of ions created in the absorption process. Furthermore, knowledge is required of the relation between this number of primary ions and the number of ions measured as is represented by the gas gain of the counter. These steps will be discussed in the next sections.

III-2 Energy deposition by ion pair creation

The particles generated in the tissue-equivalent (TE) wall, traversing the sensitive volume over a length of track, Δx, will deposit via the formation of ions an amount of energy, ΔE. From formula (II-2) it follows that $\Delta E/\Delta x$ is proportional to the number of atoms per volume unit and therefore proportional to the density, ϱ. Since, for an ideal gas, this density is proportional to the pressure, the simulated diameter, d_s, of the volume can be expressed as:

$$d_s = \frac{p}{p_n} \varrho d \tag{III-1}$$

where p is the gas pressure in the sensitive volume in pascal,
ϱ is the density of the gas at normal temperature and pressure,
d is the diameter of the gas volume of the counter and
p_n is the normal pressure in pascal at which the density is defined.

Small equivalent dimensions of the sensitive volume can consequently be readily obtained by lowering the absolute gas pressure in the counter.

The number of primary ions, N_0, formed along a track segment, Δx, of a particle and the amount of energy, ΔE, deposited by this particle in the counter are related according to the formula:

$$\Delta E = \bar{\omega} N_0 \tag{III-2}$$

where $\bar{\omega}$ is the average energy expended for the formation of an ion pair over the track length, Δx. This average energy, $\bar{\omega}$, is different from the average energy required for the formation of one ion pair, W, which is generally employed and is defined as the quotient of the energy, E, of a charged particle to the number of ion pairs, N_i, created when the particle is completely stopped.

The energy transfered to the atoms is not used only for the creation of ion pairs; a portion of it is used in the production of excitations and subexcitations. In addition, for tracks with high ionization densities, some of the created ions will recombine. Consequently, the average energy for the formation of one ion pair observed is always larger than the ionization potential.

This average energy, W, is not equal for all charged particles and depends moreover on the initial energy of the particle. Experimental data for electrons obtained by Waker and Booz [1975] in methane and TE gas [Rossi and Failla, 1956] demonstrate a strong increase in the W value with decreasing energy. The differential W values evaluated from these data demonstrate large peaks in the lower energy region corresponding to the energy region of K-shell binding. For heavy charged particles, only few experimental data [Leonard and Boring, 1973; Booz et al., 1972] for the W values of TE gases are available and conflicting conclusions with regard to the energy dependence have been drawn from these scarce data.

For neutrons, the energy deposition spectra produced by the various recoil particles (protons, alpha particles, heavy recoils) will overlap each other over very large regions. Due to this overlap, it is almost impossible to obtain the correct energy spectra of these recoil particles from these measured distributions and to introduce a W value corrected for particle energy and type of particle. Consequently, a constant mean value for $\bar{\omega}$ has been adopted to be independent of energy and particle.

III-3 Multiplication of the ion pairs originally created

Under the influence of an applied electric field, ions formed in the gas-filled cavity will drift to the electrodes. The total number of ions collected is, even for relatively small values of the electric field strength, identical to the number of ions initially produced. Mechanisms which disturb this ion collecting process are negative ion formation and recombination, but their influence can generally be neglected for the relatively high field strengths commonly used.

Increase in the field strength above a given threshold will result in a larger number of ions collected than one initially produced by the ionizing radiation. This is due to gas multiplication. There appears to be a region for the value of the electric field strength at which the number of collected ions remains proportional to the number of primary ions and therefore to the deposited energy. This is the proportional counter region. For values of the field strength beyond this region, the number of ions will also increase; however, this increase is no longer proportional to the number of primaries. Beyond this region of limited proportionality, the counter will eventually operate as a GM counter.

This increase in number of ions collected is a result of the fact that, during their travel to the collecting electrode, electrons gather enough energy from the electric field per mean free path length to ionize the atoms of the filling gas. If the value of the electric field is large enough, then multiple interactions in sequence are possible, resulting in an avalanche. The ratio between the average value of the number of ions collected to the average number of ions initially produced is called the gas multiplication factor. The mean gas multiplication factor, $\bar{G}$, in a cylindrical counter for an ionizing event at a distance, c, from the center of the counter can be given by the expression:

$$\bar{G} = \exp\left(\int_a^c \alpha \, dr\right) \tag{III-3}$$

where $2a$ is the diameter of the anode and α is Townsend's first ionization coefficient, which can be fitted by the empirical expression:

$$\frac{\alpha}{p} = A \exp\left(\frac{-Bp}{E}\right) \tag{III-4}$$

where E is the electric field strength; p, the gas pressure and A and B are constants for a given gas. Integration of equation (III-3) after substitution of equation (III-4) gives, for the gas gain in a cylindrical proportional counter with inner diameter, $2b$, and an applied anode voltage, V_a, the following expression as published by Campion [1971, 1972]:

$$\ln \bar{G} = \frac{AV_a}{B \ln(b/a)} \left[\exp\left(\frac{-aBp \ln(b/a)}{V_a}\right) - \exp\left(\frac{-cBp \ln(b/a)}{V_a}\right) \right] \tag{III-5}$$

The second term of this expression may be neglected for counters filled with

gas at conventional pressures. This means that the gas gain factor is practically constant for ions produced anywhere in the counter volume, except in a small region around the anodes where the multiplication occurs. The second term cannot be neglected at low gas pressures; consequently, the gas gain will be dependent on the site of origin of the primary ions. This variation in gas gain will cause broadening of energy deposition spectra, particularly for indirectly ionizing radiation, because, for this type of radiation, the initial sites are distributed over the sensitive volume. Apart from this loss of resolution, there will be loss due to fluctuations in the number of ion pairs primarily produced and to a variation in the gas gain. This latter variation is caused by fluctuations in the number of electrons produced per avalanche initiated by a single ionization. Several authors [Charles and Cooke, 1968; Alkhazov, 1970] have demonstrated that the relative energy resolution of a proportional counter can be given by the expression:

$$\frac{\sigma_k}{\bar{k}} = C\varepsilon^{-\frac{1}{2}} \tag{III-6}$$

where $\bar{k} = \bar{N}\bar{G}$ and $\bar{N}$ is the mean number of initial ion pairs; $\bar{G}$ is the mean gas amplification factor and ε is the energy deposited in the counter; C, a constant factor for counter and counter-gas; and σ_k, the standard deviation of the quantity k.

The ions formed in the counter gas will induce a time-dependent charge pulse on the detector electrodes during their travel to the electrodes. Because the center of ion production for the avalanche is very close to the anode, and, because the mobility of ions is much less than the mobility of electrons, the slope of the induced charge pulse is mainly determined by the slow moving ions. The fractional pulse height as a function of time can be expressed for a localized event as [Wilkinson, 1950]:

$$Q(t) = Q(0)C_c \ln(1 + t/t_0) \tag{III-7}$$

where

$$t_0 = \frac{a^2 p}{4C_c V_a \mu_0}$$

$C_c = (2\ln b/a)^{-1}$, the counter capacity per unit length, and μ_0 is the positive ion mobility at a gas pressure of 1 Pa.

For an extended ionization track, the electrons arrive at the multiplication region at different time intervals after their creation. This will reduce

the initial growth rate of the avalanche. Several authors [Hurst and Ritchie, 1953; Mathieson and Harris, 1970] have attempted to express the resulting pulse shape in an analytical form, assuming a simple relation for the electron mobility. Disregarding diffusion effects, it can be demonstrated [Neuert, 1966] that the total collection time for electrons in the proportional counter, which will be described in chapter III-4, is of the order of 0.01 μs. In agreement with the conditions for the derivation of the pulse-height formula (III-7), this time period can be ignored [Hendricks, 1973] in comparison to the total collection time of the pulse, which is about 15 μs at a gas pressure of 5 kPa.

III-4 Description of the proportional counter and gas flow system

The construction of the proportional counters with which the measurements of energy deposition were performed is given in figure III-1. The outer electrode, with an inner diameter of 5 mm and outer diameter of 11 mm,

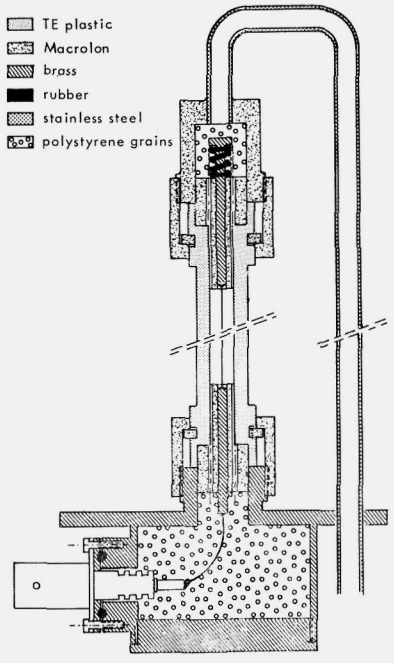

Fig. III-1. Schematic drawing of the tissue-equivalent proportional counter used for the measurement of energy deposition distributions.

Table III-1. Composition in percent by weight of "normal" tissue and some tissue-equivalent (TE) materials and commercial plastics.

	Element				
	H	C	N	O	Other
Muscle [ICRU, 1964]	10.2	12.3	3.5	72.9	
$C_5H_{40}O_{16}N$ [Rossi and Failla, 1956]	10.0	14.9	3.5	71.6	
TE-plastic A-150 [Spokas, 1975]	10.1	77.6	3.5	5.2	1.8 Ca; 1.7 F
Macrolon $(C_{16}H_{14}O_3)_n$	5.6	75.5		18.9	
Polystyrene $(C_8H_8)_n$	7.7	92.3			
Polyethylene $(C_2H_4)_n$	14.4	85.6			
Nylon 6 $(C_6H_{11}ON)_n$ [ICRU, 1977]	9.8	63.7	12.4	14.1	
TE gas [Kastner et al., 1963]	10.2	53.3	3.5		33 Ne
TE gas [Rossi and Failla, 1956]	10.2	45.6	3.5	40.7	

consists of tissue-equivalent Shonka-plastic [Shonka et al., 1958]. The composition of this Shonka-plastic in comparison to some materials, including soft tissue (ICRU), is given in table III-1.

As discussed in chapter II-5, the greater part of the energy deposition by neutrons is due to proton recoils from the hydrogen atoms in the medium. It can be seen from the table that a reasonably good match between tissue and tissue-equivalent material with regard to this hydrogen content was obtained. The evident differences in carbon and oxygen content have only a small effect on the energy deposition distribution, as demonstrated by Caswell and Coyne [1974], and are considered to be acceptable. The value of 5 mm for the inner diameter of the counter was chosen in order to achieve simulated diameters of a few hundred nanometers of unit density tissue at intermediate gas pressures. The wall thickness of 3 mm presents enough build-up material for the secondaries to obtain secondary particle equilibrium, even for neutrons of 15 MeV energy, since the range of 15 MeV recoil protons is about 2.3 mm.

A number of small holes of 0.2 mm diameter in directions perpendicular to the central wire and crossing the sensitive volume over different chord lengths were drilled in the counter wall. These holes, each closed by a Melinex window of 0.54 mg cm^{-2} thickness, permitted the introduction of α particles into the sensitive volume for studies on pulse shape and gas gain. Melinex is the trade name for the polymer polyethylene terephthalate, $(C_{10}H_8O_4)_n$, supplied by Imperial Chemical Industries Ltd., England.

For the support of the central wire, a rather unsophisticated construction without the usual field defining tubes was used. The length of the sensitive volume was restricted to the volume within the Macrolon isolators. It can

be demonstrated from Poisson's equation [Coulson, 1951] that the field strength component perpendicular to the gas-Macrolon interface is zero and that the ratio of the electric field strength in the gas to the electric field strength in the Macrolon is inversely proportional to the ratio of dielectric constants of gas and Macrolon, respectively. This ratio has a value of about 5. Macrolon is not optimal with regard to its hydrogen content, as can be seen from table III-1, but possesses good electrical and mechanical characteristics. Only a small part of the total inner surface of the sensitive volume is formed by the end pieces and, as expected, no significant differences were observed between spectra measured with Macrolon and nylon endpieces.

The central wire is made of stainless steel with a diameter of 52 μm. The lengths of the sensitive volumes of the counters are 1 and 5 cm and consequently the elongation factors are 2 and 10, respectively.

As mentioned in chapter II-6, the deposition of energy in the sensitive volume of a counter is the resultant of a number of factors, including the track length distribution. The fluence of secondary particles for detectors irradiated in a homogeneous field will be uniform when the slight preference for forward scatter is neglected. The distribution of track length under this condition belongs, according to Kellerer [1971], to the category of mean free path randomness (μ-randomness). Under this condition of μ-randomness, it can be proved that the probability density of a chord length, l, for a sphere with diameter, d, is presented by:

$$f(l) = \frac{2l}{d^2} \qquad 0 \leqslant l \leqslant d$$

Because the analytic formulation is much more complex for cylinders, Birkhoff et al. [1969] have calculated the probability densities by a Monte Carlo technique for cylinders with different elongation factors. Probability densities for cylinders with elongation factors 2 and 10, all with an identical mean track length, in comparison to the probability density for the sphere are presented in figure III-2.

It can be concluded that trajectories with the length of the diameter dominate for cylinders, especially for those with elongation factor 10. Consequently, the long cylindrical counters are favored for the measurement of lineal energy spectra.

The counters were flushed by a steady flow of approximately $5 \times 10^{-8} m^3 s^{-1}$ to ensure a constant composition of tissue-equivalent (TE) gas in the counters. This TE gas is a mixture of ethene (C_2H_4), ethane (C_2H_6), nitrogen

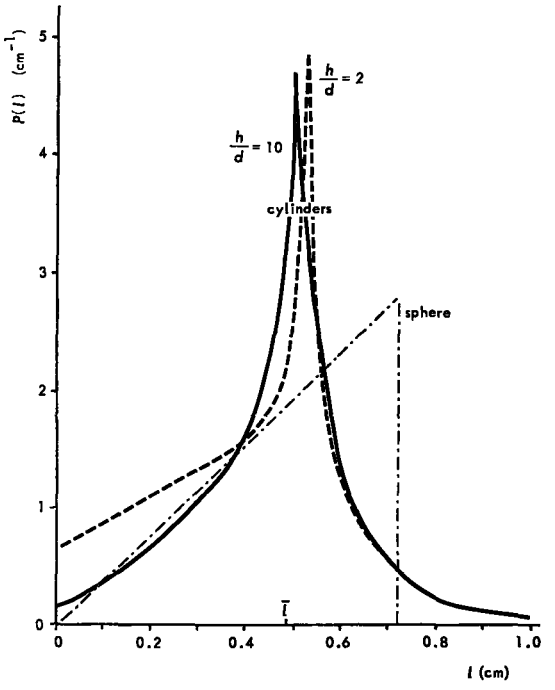

Fig. III-2. Frequency distribution, $P(l)$, for cylinders with elongation factors, h/d, equal to 2 and 10 and for a sphere. The mean track length, $\bar{l}$, is identical for the three bodies and equal to 0.48 cm.

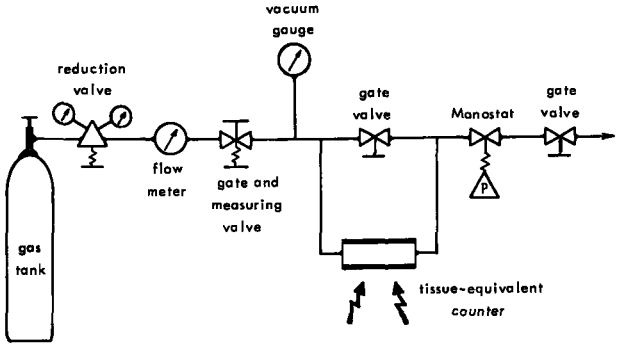

Fig. III-3. Schematic diagram of the gas pressure regulating system for the tissue-equivalent counter.

(N_2) and neon (Ne), according to Kastner [Kastner et al., 1963], in volume percentages of 39.6, 16.2, 3.1 and 41.1, respectively. This mixture was supplied in cylinders by l'Air Liquide Benelux in premixed form. The elemental composition of this TE gas in comparison to ICRU soft tissue is also given in table III-1.

A schematic diagram of the gas flow and pressure regulating system is presented in figure III-3. The TE gas mixture entering the system from the cylinder at left is reduced in pressure by a reducing valve; the flow rate set by the combined gate and measuring valve is measured with the flow meter. The pressure selected within a range of 0.7 to 101 kPa to simulate the desired volume, is maintained with a Carthesian manostat. The required vacuum is obtained from a rotating backing pump.

As will be discussed in chapter V, deviations from the expected gas gain were found at low pressures of the TE gas. In order to study the origin of these effects, additional gain measurements were performed on methane, a more commonly used counter gas.

III-5 The electronic analyzing system

The output pulses from the collecting wire of the proportional counter were amplified and analysed in an electronic system, a block diagram of which is presented in figure III-4.

Low noise charge sensitive preamplifiers of models Tennelec TC 100 C and TC 133 were alternately used. The most important specifications for the two preamplifiers are given in table III-2.

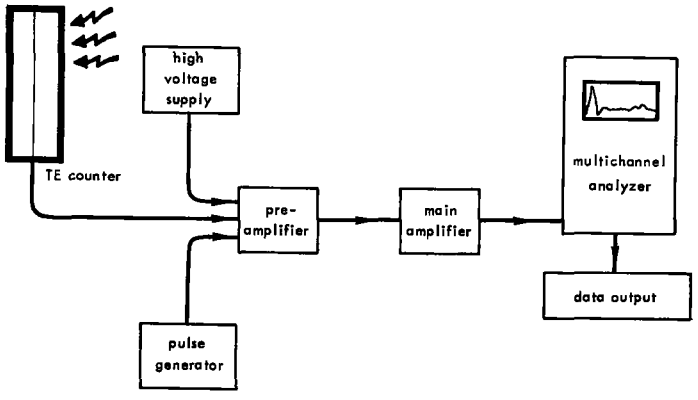

Fig. III-4. Block diagram of the electronic amplifying and analyzing equipment.

Table III-2. Electronic specifications of the preamplifiers [Tennelec, 1964 and 1967].

	Preamplifier type	
	TC 100 C	TC 133
Charge sensitivity (μV/ion pair)	0.21	0.16
Noise * (ion pairs r.m.s.)	340	420
Rise time (ns)	55	50
Decay time (μs)	47	100

* with 1.6 μs shaping for the TC 200 main amplifier

The time required for the charge pulse in a proportional counter to attain its full amplitude is relatively long; in order to minimize pile-up of sequential pulses in the analyzing equipment, the pulse has to be restricted. This can be obtained by proper pulse shaping [Fairstein and Hahn, 1965]. The preamplifier output pulses are amplified and shaped with a linear amplifier, model TC 200, having adjustable gain up to a factor 1024 and containing a first differentiator, second differentiator and integrator (double) with separate step-wise adjustable time constants in the range of 0.05 to 12.8 μs. The output pulses were analysed in a 1024 channels Laben multichannel analyser. The electronic system can be checked and calibrated by pulses fed into the test input of the preamplifier from a mercury relay pulse generator model TC 800. This test input is in parallel with the main signal input.

As mentioned above, the time for the charge pulse to attain its full amplitude is relatively long. For the TE counter used, at a gas pressure of 11.3 kPa, this time is of the order of 30 μs. The pulse shaping required to shorten the pulse duration by electronic networks will not only affect the duration of the pulse, but will also attenuate the pulse amplitude and influence the transmitted noise spectrum.

It can be shown [Gillespie, 1953] that, for a pulse shaping network performing single differentiation and integration, optimal resolution is obtained when the differentiation time constant equals the integration time constants. To determine the value of the time constant of the analyzing system for which optimal resolution could be obtained, the attenuation of exponential rising pulses of different rise times, t_0, were measured at various values of all equal time constants, τ, for differentiating and integrating networks. The exponentially rising pulses were generated by the pulse generator and fed into the test input of the preamplifier. The full-width at half maximum (f.w.h.m.) of the spectra resulting from these pulses plus noise from the preamplifier were also measured at these values of the time constants. The

gain of the main amplifier was maximal for these measurements in order to enhance the effect of loss in resolution from the preamplifier noise. The noise referred to the input of the main amplifier is hereby negligible compared to the noise from the preamplifier to the main amplifier input. As measured on an oscillograph, the rise time of the pulses used was 0.03, 0.3, 0.6, 3 and 10 μs, respectively. The decay time of the pulses was 400 μs for each of the five rise times.

The exponentially rising pulses, although not exactly representing the

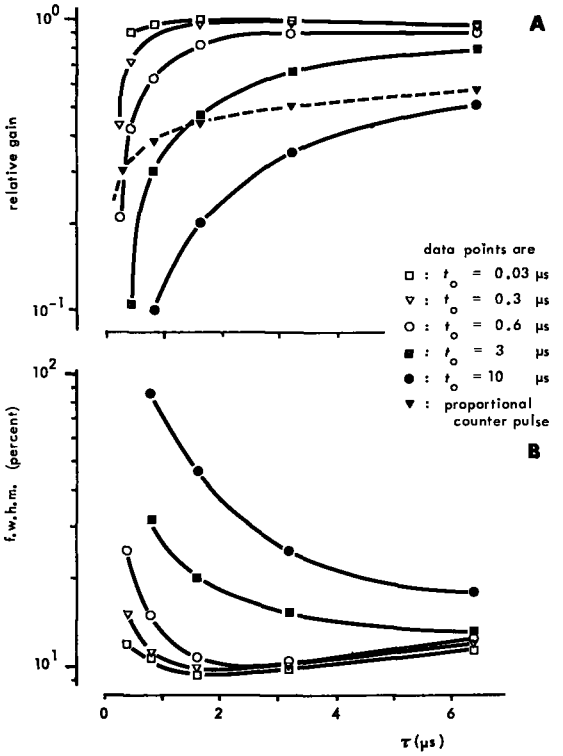

Fig. III-5. Characteristics of the electronic circuit for exponentially rising pulses with rise time, t_0.

A. Relative gain of the network as a function of amplifier time constante, τ. For comparison, the attenuation curve for an actual proportional counter pulse (at a gas pressure of 101 kPa and an applied voltage of 1600 V) is given.

B. Full-width at half maximum, f.w.h.m., (in percent of the position of the maximum) as a function of amplifier time constant, τ, derived from the pulse height distributions of the pulses modulated by amplifier noise.

counter pulses, were used to avoid the extra amplitude variations caused by differences in deposition and gain and which would be inherent in the use of actual proportional counter pulses. The resulting f.w.h.m. and attenuation curves for the TC 133 are presented in figure III-5. Identical results were obtained for the TC 100 C preamplifier. For the steep rising pulses with $t_0/\tau < 1$, the f.w.h.m. curves show weak minima, almost independent of rise time, at amplifier constants of 1.6 μs. This finding for the independency of the minima in the resolution curves is in agreement with derivations given by Gillespie [1953].

The root mean square (r.m.s.) value of the noise for the TC 133 preamplifier calculated from this measurements is 410 ion pairs and is in good agreement with the value of 420 ion pairs as given by Tennelec (table III-2). The results further demonstrate a rather high attenuation for the slow rising pulses; however, for the fast rising pulses, which can be compared to counter pulses generated at the especially important region of low gas pressures, the attenuation is small. For the fastest rising pulses, there seems to be a minimum in the attenuation curve. This effect is even more pronounced in attenuation curves measured for the TC 100 C and is caused by the decay of the pulse in the preamplifier. From these measurements with exponentially rising pulses, the value for the time constants of the main amplifier at which the event size distributions will be measured is chosen to be 1.6 μs. The absolute value for the attenuation of the charge pulse of the proportional counter which is of interest for the determination of the absolute gas gain will be discussed in relation to that subject in chapter V.

CHAPTER IV

RADIATION SOURCES

Event size spectra have been measured for a number of types of ionizing radiation. A description of the radiation sources employed and the determination of the mean energy of their radiation from energy spectra or from energy deposition spectra will be discussed in this chapter.

IV-1 Alpha particle sources

In the present investigations, the distributions of energy deposition for alpha particles in tissue-equivalent gases were measured at volumes of different sizes with a proportional counter. These alpha particles were also used, as will be discussed in chapter V, for the determination of gas gain characteristics of the proportional counters. For both measurements, alpha particles from ^{210}Po and ^{242}Cm sources were employed. The radioisotope ^{210}Po decays with a half-life time of 1.196×10^7s and emits alpha particles of 5.305 MeV energy with a relative abundance of almost 100 percent [Wilson, 1966]. In view of the short half-life time, the source had to be replaced frequently. The ^{210}Po sources used were of the type "air ionizing electrode code PDC1" supplied by The Radiochemical Centre, Amersham, England. The radioisotope is electrodeposited on the tip of a platinum wire which is encased in a brass tube. The active surface of the source was originally protected by aluminium foil of 1 mg cm^{-2} thickness. This foil was removed because this relatively thick window considerably reduced the energy of the alpha particles. These modified sources were encapsulated in order to avoid contamination of the environment with the radioisotope ^{210}Po, which, owing to its very high toxicity, is classified in class 1 [ICRP, 1964]. The capsules were constructed in such a way that the beam of ionizing radiation left the enclosure through a cylindrical collimator with an opening of 1 mm diameter covered by a Melinex window with a tissue-equivalent thickness of 0.54 mg cm^{-2}.

At a later stage, the ^{210}Po sources were no longer supplied by The Radiochemical Centre because of the high risk involved in their manufacture and use. As substitutes, ^{242}Cm sources of identical construction were used. The energies of the alpha particles emitted by ^{242}Cm are 6.066 and 6.110 MeV with a relative abundance of 23.3 and 76.7 percent, respectively; the half-life

time is 1.408×10^7 s [Wilson, 1966]. The curium sources were employed only for regular calibration of the proportional counter; all of the measurements for the determination of gas gain characteristics were performed with polonium sources.

The alpha particles of both sources have only a restricted range of about 50 μm in tissue, i.e., much less than the thickness of the counter wall. Therefore, for the measurements of spectra and for the determination of gas gain, the alpha particles were introduced into the sensitive volume of the proportional counter through the small holes drilled in the counter wall as mentioned in chapter III. By means of four micrometer adjustments of the source support, it is possible to position the particle beam in line with the entrance holes.

During their passage of source and counter window, the alpha particles will lose a part of their initial energy. The energies of the alpha particles on entry into the sensitive volume were determined for both sources by an indirect method from their average energy losses per unit path length, dE/dx, in gases. These dE/dx values were derived according to the following curve fitting method. Energy loss spectra were measured for various energies of alpha particles and the counter operated at various counter gas pressures. These spectra were fitted to their corresponding theoretical distributions. As will be discussed in chapter V-4, the mean values of the fitted theoretical distributions correspond to the mean energy loss at the various conditions. For the measurements of energy loss spectra, the energy of alpha particles was varied by introducing different numbers of additional Melinex absorbers in the beam between the source and the proportional counter. The thickness of each of these Melinex absorbers is equivalent to 0.54 mg cm^{-2} of unit density tissue. The set of mean values thus derived for the various numbers of additional absorbers was fitted to the mean energy loss versus range curve. Because this range curve has a strong maximum in the Bragg peak, this method of fitting can be rather accurately performed.

The mentioned energy loss distributions for alpha particles of different energies were measured with the counter operated at gas pressures of 101, 21.3, 11.3, 5.32, 2.66 and 1.33 kPa. These pressures correspond to values of the simulated diameters presented in table IV-1. As an example, measured distributions in TE gas at equivalent diameters of 0.075 and 1.2 μm of unit density tissue are presented in figure IV-1.

The mean values of these energy loss distributions were fitted, in accordance with the method discussed, to the curves of dE/dx versus range for alpha particles in TE gas as derived from data published by Oldenburg and

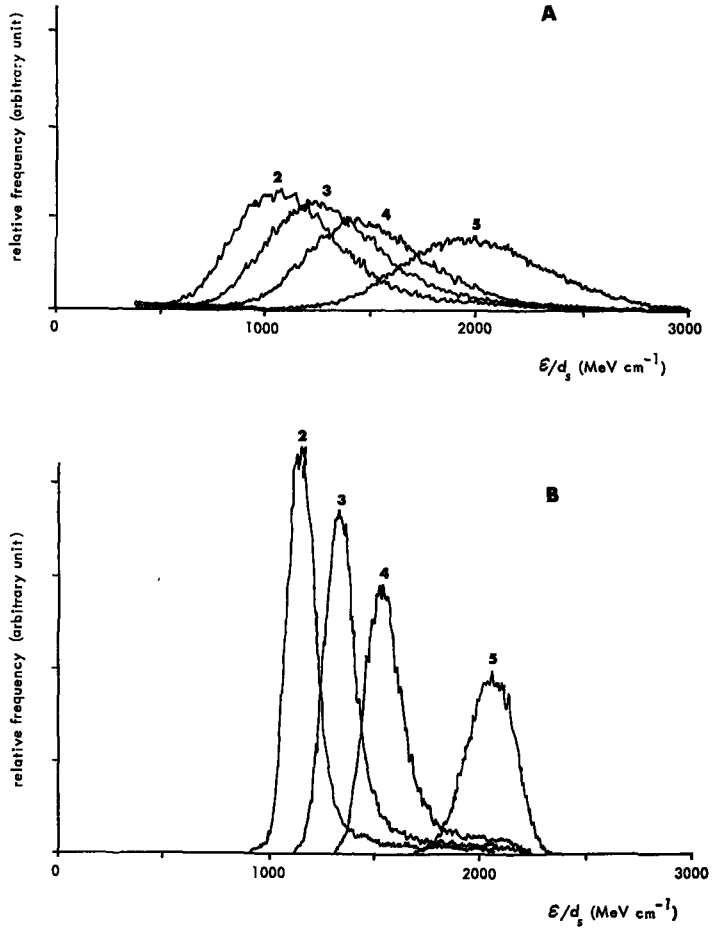

Fig. IV-1. A. Measured energy loss distributions of ^{210}Po alpha particles at equivalentdiameter of 0.075 μm in tissue of unit density after passage through different numbers of absorbers. Numbers refer to numbers of absorbers.
B. Same as A, but for an equivalent diameter of 1.2 μm in tissue of unit density.

Booz [1972] and by Walsh [1970] for soft tissue. The data of Walsh for the depth of penetration as a function of exit energy are extrapolated to an exit energy equal to zero. Results of these fitting procedures are presented in figure IV-2. The data points are related to the center of the track segments in order to correct, as a first approximation, for the fact that a track average value for dE/dx is determined. This correction is especially important for the

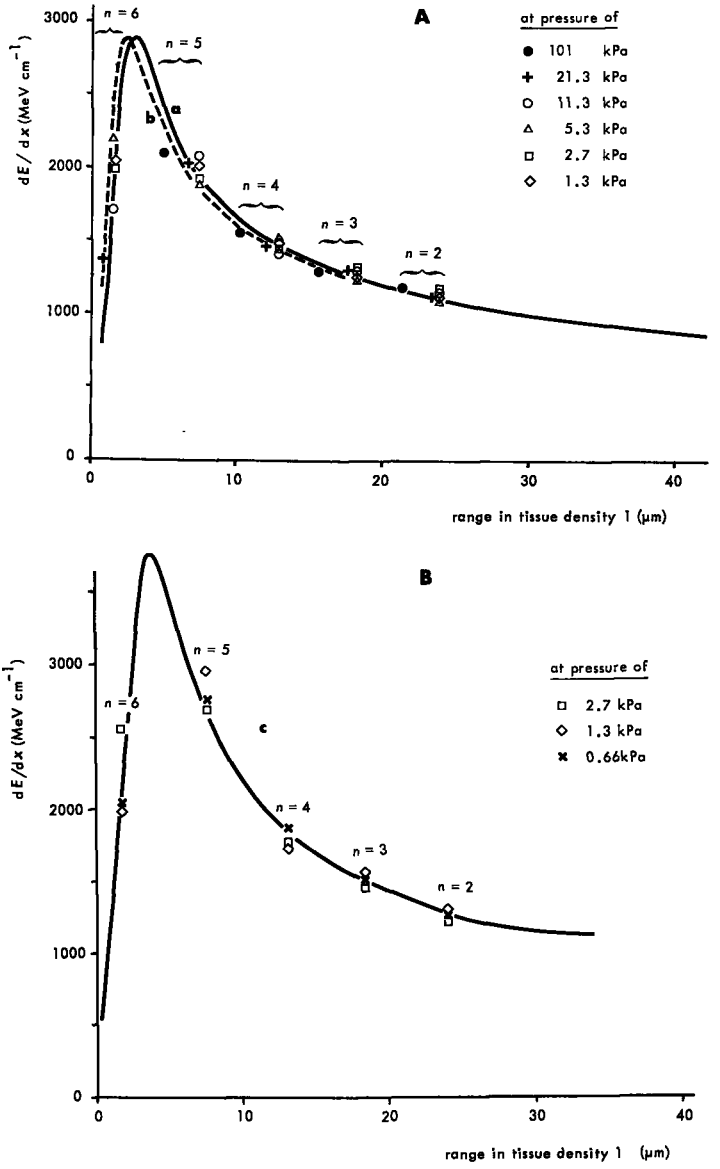

Fig. IV-2. Energy loss per unit path length, dE/dx, for alpha particles in tissue-equivalent gas and methane as a function of the range in unit density tissue.

A. dE/dx for the tissue-equivalent gas.
Curve **a** is obtained from data published by Oldenburg and Booz [1972]; curve **b** is obtained from data published by Walsh [1970].

B. dE/dx for methane.
Curve **c** is obtained from data published by Rotondi [1968].

Data points are for ^{210}Po alpha particles after passage through different numbers, n, of absorbers at different gas pressures.

larger simulated diameters. For decreasing sizes of simulated volumes, the number of energetic delta rays depositing part of their energy outside the detector volume will increase and consequently the mean of the distribution will no longer be representative for the value of dE/dx estimated from stopping power theories (see chapter II). From the fact that the respective values for $d < 1.2$ µm are close together along the curve, it can be concluded that, even for the situation of the smallest simulated diameter of 0.075 µm of unit density tissue, equilibrium conditions still apply and the factor of escaping delta rays does not present a serious problem.

From the curve of figure IV-2, a value of $dE/dx = 1100 \pm 20$ MeV cm^{-1} of unit density tissue is determined for the polonium alpha particles entering the sensitive volume with no additional absorption between source and the counter. By the same method, the mean dE/dx value on entry into the sensitive volume for alpha particles originating from the curium source is determined to be 950 ± 20 MeV cm^{-1} in unit density tissue. For diameters larger than 0.5 µm, a track average value for dE/dx (table IV-1) is used in the calculations of the energy deposition instead of dE/dx at the entrance.

Table IV-1. Review of the tissue-equivalent (TE) gas pressures used in the TE counter and the corresponding simulated diameters, d_s, and mean stopping powers, dE/dx, for the ^{210}Po alpha particles traversing the counter.

Gas pressure (kPa)	1.33	2.66	5.32	11.3	21.3	101
d_s (µm unit density tissue)	0.075	0.15	0.30	0.63	1.2	5.6
Mean dE/dx (MeV cm^{-1} of unit density)	1100	1100	1100	1120	1140	1180

As will be discussed in chapter V-4, unexpected differences in gas gain were measured for particle tracks of different length at very low pressures. To investigate whether these effects are related to gas composition, the counters were also flushed with methane. The mean dE/dx value for the polonium alpha particles in this methane gas was derived by the same curve fitting method as described for the TE gas. Mean values of the measured energy loss distributions for the alpha particles in this gas were fitted to a curve of the stopping power in methane versus range in tissue as derived from data published by Rotondi [1968]. From this result (figure IV-2), a mean value of $dE/dx = 1260 \pm 20$ MeV cm^{-1} of unit density methane is derived for the polonium alpha particles. The values of dE/dx which were derived for the polonium and curium alpha particles in TE gas and methane demonstrate differences, such as decrease in dE/dx with increasing particle energy, which are to be expected on stopping power theory. A further comparison shows

that the derived values of 1100 MeV cm^{-1} in TE gas and 1260 MeV cm^{-1} in methane are in good agreement. This agreement can be deduced from the equal rest ranges of 24 μm of unit density tissue which correspond to these stopping power values of both gases. The rest range of 24 μm of unit density tissue corresponds to an effective energy of the alpha particles of 4 MeV. The decrease in the original particle energy from 5.3 MeV to an effective energy of 4 MeV is due, as mentioned, to the passage of the particles through the enclosure of source and counter and the passage through the small air gap between both. For these absorbing materials, a total equivalent thickness of 13.1 μm of unit density tissue can be calculated from the difference between the range corresponding to the original energy and to the derived rest range.

The stopping power value of 950 MeV cm^{-1} determined for the alpha particles of the curium source corresponds to an effective energy of 5 MeV and a rest range of 33.2 μm unit density tissue. The thickness of the absorbing material corresponding to this rest range is 12.9 μm of unit density tissue, which is in good agreement with the value of 13.1 μm in unit density tissue derived from the results for polonium alpha particles. These results clearly demonstrate the validity of the curve fitting method for the determination of the energy loss per unit path length for the alpha particles in the counter volume.

IV-2 Proton sources

For the measurement of energy loss distributions of protons in tissue-equivalent volumes, H_1^+ ions were accelerated in a double belt K2N-3750 Van de Graaff electrostatic positive ion accelerator to energies of 1.5 and 3.0 MeV. The ions were produced in a radiofrequency ion source and were analysed, after extraction, in a magnetic field before entering the accelerating tube. The protons leave the beam pipe through a hole of 0.2 mm drilled in the end plate. The end plate is provided with a carbon backing in order to decrease the amount of gamma radiation generated in the end plate material. The exit opening is closed by a Melinex window with an equivalent thickness of 0.54 mg cm^{-2}, to prevent leakage of air into the beam pipe.

The proportional counter was lined in such a way that the proton beam entered the sensitive volume through the small apertures in the counter wall. Identically as for the alpha particles, the energy was varied by insertion of extra absorbers in the beam. The mean values of the measured energy loss distributions after passage of these various energies were fitted to the dE/dx versus range curve derived from data published bij Oldenburg and Booz

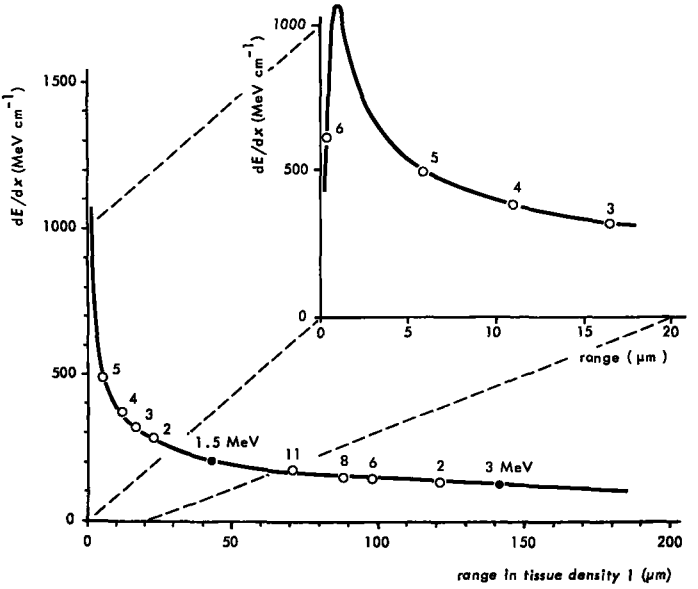

Fig. IV-3. Energy loss per unit path length, dE/dx, in tissue-equivalent gas versus range in tissue for protons.
Data points are for 1.5 and 3 MeV protons after passage through different numbers of Melinex absorbers, each having an equivalent thickness of 0.54 mg cm^{-2}. Numbers refer to numbers of absorbers.
The curve is obtained from data published by Oldenburg and Booz [1972].

[1972]. The results of this fitting procedure are presented in figure IV-3.

From this curve, the energy loss per unit path length of the protons in the sensitive volume after passage of the beam tube exit window and proportional counter entrance window is determined to be 280 ± 10 and 130 ± 10 MeV cm^{-1} for accelerating voltages of 1.5 and 3.0 MeV, respectively. The mean energies of the protons corresponding to these values for the energy loss per unit path length, derived from Oldenburg and Booz data, are approximately 1.0 and 2.7 MeV, respectively. Identically as for the alpha particles, the total equivalent thickness of absorbing material (Melinex absorbers plus air gap between source and counter) can be calculated for these proton experiments. This results in an equivalent thickness of about 20 μm of unit density tissue, a value which is larger than the value of 12 μm which was derived from the experiments with alpha particles. This is due to a larger air gap (defined by the experimental condition) between tube exit and counter entrance window than that between alpha source and counter.

IV-3 Neutron sources

Collimated as well as uncollimated neutron beams of various energies were used for the measurement of the energy loss distributions and will be described separately below.

15 MeV neutrons were produced by the $T(d,n)^4He$ reaction, which is commonly referred to as the d-T reaction. Because of the high values for the reaction energy, Q, ($Q = 17.590$ MeV) and for the reaction cross section, fast neutrons can be produced at relatively low accelerating voltages [Brolley and Fowler, 1960; Liskien and Paulsen, 1973]. Deuterium ions used for the reaction were accelerated in a Van de Graaff electrostatic generator type AN-400, in a Texas Nuclear generator model 9909 S or in a double-belt Van de Graaff electrostatic generator type K2N-3750.

The deuterium ions accelerated in the AN-400 to 400 keV impinge on a stationary tritium loaded titanium target plated on a copper backing. The water-cooled target holder is of the construction described by Broerse [1966]. The accelerating voltage for this machine is restricted to an upper limit of 400 kV, while the beam current is restricted to about 250 μA.

The Texas Nuclear generator is a modified model 9909 S accelerator with an oil transformer power supply delivering a maximum accelerating voltage of about 270–280 kV and having a maximum beam current of 6 mA [Broerse et al., 1972]. The targets used for this machine were also tritium loaded titanium layers plated on a water-cooled copper backing. The Texas Nuclear generator is constructed for high output yields of neutrons, such as are required for the irradiation of larger biological objects and for radiotherapy. The thermal load per unit area of the target and consequently the target-lifetime is improved by employing a rotating target construction of the type RTE 2 as supplied by NUKEM. The total yield of neutrons which can be produced under optimal target conditions is 6×10^{11} neutrons per second for the d-T reaction with the described accelerating voltage and beam current.

These high outputs are undesirable for the measurements of energy deposition distributions, since pile-up effects in the detector can cause distortions of the spectra; consequently, the machines were run on very low ion currents. Apart from these changes to low output values, other conditions were kept similar to the set-up as used for biological experiments and clinical applications.

Deuterium ions for the production of 15 MeV neutrons with the double-belt K2N-3750 Van de Graaff generator were accelerated at a voltage of

500 kV, the lower limit for the accelerating voltage obtainable for this machine.

The differences in applied voltages for the various accelerators will influence the energy distributions of the generated neutrons to only a small extent, as will be discussed in the section on energy spectra. The constructions of target holders differ only slightly and accordingly negligibly small differences in the energy loss distributions are obtained.

3 and 5 MeV neutrons were generated by the D(d,n) ^{3}He reaction, commonly referred to as the d-D reaction. This reaction is also exothermic; however, the reaction energy ($Q = 3.269$) and the production cross sections are considerably smaller than for the d-T reaction. As a consequence, the energy and energy distribution depend more significantly on the accelerating voltage, and higher beam currents are required for similar neutron outputs as compared to the d-T reaction.

Neutrons with a maximum energy of 3.37 MeV result from 400 keV deuterium ions accelerated in the AN-400 impinging on the deuterium loaded titanium targets. The maximum energy is 5.55 MeV for neutrons produced in the Van de Graaff K2N-3750 by the 2.3 MeV deuterium ions. The constructions of the targets are identical to the constructions mentioned for the d-T reaction.

0.51 and 0.89 MeV neutrons were produced by the T(p,n) ^{3}He reaction. This is an endothermic reaction with a Q value of –0.764 MeV [Liskien and Paulsen, 1973]; it has an acceptable production cross section and the neutrons are emitted mainly in the forward direction at low energies. The reaction is, nevertheless, very useful in the production of high fluxes of low energy monoenergetic neutrons for biological studies.

Analysed positive atomic hydrogen ions were accelerated in the K2N-3750 generator to 1.340 and 1.700 MeV, producing neutrons with maximum energies of 0.51 and 0.89 MeV, respectively, in the forward direction. The usual target assembly of this machine was employed.

The 15 and 3 MeV neutrons produced in the AN-400 Van de Graaff generator were used for the measurements of energy loss distributions "free-in-air" and for the measurement of these distributions behind a collimator with a conically shaped outlet employed for various types of radiobiological studies. The neutrons of 15, 5, 0.9 and 0.5 MeV energy produced with the Texas Nuclear generator and with the Van de Graaff K2N-3750 generator were used for studies on collimated beams. For this purpose, collimation was

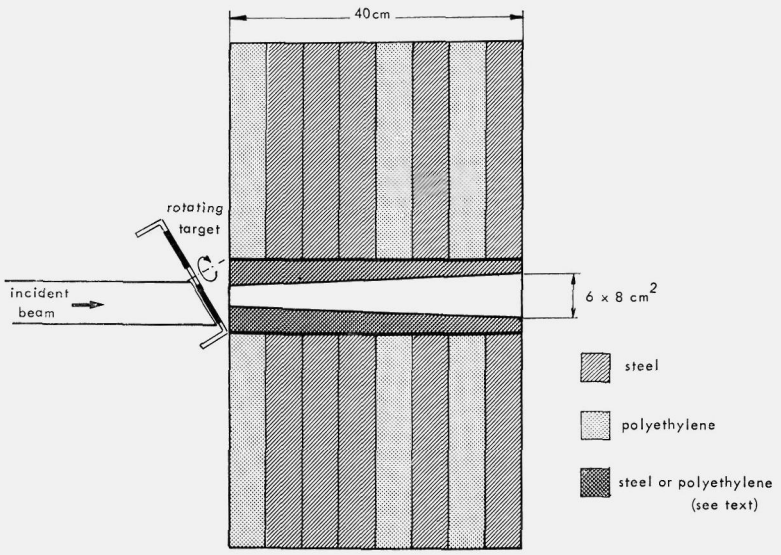

Fig. IV-4. Schematic drawing of the collimator as used in the clinical trial of fast neutron cancer therapy [Broerse et al., 1973].

obtained with the collimator employed in clinical studies of neutron cancer therapy on patients with lung metastases [Van Peperzeel et al., 1974].

The collimator, built of multilayers of steel and polyethylene to a total thickness of 40 cm, is of the construction reported by Broerse et al. [1973] and Mijnheer et al. [1975]. A schematic representation of the construction is presented in figure IV-4. The inside surface of the outlet was lined with a tapered steel or polyethylene layer. The field defined by both cones was a 6×8 cm^2 field at 45 cm from the target; the opening at the target side measured 3×3 cm^2.

(α-n) sources are the oldest type of neutron sources. In fact the neutron was discovered in 1932 by Chadwick using an alpha-berylium source. Because of the wide energy distributions in combination with low intensities of the produced neutrons and the relatively large contribution of accompanying gamma rays, reactions other than those with alpha particles are usually more convenient for biological experiments. For applications as calibration sources there are some advantages, since these sources are easy to operate, are stable in output and can be prepared carefully enough to be used as standards.

Energy loss distributions have been measured for two types of Be(α,n) calibration sources, namely, an ^{241}Am Be source and a ^{239}Pu Be source. These sources and their characteristics have been described by Pauw [1970]. A review of the main characteristics is presented in table IV-2.

Table IV-2. Characteristics of (α, n) sources employed.

	Type of sources	
	241 Am Be	239 Pu Be
Manufacturer	Radiochemical Centre Amersham	NUMEC
Container material	stainless steel	tantalum, stainless steel
Height (mm)	48.5	52.3
Diameter (mm)	22.4	39.5
Activity approx. (Bq)	11.1×10^{10}	18.5×10^{10}
Half-time (s)	14.45×10^{10}	77.0×10^{10}
Neutron emission rate (s^{-1})	8.6×10^{10}	10.0×10^{10}

IV-4 Energy distributions of the neutron sources

The energies of the monoenergetic neutrons produced in the d-D and d-T reactions for thin targets are well established and have been discussed by a number of authors. Neutrons produced with practical targets will have much wider distributions due to a number of complicating factors. Some of these complicating factors are target thickness, construction of target holder and accompanying reactions. Firstly, the accelerated particles lose energy when penetrating into the target layer; consequently, the energy of the neutrons produced will vary with penetration depth. Secondly, attenuated neutrons and gamma rays resulting from neutron interactions with target and target assembly materials will contaminate the original beam. Furthermore, contamination with carbon films on target and other beam tube parts can result in additional contributions of low energy neutrons from deuterium ions in the ^{12}C(d,n)^{13}N reaction, having a Q value of –0.281 MeV [Hanson et al., 1949].

For the 3, 5 and 15 MeV neutrons, energy spectra were determined experimentally with an organic scintillator proton-recoil spectrometer.

The detector employed for the spectrometer is a cylindrical cell of NE 213 liquid scintillator, with a diameter of 5 cm (Nuclear Enterprise Ltd., Type VH1) mounted directly onto a photomultiplier (Philips, type 56 DVP).

The principle of the detector of the recoil-proton spectrometer is based on the fact that the protons produced by neutron interactions deposit their

total energy in the detector volume. It can be demonstrated that these recoil protons produced by single scattering collisions of monoenergetic neutrons with the hydrogen atoms are distributed with equal probability in the energy range from zero to the maximum energy [Jones and Toms, 1971]. This maximum proton energy is identical to the neutron energy (chapter II). Differentiation of the rectangular energy distribution of the protons results in a delta function at a value for the energy equal to this maximum energy. The practical application is somewhat complicated by a number of factors, which will be briefly discussed.

The luminous output from the scintillator is a nonlinear function of the energy lost by heavy particles in the scintillator [Birks, 1964]. Consequently the height of the pulse as collected in an analyzer is not proportional to the energy of the proton recoil. The measured pulse-height distributions can be converted into proton energy spectra if the response of the scintillator is known. This response of the scintillator to protons of energy, E_p, can be expressed in terms of an electron energy, E_e, for equal light output as an approximation by the two parameter expression:

$$E_e = aE_p^b \tag{IV-1}$$

Where a and b are two curve fitting parameters. Calibration of the detector for electrons of various energies can be obtained from calibrations with Compton electron spectra produced by gamma rays of different energy.

Neutrons will be detected by the scintillator with varying efficiency. It can be demonstrated that the efficiency, $\eta(E_n)$, for detection of neutrons with energy, E_n, due to single scattering (ignoring the carbon contribution) is approximately [Swartz and Owen, 1960]

$$\eta(E_n) \approx n_H \sigma_H L \left[\frac{1-\exp(-aL)}{aL}\right] \tag{IV-2}$$

where: L is detector length
$a = n_H\sigma_H + n_C\sigma_C$
n_H and n_C are the number of hydrogen and carbon atoms per cm^3 of the scintillator
σ_H and σ_C are the neutron scattering cross sections for hydrogen and carbon

It is evident from the decrease in the cross section with increasing energy that the efficiency is a decreasing function with increasing energy. Numerical values for the efficiencies have been calculated for stilbene [Swartz and Owen,

1960] and NE 213 [Verbinski et al., 1969]. Knowledge of both of these efficiency and light output functions is required for the unfolding of measured spectra.

The detector is not only sensitive to neutrons, for, when it is exposed to a mixed field, gamma rays will also be detected. It has been found that pulses produced by different types of charged particles vary in decay time and that these differences are related to the ionization density of the particles. These differences in pulse shape can be used to distinguish and separate recoil proton pulses from electron pulses [McBeth et al., 1971].

In the practical application, the discrimination between neutrons and gamma rays is provided by the time difference in the zero crossing of the doubly differentiated pulse. A block diagram of the pulse shape discriminator circuit is presented in figure IV-5.

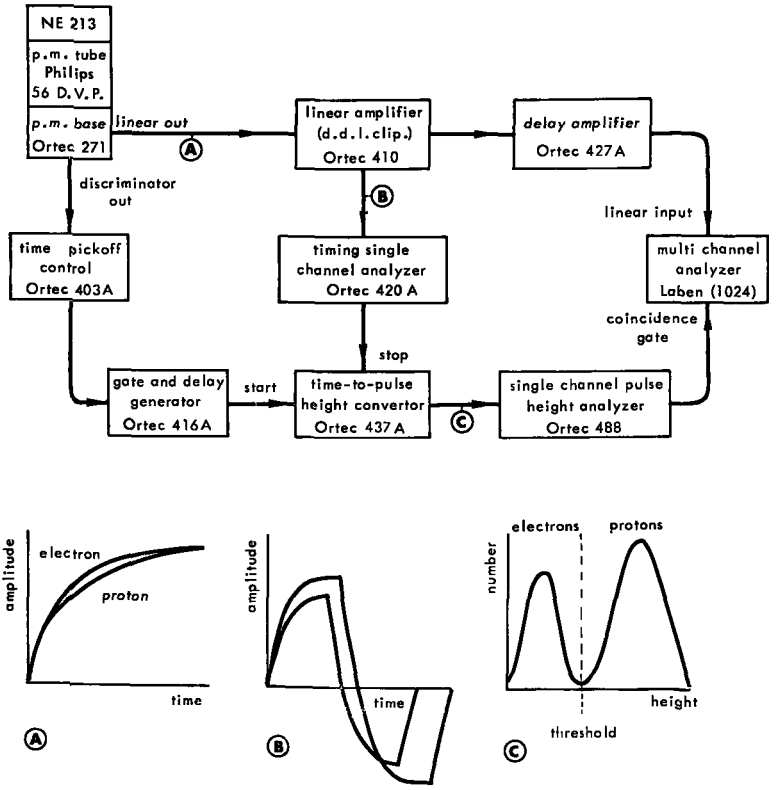

Fig. IV-5. Block diagram of the proton-recoil neutron spectrometer. Pulse shape and spectra measured at points A, B and C in the circuit are presented schematically.

A timing signal related to the pulse start is produced by a constant fraction timing unit: this pulse starts the time-to-pulse height converter. The linear output pulse, representing the energy information, is differentiated in the double delay line amplifier; the output pulse **B** from this amplifier triggers the timing single channel analyzer at a time that is dependent on the zero crossing of the doubly differentiated pulse. The pulse from the timing single channel analyzer stops the time-to-pulse height converter and, as a result, the pulses generated in this converter will vary in height corresponding to the time difference between start and zero crossing of the differentiated pulse. Two peaks can be measured at **C**: one due to electrons induced by gamma rays and one to protons induced by neutrons. The threshold for the single channel analyzer is set in such a manner that only the pulses correlated to neutrons can produce a coincidence pulse. The linear output pulses and coincidence pulses are fed to the multichannel analyzer and this provides spectra which can be transformed into neutron energy distributions by means of the efficiency function and the light output function. The pulse height spectra were analysed in cooperation with the Centre d'Etudes Nucleaires, de Fontenay-aux-Roses, France, employing a computer code as developed by Benezech [1975]; this code is based on principles published by Toms [1971].

The coefficients a and b in the light output relation are not uniquely defined for the whole range of proton energies and are system-dependent. Values for a and b were determined from calibrations with Compton electrons induced by ^{22}Na and ^{137}Cs gamma rays and from the "most likely" neutron energies for beams of 5 and 15 MeV neutrons, respectively. These "most likely" energy values were determined from calculated neutron energy spectra (presented in figure IV-6) as were derived for the relatively thick targets employed for the neutron production. For the calculation of these theoretical spectra, the accelerated ions were assumed to slow down continuously. Ranges of these ions in the targets were calculated by employing the empirical range formula published by Zaidins [1974], while range straggling was ignored. Neutron energy and production cross sections of the neutron producing reactions published by Liskien and Paulsen [1973] were used. Effects of scatter in the target assembly were also not taken into account.

The "most likely" energy of neutrons produced by the d-D reaction with an accelerating voltage of 2.3 MeV and a 3.0 mg cm^{-2} thick target was calculated by this method to be 5.3 MeV. For 15 MeV neutrons produced by the d-T reaction with deuterons impinging on a 2.2 mg cm^{-2} thick target, a "most likely" energy was determined to 14.8 MeV. This latter value

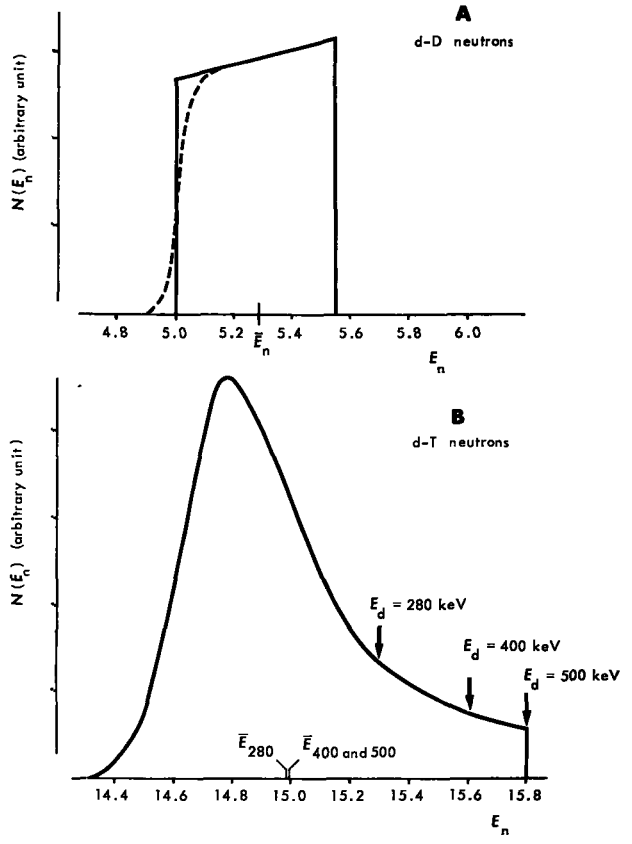

Fig. IV-6. Calculated neutron spectra for 5 and 15 MeV.

A. For the 5 MeV neutrons produced by 2.3 MeV deuterium ions on a 3.0 mg cm^{-2} thick titanium-deuterium target. The calculated mean neutron energy, $\bar{E}_n$, is 5.3 MeV.

B. For the 15 MeV neutrons produced by deuterium ions with energy, E_d, of 280, 400 and 500 keV, respectively, on a 2.2 mg cm^{-2} thick titanium-tritium target. The arrows indicate the maximum energy for the different energies of deuterium ions. Calculated mean neutron energies, $\bar{E}_n$, are indicated for the various deuterium energies.

corresponds to the energy at which the neutron production cross section is maximal. The mean neutron energies produced by the various accelerating voltages employed can be determined on the basis of this theoretical neutron flux density distribution. For deuterium ions of energies of 280, 400 and 500 keV, the calculated mean values are 14.86, 14.93 and 14.97 MeV, respectively. These differences can be neglected, as stated earlier. Employing

these values for the "likely" energies, the resulting values for the parameters a and b are, for 5 MeV neutrons, $a = 1.46 \times 10^{-1}$ and $b = 1.67$ and, for 15 MeV neutrons, $a = 1.16 \times 10^{-1}$ and $b = 1.60$.

Differential density distributions of the fluence obtained from measured distributions for 3, 5 and 15 MeV neutrons are presented in figure IV-7. In the measured region, it appears that the generated neutrons are reasonably monoenergetic and that a rather good similarity can be observed between the shapes of measured and calculated distributions for the 15 MeV neutrons. The lower limit of the spectra at around 2 MeV is set by imperfections in the discriminator circuit. In the measured energy distributions, the frequency is larger than zero for neutrons having energies in excess of the theoretical limits as a consequence of the resolution of the system. The resolution for ^{137}Cs gamma rays is determined by a comparison of a measured spectrum to a convolution distribution resulting from the theoretical Compton electron distribution with a Gaussian distribution. A good fit was obtained for a

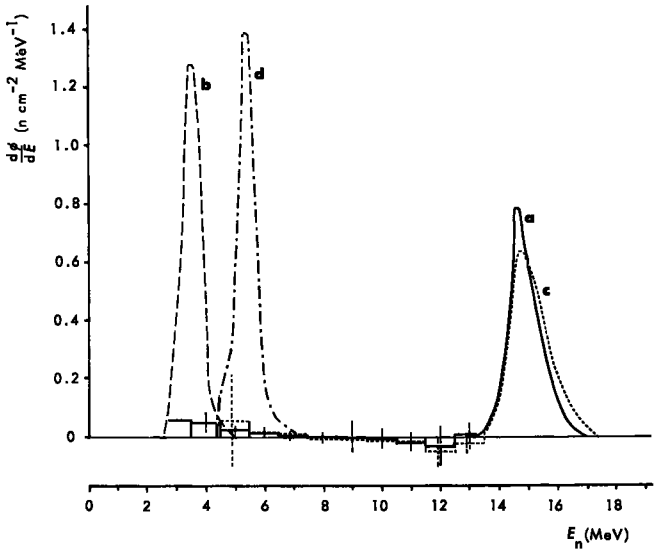

Fig. IV-7. Differential distributions of the fluence, $d\Phi/dE$, as a function of neutron energy, E_n. Curves **a** and **b** are for 15 and 3 MeV neutrons, respectively, produced with the AN-400 generator and are measured "free-in-air". Curves **c** and **d** are for 15 and 5.3 MeV collimated neutron beams produced with the K2N–3750 generator and are measured "free-in-air" behind the collimator in the center of the beam.

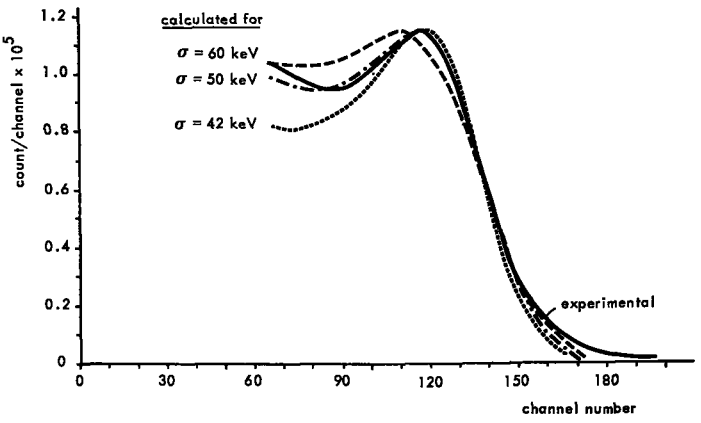

Fig. IV-8. Experimental and calculated Compton spectrum of ^{137}Cs gamma rays for the two inch NE-213 neutron scintillation detector. The calculated curves are the result of the convolution of the theoretical Compton-electron distribution for ^{137}Cs gamma rays and a normal distribution having a standard deviation, σ, of 42,50 and 60 keV, respectively, as is indicated.

Gaussian distribution having a standard deviation of 50 keV, as is demonstrated in figure IV-8.

Energy distributions for the (α,n) sources have been published by Pauw [1970]. The energy distributions of both sources are almost identical, because the energies of the alpha particles emitted by americium and polonium are nearly the same. The sources differ mainly in their relative gamma contributions.

CHAPTER V

DETERMINATION OF THE GAS GAIN CHARACTERISTICS OF THE PROPORTIONAL COUNTER

V-1 Introduction

The total net charge of a proportional counter pulse as induced at the anode can be expressed, according to the definition of the gas gain factor, as the product of the gas gain and the charge of the ions initially produced in the sensitive volume by an energy deposition event. Consequently, the gas gain can be determined from the measurement of both charges.

The gas gain is not a factor with a constant value; it is a function of the applied voltage, gas pressure and the starting point of the avalanche. The range of proportionality and, accordingly, the practical range as a detector for the measurement of energy deposition distributions, is determined by these gas gain characteristics.

A number of methods for the determination of the gas gain using monoenergetic x-rays or gamma rays have been reported in the literature [Kiser, 1960; Campion, 1968; Charles, 1972; Hendricks, 1973; Wolf, 1974]. The energy of these x or gamma rays must be totally absorbed in the gas, a condition which can hardly be fulfilled at low gas densities.

As an alternative method, alpha particles with a known energy loss per unit path length were used for the creation of the initial ion pairs. The ^{210}Po alpha particles which were employed enter the sensitive volume of the counter through the small holes with a diameter of 0.2 mm which are drilled in the counter wall. The alpha particles traverse the counter in a direction perpendicular to the central wire over a path length equal to a known chord length. The lengths of these chords are different for the various holes in the counter. Two Melinex absorbers were necessarily introduced into the path of the particles to enclose the counter and the source. These Melinex absorbers degrade the energy of the particles from the initial value to a lower value and this results in an increased energy loss per unit path length. Methods for the determination of this average energy loss per unit track length for the particles in the sensitive volume and the values derived were presented in chapter IV.

The mean energy deposited in the sensitive volume by the alpha particles is equal to the product of the pressure-dependent mean track length and the

mean energy loss per unit path length. The number of ion pairs initially produced by this energy deposition is equal to the amount of energy divided by a factor, W, which expresses the energy expended in the creation of one ion pair (chapter III).

The other quantity which is required for the calculation of the gas gain factor is the total charge induced by the counter pulse on the anode. This charge was determined, analogous to the methods reported in the literature, by comparison with the known charge of an unipolar voltage step pulse from a precision pulse generator which was fed into the test input of the preamplifier (see figure III-3). Because the proportional counter pulse and the calibration pulse differ markedly in shape, the attenuation introduced by the electronic time constants in the amplifiers will be different for both pulses. Consequently, a counter pulse and a calibration pulse of equal charge will induce pulses of unequal amplitude at the amplifier output. For the determination of the amounts of charge in the counter pulses at the preamplifier input from the amplitudes of corresponding pulses at the amplifier output, a correction factor for this difference in ballistic deficit between counter and calibration pulse must be applied [Breyer and Cimerman, 1971].

Calculations and measurements of W value and ballistic deficit, as necessary for the estimation of the gas gain factors of the detector, will be discussed in the next sections.

V-2 Average energy expended for the creation of one ion pair

In order to calculate the average number of ion pairs created in the counter volume by the energy deposited from a passing alpha particle, the average energy, W, expended in the formation of one ion pair must be known. W values of various gases, including the Rossi-Failla TE gas [Rossi and Failla, 1956], for different ionizing radiations have been reported [Myers, 1968; Booz, 1968; Leonard and Boring, 1973; Kemmochi, 1976]. However, for the Kastner TE gas mixture [Kastner et al., 1963] employed for the measurements of energy deposition distributions, which is composed of ethene, ethane, nitrogen and neon (see table III-1), no measured values have been reported. The TE gas mixture composed of ethene, ethane, nitrogen and neon used by Kemmochi deviates strongly from the standard gas mixture recommended by Kastner et al.; therefore, his reported W value cannot be applied.

The W_α value for the alpha particles was determined in an indirect way from a measured W_e value for electrons and a calculated ratio of the energies

expended in the formation of ion pairs by alpha particles and by electrons, respectively. W_e, the mean energy required by electrons to create one ion pair, was determined from a comparison of the ionization currents for various gases measured with a cavity ionization chamber which was exposed to gamma rays.

The energy deposited by the gamma rays in the gas of a cavity ionization chamber is the result of energy deposited by stopping and crossing electrons generated in the cavity wall and by starting electrons generated in the gas. For a small cavity (small with respect to the mean range of the electrons), the contribution of starters accounts for only a small negligible fraction of the total amount of absorbed energy, because of the large difference in density between wall and gas. Under this condition, the electron spectrum in the cavity is determined only by the energy of the gamma radiation and the composition of the cavity wall. On the basis of cavity-chamber theory [Burlin, 1968], it can be demonstrated that the ratio of ionization currents per unit mass for two gases in the same chamber can be expressed as:

$$\frac{J_2}{J_1} = \hat{s}_{1-2} \frac{W_1}{W_2} \tag{V-1}$$

where J_1 and J_2 are the ionizations per unit mass for the two gases indicated as 1 and 2, and $\hat{s}_{1-2}$ is the ratio of the mass stopping power, averaged over the electron spectrum, of gas number 1 and gas number 2.

Applying two "standard" gases with well known W values, it is evident that from equation (V-1) a mean ratio for the stopping power of both gases can be derived. According to the stopping power formula, this ratio depends only slightly on the electron energy. Consequently, it is possible to estimate from the ratio an effective energy for the electron spectrum in the cavity. This value of the effective energy was used for the calculation of the mass stopping power ratio of a "standard" gas and the TE gas for which W was to be determined.

Two spherical cavity ionization chambers of identical construction (outer diameter 23 mm and wall thickness 3 mm) with wall materials of A-150 TE plastic [Spokas, 1975; Smathers et al., 1977] and Magnox, respectively, were each exposed to ^{137}Cs gamma rays at a constant exposure rate. The chambers were flushed with argon and methane as "standard" gases and with two different TE gas mixtures of compositions according to Rossi-Failla and to Kastner. The purity grades of the "standard" gases argon and methane were more than 99.99 and 99.97 percent, respectively. The TE gases employed

were supplied in pressure bottles by l'Air Liquide Precigaz in premixed composition.

The stopping powers for the various gases were calculated by using the tabulated data published by Berger and Seltzer [1964]. Values for mixtures were obtained by employing the well-known sum rules. For the "standard" gases argon and methane, W values as summarized by Myers [1968] were applied.

The effective energy of the electron spectra in the cavity when calculated as described was 280 keV for the cavity chamber with Magnox wall and 300 keV for the chamber with A-150 TE plastic wall. Although these values for the effective energy do not differ significantly, the slight increase in the value derived for the TE wall in comparison to that for the Magnox wall may be attributed to the increasing contribution of the Compton effect with decreasing atomic number.

A review of the most important parameters which are employed in the calculations in combination with the resulting W values are presented in table V-1.

Table V-1. Review of parameters used for the determination of W_e and resulting W_α values for TE gases.

Gas	I_{adj} (eV)	ϱ (kg m^{-3})	W_e (eV/ip)	W_α/W_e	W_α(eV/ip)
Argon	210 (1)	1.784 (3)	26.2±0.2 (5)	1.004 (5)	
Methane	44.6 (1)	0.7168 (3)	27.3±0.2 (5)	1.066 (5)	
TE [Kastner]	70 (2)	1.138 (4)	26.7	1.04 (6)	27.8
TE [Rossi-Failla]	63 (2)	1.119 (4)	30.2	1.06 (6)	32.0

(1): Berger and Seltzer, 1964
(2): Calculated employing sum rule and data of (1)
(3): Handbook of Chemistry and Physics, 1964
(4): Calculated employing sum rule and data of (3)
(5): Myers, 1968
(6): Calculated employing sum rule and data of (5)

The W_e value of 30.2 eV/ip obtained for the Rossi-Failla gas is in good agreement with a value of 31.3±0.7 eV/ip for electrons produced by low energy x-rays as reported by Booz [1968] and values of 30.2±0.7 and 29.2±0.6 eV/ip as measured at the Armed Forces Radiobiology Institute [Leonard and Boring, 1973] for electrons produced by 250 kVp x-rays and ^{60}Co gamma rays, respectively. The W_e value of 26.7 eV/ip for the Kastner TE gas is in good agreement with a calculated W value of 26.1±0.4 eV/ip, using in the calculation a reduced W value of 26.1 eV/ip for neon gas in the

mixture instead of 36.2 eV/ip, which is valid for pure neon gas [Jesse and Sadauskis, 1952].

The uncertainties in the evaluation of W by this method are estimated to be about 3 percent; they are due to uncertainties in the quoted W values for the "standard" gases, which are of the order of 0.3 eV/ip, and to uncertainties in the stopping power ratios and the reproducibility of the electrometer readings. The uncertainties in the stopping power ratios are estimated to be about 1 percent, while the reproducibility of electrometer readings is better than 1 percent, as estimated from repeated measurements.

The ratio of W_α and W_e for the various gases reviewed in Myers table [1968] varies, without clear trends, between values of 0.98 for hydrogen sulfide and 1.20 for methylbromide. Calculated values of the ratio for the Rossi-Failla TE gas and the Kastner TE gas, using the data from the table mentioned, were 1.06 and 1.04, respectively. Values of W_α derived from these factors in combination with the corresponding values of W_e are 27.8 eV/ip for the neon TE gas and 32.0 eV/ip for the methane TE gas.

V-3 Attenuation of the counter pulses

As discussed above, the charge of the proportional counter pulse is proportional to the amount of energy absorbed per event. It is standard practice to calibrate the charge sensitivity of the input by means of pulses from a precision pulser fed to a test pulse input parallel to the main input of the amplifier. The shape of this calibration pulse approximates a step function, since the rise time is short compared to the time constants of the circuit. The attenuation of the unit step function in the amplifier having a doubly differentiating, doubly integrating network with equal time constants, τ, can be calculated from the relative response function, $f(t/\tau)$, by the formula:

$$f(t/\tau) = \left\{ \frac{(t/\tau)^2}{2} - \frac{(t/\tau)^3}{6} \right\} e^{-t/\tau} \qquad \text{(V-2)}$$

This function has a first maximum at $(t/\tau) = 3 - \sqrt{3}$, resulting in an attenuated value, f_s, for the unit step function of about 0.1306.

The time dependency of a proportional counter pulse can be expressed as discussed in chapter III by a function of the form $Q(t) = Q(0)C_c \ln(1 + t/t_0)$. This shape does not approximate a step function for practical values of the ratio, τ/t_0, of characteristic time constant of the amplifier and of the pulse. Consequently the counter pulse will be attenuated differently. Since the

attenuation for this log-pulse cannot be calculated analytically, various approaches have been used. Cutler et al. [1969] solved the problem by approximating the log-pulse by a generator pulse of the form $[1\text{-}\exp(-t/t_1)]$ and measuring the attenuation of this pulse. This method offers the possibility of measuring directly the attenuation of the total system, but, due to the poor approximation of the counter pulse by the suggested exponential pulse, the derived attenuation will not have the correct value. Others [Kemshall et al., 1969; Mathieson and Charles, 1969; Breyer and Cimerman, 1971; Hendricks, 1973] calculated the attenuation of the theoretical predicted counter pulse for different circuits from the single differentiation, single integration to single differentiation active filter integration combination having equal *RC*-time constants. Mathieson and Charles demonstrated that the attenuation of a counter pulse in the range $30 < \tau/t_0 < 800$ for a shaping network consisting of equal integrating and differentiating time constants can be described with considerable accuracy (≈ 0.1 percent) by a simple linear relationship. The normalised pulse height, f_m/C_c, was suggested to be written by the relation:

$$f_m/C_c = a' + b' \log \tau/t_0 \tag{V-3}$$

where C_c is the counter capacity per unit length given in formula (III-7); a' and b' are fitted parameters.

It was found that, for shaping networks consisting of single differentiation in combinations with double *RC* integration, fourfold *RC* integration or active filter integration, the attenuation calculated by Breyer and Cimerman can also be described by the same formula (V-3).

For an amplifier with double integration and double differentiation as used for our measurements of energy deposition distributions in order to minimize pulse pile-up, such data were not available and were calculated with a Data General Computer ECLIPSE-C/300 using a fast Fourier transformation program [Oostenbrug, 1976]. Values of f_m/C_c were calculated for three networks, namely, single differentiation plus single integration, single differentiation plus double integration and double differentiation plus double integration. The results of this computer analysis are presented in table V-2 and show excellent agreement with the results for the networks reported by Breyer and Cimermann [1971].

The normalised pulse height, f_m/C_c, for these three networks can also be described with identical accuracy, even for a larger range of $30 < \tau/t_0 < 2000$, by the linear relationship (V-3). The fitted parameters a' and b' of this function for the studied networks are given in table V-2.

Table V-2. Values of f_m/C_c as dependent on the ratio τ/t_0 and values of the fitted parameters a' and b' for *RC* networks of different compositions.

	RC networks		
τ/t_0	1×diff.+1×int.	1×diff.+2×int.	2×diff.+2×int.
80	1.669	1.330	0.572
90	1.702	1.331	0.585
100	1.745	1.356	0.592
200	1.945	1.527	0.673
300	2.076	1.630	0.723
400	2.172	1.704	0.758
500	2.247	1.762	0.785
600	2.309	1.810	0.808
700	2.362	1.850	0.827
800	2.408	1.885	0.844
900	2.449	1.916	0.859
1000	2.486	1.943	0.872
2000	2.731	2.136	0.942
a'	0.228	0.172	0.051
b'	0.752	0.591	0.272

For identical shaping networks, the values of the attenuation given by the various authors differ only slightly. These differences are probably due to differences in approximations of the continuous function for the pulse in the discrete Laplace transformation form.

From the attenuation of the step-pulse ($f_s = 0.1306$) and the attenuation function of the proportional counter pulse for the circuit used, it follows that the normalised correction factor, f/C_c, is given by:

$$f/C_c = f_m/f_s C_c = 0.391 + 2.083 \log \tau/t_0 \qquad \text{(V-4)}$$

The values of the constants are derived from the corresponding values of a' and b'.

For the measurements of energy deposition distributions (as discussed in chapter III-5), the value of the amplifier time constant, τ, was chosen to be 1.6 μs. The value of the other parameter, t_0, required for the calculation of the correction factor can be derived from formula (III-7) for the various counter conditions. The parameter ion mobility, μ_0, used in this formula was determined for the TE gas from the shape of the counter pulses according to the following method.

Amplified counter pulses generated by alpha particles crossing the sensitive volume of the counter (at an applied voltage of 1600 V and a gas pressure

of 101 kPa) were photographed from an oscilloscope display. The counter pulses were amplified for these measurements by a broadband low-gain amplifier, which modifies the pulse shape to only a negligibly small extent. The low amplifier gain necessitates the use of a high gas pressure in order to obtain pulses of acceptable amplitudes on the display unit. An additional advantage of the use of the high gas pressure in the counter is that straggling and the consequent gain variations are much smaller at this pressure. The measured amplitudes versus time curves were fitted to a theoretical curve as represented by formula (III-7). This yields a value for t_0 of 26 ns, which results in a value of $\mu_0 = 3.52\,\mathrm{NV^{-1}s^{-1}}$ and mobility $\mu = 35 \times 10^{-6}\mathrm{m^2V^{-1}s^{-1}}$ at atmospheric gas pressure of 101 KPa.

This latter value of μ is in reasonable agreement with a calculated value of $51 \times 10^{-6}\mathrm{m^2V^{-1}s^{-1}}$, based on values of the mobilities for neon and nitrogen of 500×10^{-6} and $127 \times 10^{-6}\mathrm{m^2V^{-1}s^{-1}}$ and using for ethene and ethane a mobility value of $34 \times 10^{-6}\mathrm{m^2V^{-1}s^{-1}}$ as is given for ethanol [Neuert, 1966] and utilizing the sum rule for their relative contributions. The lower experimental value of the mobility in comparison to the calculated value might be due to the effect of charge exchange between neon and the compound gases [Wilkinson, 1950].

Substituting for the TE gas the value of the mobility, $\mu_0 = 3.52\ \mathrm{NV^{-1}s^{-1}}$, in the formula for t_0 (III-7), combining this result with the calibration formula (V-4) and also using the value of the amplifier time constant, $\tau = 1.6\ \mu\mathrm{s}$, yields a correction formula:

$$f = 0.86 + 0.23 \log(V_a/p) \tag{V-5}$$

where V_a is the applied counter voltage and p is the counter gas pressure in pascal. A similar formula can be derived for the attenuation of proportional counter pulses produced in methane. Using a value for the mobility, $\mu_0 = 27.8\ \mathrm{NV^{-1}s^{-1}}$ [Neuert, 1966], this correction factor can be represented by the expression:

$$f = 1.06 + 0.23 \log(V_a/p) \tag{V-5a}$$

Results of the absolute gas gain, corrected for the differences in pulse attenuation according to the method described, will be presented in the next section.

V-4 Results of gas gain and counter resolution

Gas gain measurements were performed for the two counters of different

length flushed by neon TE gas and methane at various gas pressures in the range of 1.33 to 101 kPa and various applied voltages in ranges which were restricted due to sparking phenomena.

The alpha particles crossed the sensitive volume of the short counter with elongation factor 2 over trajectories of 3.9 and 4.7 mm, situated in the mid-plane perpendicular to the central wire. These trajectories permitted the measurement of gas gain for two different distances of the origin of the avalanche to the central anode wire.

The three alpha particle trajectories in the counter having an elongation factor 10 were 4.8, 4.9 and 4.9 mm and spread over the length of the sensitive volume. This permitted the study of possible variations in gas gain with the position of the avalanche along the length of the central wire.

The measured energy deposition distributions were fitted to corresponding theoretical energy loss distributions to correct for differences between average energy loss and the value of energy loss at the maximum of the distribution. Results for the gas gain of TE gas derived by the method described are presented in figure V-1. They demonstrate a significant difference in gas gain obtained for alpha particles crossing the sensitive volume over path lengths of 3.9 and 4.7 mm at gas pressures of 1.33 and 2.66 kPa. The origin of the differences will be discussed later. Similar results were derived when methane

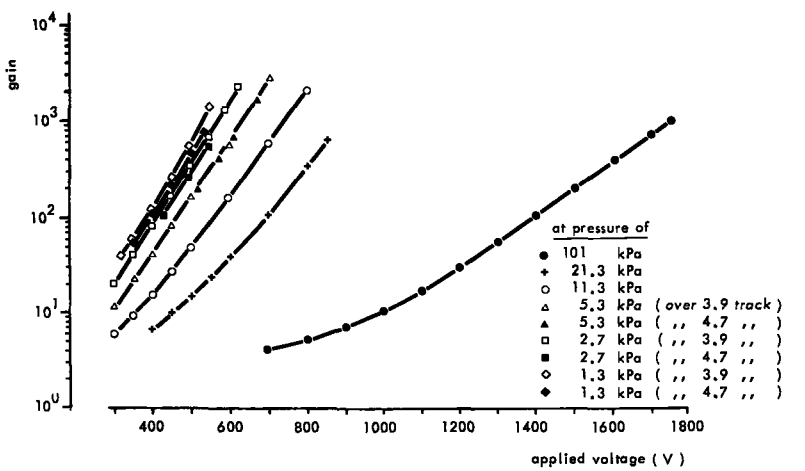

Fig. V-1. Gas gain as a function of applied voltage for the TE proportional counter at different gas pressure, *p*. At the gas pressures of 1.3, 2.7 and 5.3 kPa, the gain was measured for alpha particles passing the sensitive volume over the chord lengths of 3.9 and 4.7 mm, respectively.

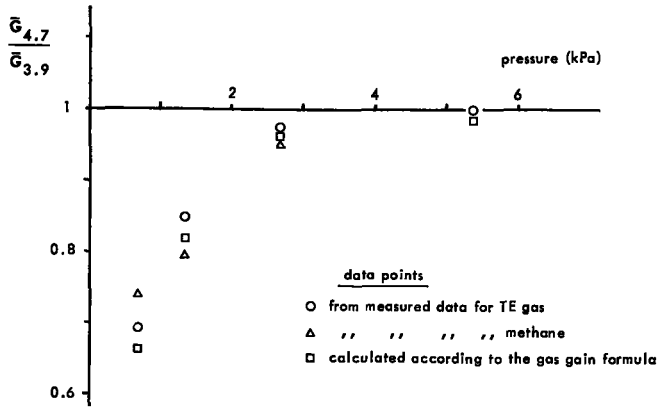

Fig. V-2. Ratio of the mean gain values, $\bar{G}_{4.7}$ and $\bar{G}_{3.9}$, for alpha particles passing the sensitive volume over a chord length of 4.7 and 3.9 mm, derived at different gas pressures. The experimental data points are derived from gain measurements for TE gas and methane. The theoretical values are calculated according to the gas gain formula (III-5).

was employed as the counting gas. This is demonstrated in figure V-2, which represents the ratio of the gas gain measured over chord lengths of 4.7 to 3.9 mm for both gases. It can be concluded from this figure that the decrease in gas gain as presented for the longer track length at low gas pressure is not dependent on gas composition and that the calculated values are in good agreement with the measured data.

Significant differences in the gas gain for longitudinally different positions have not been detected; the absolute values of the gas gain were, within experimental errors, in good agreement with those measured at a track length of 4.7 mm.

The validity of the theoretical expression for the gas gain as given in equation 5 of chapter III is demonstrated for a wide range of the ratio V_a/p, in figure V-3, where the derived data points are presented in comparison with the theoretical curve. The constants A and B of the theoretical expression were determined to be, for the neon TE mixture, $A = 10.7\ \mathrm{N^{-1}m}$ and $B = 185\ \mathrm{VN^{-1}m}$, and for methane, $A = 8.1\ \mathrm{N^{-1}m}$ and $B = 160\ \mathrm{VN^{-1}m}$. The value of A derived for methane is slightly higher than the values of 6.24 and 5.34–6.61 $\mathrm{N^{-1}m}$ reported, respectively, by Le Blanc and Devins [1960] and by Heylen [1963], whereas the value of B is in good agreement with the published data of Le Blanc and Devins and of Heylen of 149 and 145–158 $\mathrm{VN^{-1}m}$, respectively.

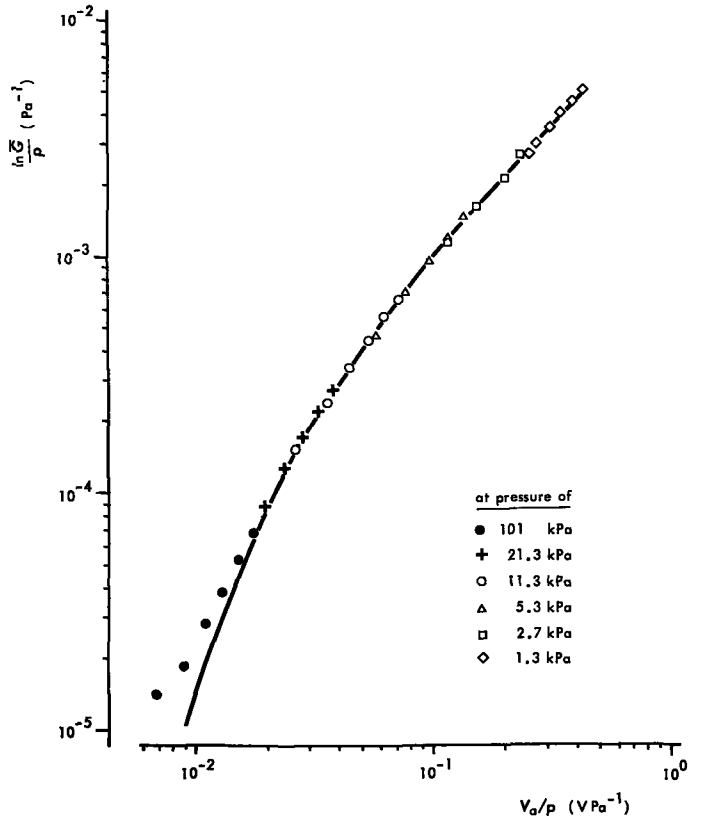

Fig. V-3. Characteristic curve for the gain parameter, $(\ln \bar{G})/p$, versus V_a/p. The solid line is a theoretical curve for $A = 10.7\ N^{-1}m$ and $B = 185\ VN^{-1}m$ (see formula III-5). The data points are derived from gain measurements performed at different pressures of the counter gas.

The measured differences in gas gain for the two chord lengths at lower gas pressures can be explained on the basis of the fact that, for these gas pressures, the second term of the theoretical expression for the gain cannot be neglected. This is demonstrated in figure V-4, where $(\ln G)/p$ is plotted as a function of the radial distance of the avalanche starting point in the TE counter at different values of V_a/p. The curves show that, for high values of V_a/p, the gain is strongly position-dependent and that, even for lower values of V_a/p, the gas gain varies for avalanches starting close to the central wire for these conditions. The physical significance of this effect is that the mean free path length for these conditions is relatively long in comparison to the distances

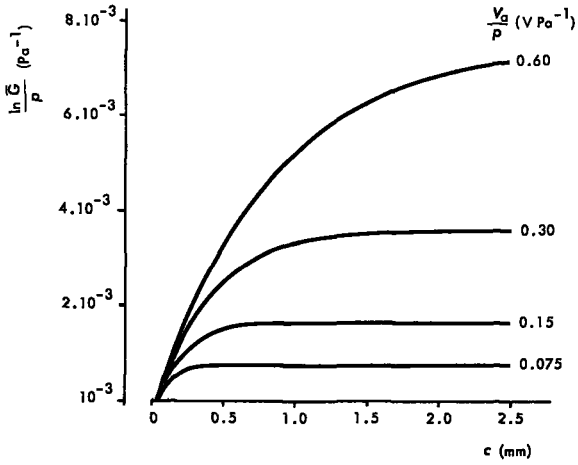

Fig. V-4. Characteristic gain parameter, $(\ln \bar{G})/p$, as a function of radial distance, c, of the avalanche starting point for different values of the parameter V_a/p.

between anode and site of origin of these avalanches and that, consequently, the ions do not cause a sufficient number of collisions to achieve full multiplication.

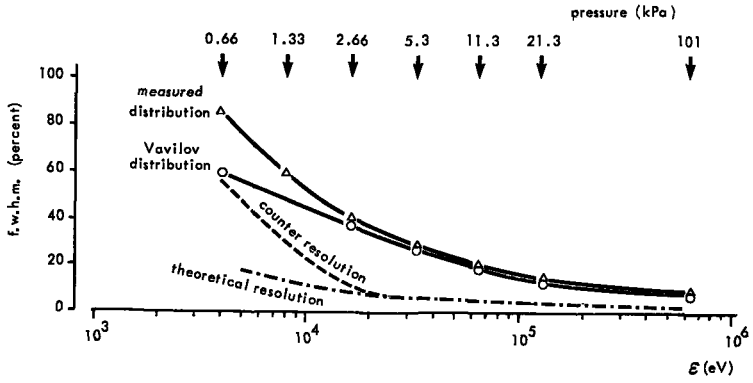

Fig. V-5. Measured and calculated curves of the full-width at half maximum, f.w.h.m. (in percentage of the maximum), determined from energy deposition distributions of the ^{210}Po alpha particles passing the sensitive volume of the TE counter. The curves are plotted as a function of deposited energy, ε, while corresponding gas pressures of the counter are indicated. The counter resolution is derived from the widths of the measured distribution and the Vavilov distribution. The curve of this counter resolution is compared to a theoretical curve as is given by formula (III-6).

The measured energy deposition distributions are composite distributions of a number of statistically independent variables such as energy deposition, track length, electronic gain and proportional counter gain. For the determination of the resolution of the proportional counter, it was assumed that the variance of the energy deposition distribution for the alpha particles is the sum of the variances of these contributions. The theoretical distributions of energy deposition by alpha particles were approximated by corresponding Vavilov distributions (chapter II), while the distributions of track length and electronic gain were calculated and measured.

The net result of the resolution, expressed as full-width at half maximum as a percentage of the maximum, are presented in comparison with a theoretical curve, f.w.h.m. (percent) $= 2.35\ C\varepsilon^{-\frac{1}{2}}$ (chapter III), in figure V-5. The factor 2.35 expresses the conversion from standard deviation to f.w.h.m. It can be seen that the measured resolution curve follows the theoretical curve reasonably well down to a pressure of 4 kPa and that the resolution loss increases more strongly than should be expected below this pressure.

V-5 Implications of the gas gain characteristics

From these results for gas gain and counter resolution, it can be concluded that the proportional counter does not function adequately below a gas pressure of 5 kPa, corresponding to a simulated volume of about 0.3 μm of unit density tissue. The starting point of the avalanche has significant influence below this pressure and will result in spectrum deterioration, especially for indirectly ionizing radiations which produce ionizations distributed at random over the volume. Similar effects as described here have been reported by others for counters of larger diameters; only the magnitude of simulated tissue volume for which deviations from "normal" gas gain behaviour are registered differ slightly [Srdoc and Kellerer, 1972; Campion, 1972].

The significance of this conclusion is that event size distributions for tissue volumes of dimensions less than 0.3 μm cannot be obtained from these physical measurements. As will be discussed in chapter VI, event size distributions for these small dimensions are of great interest for the interpretation of dose-effect relations in radiobiology. It would be of great importance if other detector types which do not have this inherent limitation could be developed.

CHAPTER VI

DETERMINATION OF CRITERIAL SITE DIMENSIONS FROM LINEAL ENERGY DISTRIBUTIONS

VI-1 Introduction

As mentioned in the general introduction (chapter I), the primary action of ionizing radiation in biological material results mainly from ionizations of the molecules of cell constituents. It is probable that these ionizations initially cause rupture of bonds and chemical changes in elementary critical structures of subcellular dimensions which will result in macroscopically observable changes at later stages. As will be justified later in this section, only biological effects from radiation on individual cells will be considered for the determination of the dimensions of these critical sites for the present investigations.

The probability that a given effect is induced at the cellular level will depend in a complex way on the absorbed dose. If only a single ionization is required for the induction, then at low doses the probability is proportional to the dose. However, if interaction between chemically changed molecules is required, the dose dependence of the probability of the final effect is to be described by quadratic or even more complex functions.

In addition to this dependence on the total number of ionized molecules, it can be expected that the density of the centres produced per cellular or subcellular volume will be of importance for the probability of interaction and hence for the frequency and degree of the final biological effects. These expected dependences on dose and lineal energy have been demonstrated in many studies on various biological test systems with ionizing radiation of different lineal energies.

A commonly used quantitative parameter for the effectiveness of a radiation type *a* is the relative biological effectiveness (r.b.e.). This r.b.e. is defined as the ratio of the dose of a standard radiation (medium energy x-rays produced by generating voltages of about 250–300 kVp) to the dose of radiation type *a* required for a specified endpoint to be induced by both types of radiation (see figure VI-1). The dependence of r.b.e. on ionization density has been used in various attempts to derive biophysical models of the mechanisms by which the final action is caused. These studies are of interest with respect to biological as well as to physical aspects. Biologically, because the model, together with the derived target candidate, can give a better

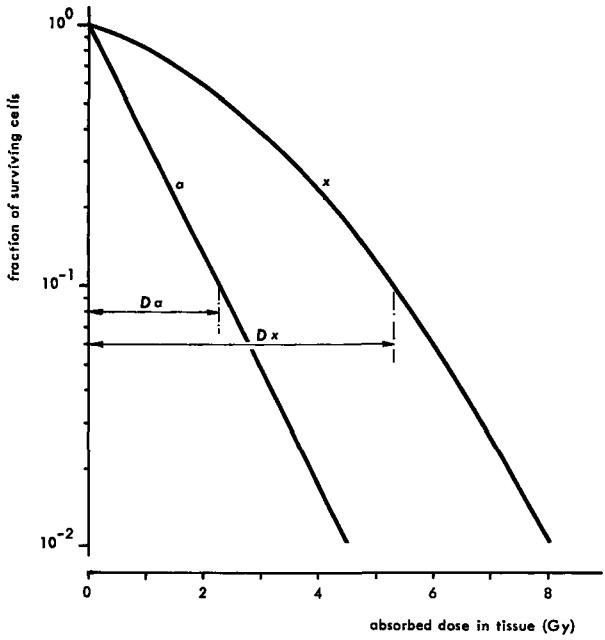

Fig. VI-1. Reduction in the colony forming capacity of cultured cells by radiation, presented as the fraction of surviving cells, as function of the dose.
Curve x is an example of a survival curve as commonly derived for x-rays; curve a is an exponential curve as will be generally observed for heavy charged particle irradiation. The r.b.e. of radiation type a for a defined endpoint (in this figure, as an example for 10 percent survival), is defined as the ratio of the dose D_x to D_a in the radiation types x and a; where x is the standard radiation type.

understanding of the mechanisms involved in the radiation action and can offer suggestions for additional research. From the physical point of view, the size of the target determines the ultimate dimensions of the volumes for which event size distributions must be derived either by measurements or by calculations. These latter aspects are of particular interest in the scope of this thesis.

For a quantitative analysis of the r.b.e. in relation to energy deposition distributions, the best approach is provided by investigations on the most simple experimental systems. Energy deposition by indirect ionizing radiation is always characterized by wide distributions of specific energy and this makes the interpretation of radiobiological data in terms of microdosimetric quantities needlessly complex. Therefore, with regard to physical aspects, many complicating factors are reduced or eliminated if monoenergetic direct-

ly ionizing particles are used under conditions in which the biological objects are traversed by a short portion of the particle track [Zirkle, 1954]. Under this condition, the amount of energy deposited during passage is small compared to the initial energy of the particle, while the energy deposition distributions will be relatively narrow.

With respect to the biological systems, it is important to employ the most simple one for which a distinct dependence of the r.b.e. on ionization density has been observed. For the inactivation of simple systems such as phages or enzymes, the r.b.e. depends only to a small extent on the l.e.t.; consequently, the more complex single cell systems must be employed. The response of a multicellular system will be too complicated due to interactions between damaged and unaffected cells in the population.

In a series of experiments performed during the past two decades, the track segment method has been employed for the measurement of reproductive death of cultured mammalian cells after irradiation by charged particles of various energies [Barendsen et al., 1960; Barendsen et al., 1963; Barendsen, 1964; Todd, 1967]. Barendsen has previously made attempts [1964 and 1967] to analyze his data in terms of a hypothesis in which it was assumed that a minimum number of primary molecular lesions within a restricted distance is required for the impairment of the clonogenic capacity. With the limited data available for the energy deposition distributions, he arrived at the conclusion that between 10 and 15 ionizations are required within a distance of about 7 to 10 nm. In this chapter, measured and calculated energy distributions will be reported and these distributions will be employed in an analysis of Barendsen's experimental data on the basis of an essentially identical hypothesis.

VI-2 Measurement of energy deposition distributions of alpha particles

Energy deposition distributions for alpha particles from ^{210}Po were measured with the TE proportional counter at energies and under conditions comparable to those for which the survival curves for cultured cells of human kidney origin were obtained [Barendsen and Beusker, 1960]. Entry into and passage through the sensitive volume of the counter by the alpha particles and the change in their energy was achieved as described in chapter IV-1. The length of the particle track in the sensitive volume for which the energy loss distributions were measured corresponded to 5.6, 1.2, 0.63, 0.3, 0.15 and 0.075 μm of unit density tissue.

These various simulated track lengths were attained, as discussed in chap-

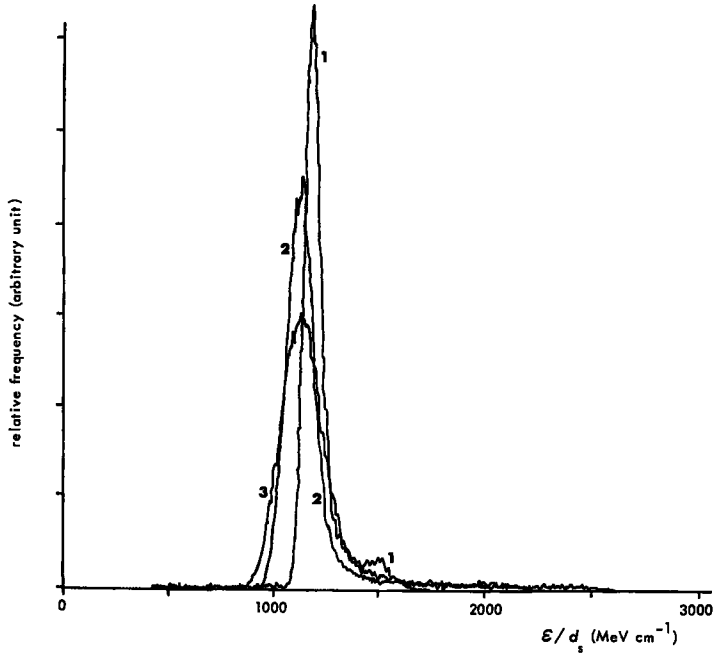

Fig. VI-2. Energy loss, ε, distributions of ^{210}Po alpha particles with a mean l.e.t. of 1100 MeV cm^{-1}, measured for different simulated diameters, d_s.
Curves 1,2 and 3 correspond to distributions measured for values of d_s equal to 5.6, 1.2 and 0.63 μm of unit density tissue, respectively. The different distributions are presented as a function of their lineal energy, ε/d_s.

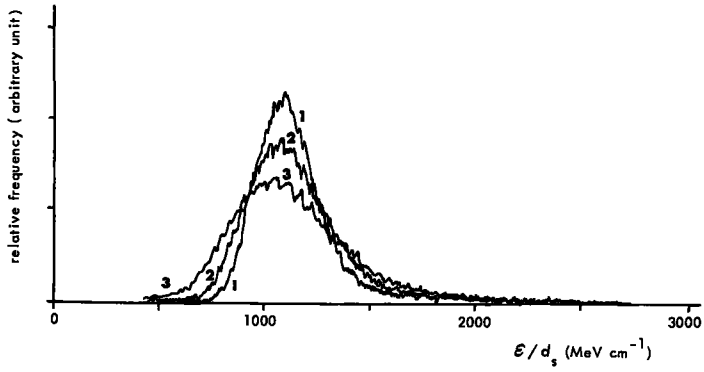

Fig. VI-3. Energy loss, ε, distributions of ^{210}Po alpha particles having a mean l.e.t. of 1100 MeV cm^{-1}, measured for different simulated diameters, d_s.
Curves 1, 2 and 3 correspond to distributions measured for values of d_s equal to 0.30, 0.15 and 0.75 μm, respectively. The different distributions are presented as a function of their lineal energy, ε/d_s.

ter III-2, by reduction of the counter gas pressure. Gas multiplication factors employed were in the range of 500 to 1000, in order to satisfy sensitivity as well as proportionality requirements (for high gain factors the proportionality is affected by space-charge effects).

Measured distributions of energy loss, ε, for alpha particles with a l.e.t. of 1100 MeV cm^{-1} at different simulated diameters, d_s, are presented in figures VI-2 and VI-3. The frequency distributions are plotted as a function of the

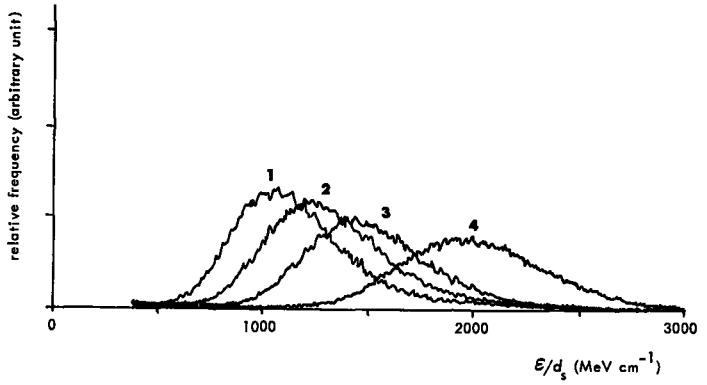

Fig. VI-4. Energy loss, ε, distributions at a simulated diameter, d_s, of 0.15 μm for ^{210}Po alpha particles, which, after passage through various numbers of absorbers, have different l.e.t. values. Curves 1, 2, 3 and 4 correspond to distributions at l.e.t. values of 1100, 1260, 1480 and 2000 MeV cm^{-1} in tissue of unit density.

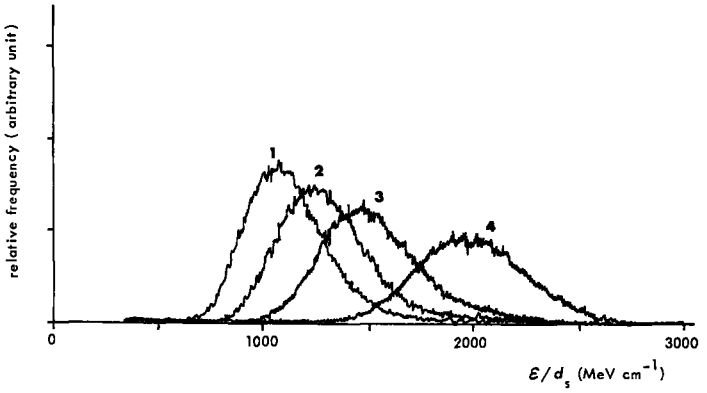

Fig. VI-5. Energy loss ε, distributions at a simulated diameter, d_s, of 0.075 μm for ^{210}Po alpha particles, which, after passage through various numbers of absorbers, have different l.e.t. values. Curves 1, 2, 3 and 4 correspond to distributions at l.e.t. values of 1100, 1260, 1480 and 2000 MeV cm^{-1} in tissue of unit density.

lineal energy, ε/d_s. These results clearly demonstrate the widening of the distributions with decreasing track lengths, as predicted from theoretical distributions. The small but significant contribution at the lineal value of 1500 MeV cm^{-1} manifest at $d_s = 5.6$ μm might be attributed to contamination of the incident spectrum with alpha particles of energies around 0.8 MeV, which are completely stopped in the sensitive volume.

Energy loss distributions for alpha particles with an average energy loss per unit path length of 1100, 1260, 1480 and 2000 MeV cm^{-1} over track lengths of 0.15 and 0.075 μm are presented in figures VI-4 and VI-5, respectively. These figures show similar changes in the various spectra with decreasing size of the simulated volume as demonstrated in the foregoing figures.

A comparison between the measured distribution for alpha particles with an average energy loss per unit path length of 1100 MeV cm^{-1} and the corresponding calculated distributions for a simulated diameter of 0.075 μm is presented in figure VI-6. The measured distribution is not corrected for additional loss in resolution induced by variation in the gas gain and by variation in the electronic gain of the amplifiers resulting from noise and for geometrical resolution loss. The values of the f.w.h.m. as a percentage of

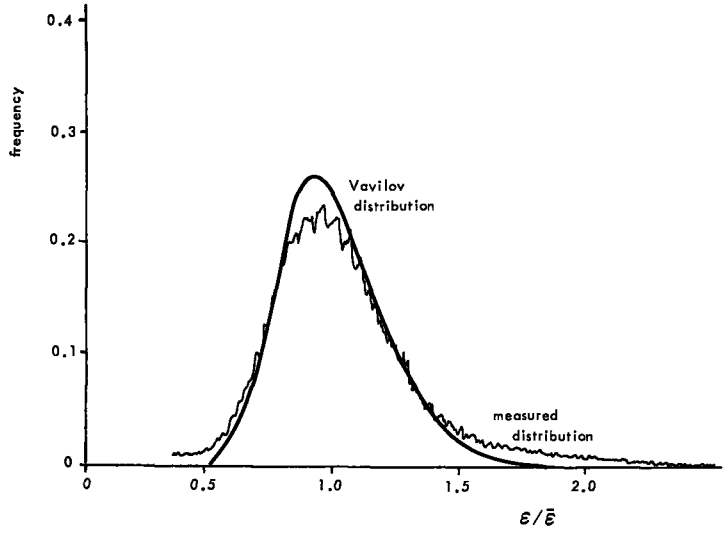

Fig. VI-6. Measured and theoretical energy loss, ε, distributions (at a simulated diameter of 0.075 μm) for alpha particles having a mean energy loss, $\bar{\varepsilon}$, per unit path length in unit density tissue of 1100 cm^{-1}.

the mean for these three resolution loss contributions are 26, 10 and 6 percent, respectively. This results in a total loss of resolution for the measured spectrum with respect to the actual distribution of about 29 percent. According to the Blunck-Leisegang theory (chapter II-4), a correction must be applied to the Vavilov distribution in order to obtain the correct energy loss distribution. For the conditions employed for the measurement of the spectrum, the value for the correction is 31 percent. This value is not significantly different from the value of the resolution loss of 29 percent. The good fit which is found between the corrected Vavilov distribution and the measured distribution is therefore fortuitous. This finding is in agreement with the conclusion of Chechin and Ermilova (chapter II-4) that the Blunck-Leisegang corrected distribution overestimates the effect of straggling. Because of the fact that the loss in resolution is almost equal to the theoretical correction factor, it can be concluded that the uncorrected Vavilov distributions can be used as a good first approximation for energy deposition distributions of heavy charged particles at very small track lengths and for which no measured data are available.

VI-3 Measurement of energy deposition distributions of protons

The polonium alpha particles permitted only measurements of energy deposition distributions with an average value of 1100 MeV cm^{-1} or more. For a comparison of the relation between the biological effectiveness of alpha particles and their energy deposition distributions, it is of interest to obtain equivalent distributions in the l.e.t. range of 100 to 1000 MeV cm^{-1}.

Energy loss and energy loss distributions of alpha particles can, on a theoretical basis (chapter II), be simulated by protons having a mass corrected equivalent energy. Based on this idea, energy loss distributions were measured for protons in the required range.

The protons generated by the 3 MeV Van de Graaff generator (see chapter IV-2) were introduced into the sensitive volume in the same manner as described for the alpha particles. The energy of the protons, accelerated to initial energies of 1.5 and 3.0 MeV, was varied by introducing different numbers of absorbers in their path between generator and counter. Energy loss distributions for these protons after passage through various numbers of energy modifying absorbers were measured at a simulated diameter of 0.3 μm. The results are presented in figures VI-7 and VI-8. Each set of distributions was measured for equal fluxes of charged particles.

Analogous spectra [Hogeweg et al., 1973] were measured for a simulated

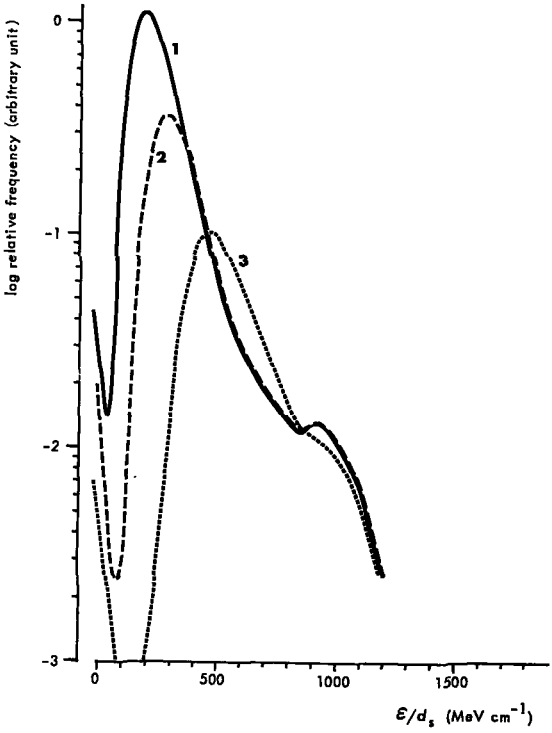

Fig. VI-7. Energy loss, ε, distributions (at a simulated diameter, d_s, of 0.3 μm unit density tissue) for 1.5 MeV protons which, after passage through various numbers of absorbers, have different l.e.t. values. Curves 1, 2 and 3 correspond to distributions at l.e.t. values of 280, 370 and 610 MeV cm^{-1}.

diameter of 0.15 μm. The measured distributions for the 1.5 MeV as well as for the 3 MeV protons are much wider than the corresponding Blunck-Leisegang corrected Vavilov distributions. In the bimodal distributions measured for protons with initial energies of 1.5 MeV, the small but significant contribution with a peak at 1000 MeV cm^{-1} is probably due to low energy protons having energies corresponding to the peak region in the stopping power curve (see figure II-2). Since these contributions of low energy protons appear to be independent of the pressure of the counter gas and the number of energy modifying absorbers, they are likely to have resulted from neutrons produced by the accelerated protons in interactions with the beam pipe assembly. Because of these complicating experimental factors, the proton experiments were not extended to other conditions and the required energy

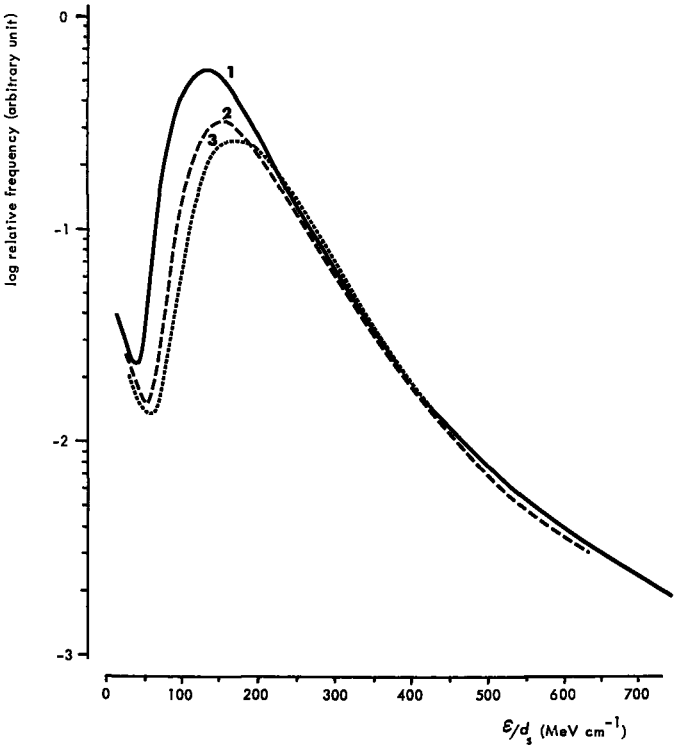

Fig. VI-8. Energy loss, ε, distributions (at a simulated diameter, d_s, of 0.3 μm unit density tissue) for 3 MeV protons which, after passage through various numbers of absorbers, have different l.e.t. values. Curves 1, 2 and 3 correspond to distributions at l.e.t. values of 130, 160 and 180 MeV cm^{-1}.

deposition spectra for the interpretation of biological effectiveness were calculated on the basis of the Vavilov distributions.

With these experimental and theoretical data on energy depositions, an attempt will be made to interpret r.b.e. versus l.e.t. relations for induction of cell reproductive death in mammalian cells of human kidney origin.

VI-4 Survival of cells following ionizing radiation

Before analysis of the dependence of r.b.e. on the energy deposition spectra, a brief discussion of cellular survival and derived parameters will be presented.

In radiobiological studies, the criterion "survival of cultured mammalian

cells" is generally connected with the capacity of vital nonresting cells to proliferate indefinitely. This reproductice capacity can be measured by the cloning technique introduced by Puck and his colleagues [1956], in which single cells are plated. By selection of suitable environmental conditions, these cells are stimulated to grow into an observable colony during a selected time interval. The fraction of cells capable of growing into colonies after treatment compared to nontreated controls is used as a measure for the criterion of reproductive death of these cells. In irradiated cultures, this fraction of cells developing into clones decreases with increasing dose. This effect is of obvious importance for cancer radiotherapy research, because the aim of this therapy is to destroy the proliferative capacity of all cancer cells.

The fraction of surviving cells can be determined with sufficient accuracy in a range down to about 10^{-4}. Because of this wide range of surviving fraction, it is customary to plot the surviving fraction on a logarithmic scale versus dose on a linear scale. The shape of such survival curves are found to vary, depending on synchrony of the cells, types of radiation and environmental conditions for a given cell line. According to their shape, survival curves are classified as exponential and nonexponential curves. Survival curves with an exponential shape are obtained for densely ionizing radiation, e.g., charged heavy particles, while nonexponential curves are usually obtained for sparsely ionizing radiations. Both types of curves, presented schematically in figure VI-1, have been explained on the basis of the theory that there are certain "targets" or combinations of targets which are essential for the reproductive function. It can be demonstrated [Fowler, 1964], that the general form of the curves describing the relative survival, S, after a dose, D, of a sample of identical individuals having m targets each requiring a minimum of n hits before the individual is inactivated, is given by:

$$S = 1-(1-B)^m$$

where

$$B = e^{-x}\left(1+x+\frac{x^2}{2!}+\ldots.+\frac{x^{n-1}}{(n-1)!}\right) \qquad \text{(VI-1)}$$

and

$$x = D/D_0$$

D_0 represents the dose required to give an average of one "hit" per site. Not involved in this general formulation is the possibility of repair of sublethally damaged target sites with time, a situation frequently occurring with sparsely ionizing radiations [Todd, 1968; Elkind and Sutton, 1960].

The exponential survival curve appears as a special case of this general formula for $m = 1$ and $n = 1$; consequently, these curves are usually designated as "one-hit" curves. The terminology of "one-hit" is, however, somewhat ambiguous, being used in different ways as either "energy absorption event" or "excitation or ionization" and this may lead to erroneous simplifications of the mechanisms involved. The concept of "one-hit and one-target" must be viewed from a less restricted mathematical-physical point without any direct biochemical connection. In order to avoid this confusion, Gray therefore suggested the use of the word "monotopic" [Gray, 1951].

Experimental survival curves of cultured mammalian cells of human kidney origin for irradiations with heavy charged particles, as measured by Barendsen and co-workers [1960, 1963, 1964], are indistinguishable from exponential monotopic curves over a significant range of doses. These survival data will be used to determine the dimensions of the critical elements for these cells.

VI-5 The hypothesis of monotopic action and derivation of the cross-section of the critical assembly

In the theory of monotopic action, interference with the proliferative capacity of mammalian cells by irradiations with charged particles is explained by the assumption that, for reproductive death of cells, inactivation of one critical element from a relatively large set of such elements is required. The onset of the inactivation process of a critical element, which may involve a series of steps after initiation, will occur only when the amount of energy deposited in the element per traversal of a particle exceeds a certain threshold level.

It should be stressed again that this interpretation of exponential survival curves does not imply that the loss of reproductive capacity is due to a single type of inactivation event in a single type of site or structure.

The hypothesis is supported by the observations of Pollard and co-workers [Pollard and Tilburg, 1972; Pollard and Kraus, 1973] that, in sensitive strains of *Escherichia Coli* B, the DNA degradation occurs in an "all-or-nothing" fashion.

In mathematical formulation, the inactivation, I, can be presented as:

$$I = \begin{cases} 0 \text{ for } \varepsilon < E_0\text{: no inactivation; the cell retains its capacity for unlimited proliferation} \\ 1 \text{ for } \varepsilon \geqslant E_0\text{: inactivation; the cell is killed} \end{cases} \quad \text{(VI-2)}$$

where ε is the energy deposited in the volume of the critical element and E_0 the threshold energy for inactivation of the proliferative capacity.

On the basis of this hypothetical model, both the cross-section of the volume comprising the set of critical elements and the mean size of these critical elements can be derived from the D_0 values of the survival curves employing a statistical method discussed hereafter.

The absorbed dose, D, given to the cells which are irradiated in conditions according to the track segment method, can be calculated from the energy loss per unit path length, $\mathrm{d}E/\mathrm{d}x$, and the flux, F, by the formula:

$$D = 1.6F\,\mathrm{d}E/\mathrm{d}x \qquad \text{(VI-3)}$$

where the dose is given in gray, $\mathrm{d}E/\mathrm{d}x$ in MeV cm^{-1} and the flux in particles per cm^2. Employing this expression, Barendsen calculated from the D_0

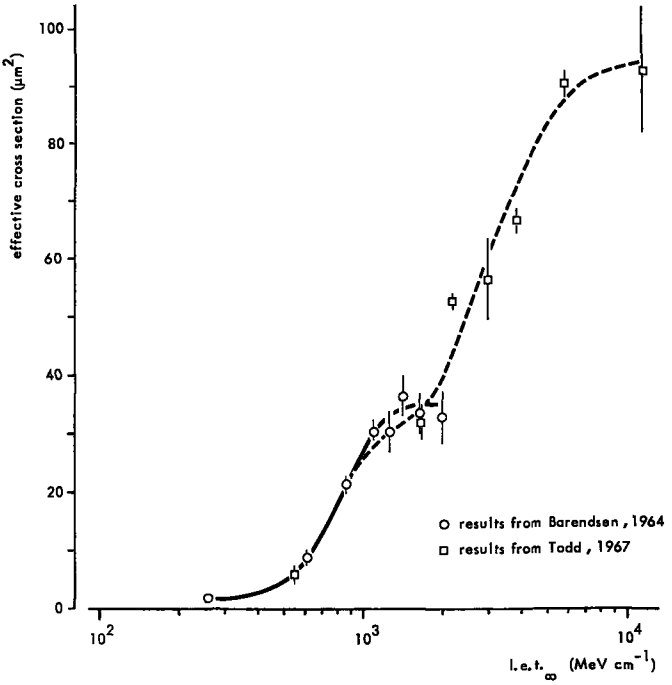

Fig. VI-9. Effective cross section of human kidney (T-1) cells irradiated and assayed *in vitro* after exposure to heavy charged particles of different l.e.t.$_\infty$. Data points are from results published by Barendsen [1964] and Todd [1967]. The bars indicate standard errors.

values of the various survival curves an average flux, F_0, at which one effective particle passes through one of the set of critical elements. The inverse value of this flux (expressed as an effective cross-section, σ) represents a probability factor for impairment of the clonogenic capacity by the various radiations. His results on the effective cross-section are presented in figure VI-9. The asymptotic characteristics of this probability curve at high l.e.t. values reflects the excess killing capacity of particles passing through the set of critical elements with l.e.t. values larger than 2000 MeV cm^{-1}. It is most likely that the limiting value of about 35 μm^2 corresponds to the average value for the area of the projective of the sets of critical elements.

Values for the effective cross-sections derived from survival curves for the same cell line irradiated with heavy ions, as measured by Todd [1967], are also presented in figure VI-9. The shape of this curve shows identical characteristics; however, the asymptotic value of the cross section approaches a much higher value of about 100 μm^2. This higher value is unlikely to be due to differences in the cells employed by Barendsen and Todd, since they are of the same origin. It more likely results from the larger effective track width [Katz et al., 1971] as illustrated by figure VI-10.

Different particles of the same l.e.t. do not necessarily have equal energy distributions of secondary particles. Because of this, the track width determined by the spatial distribution of energy deposited around the path can differ markedly for particles with the same l.e.t. Scanning of a set of critical

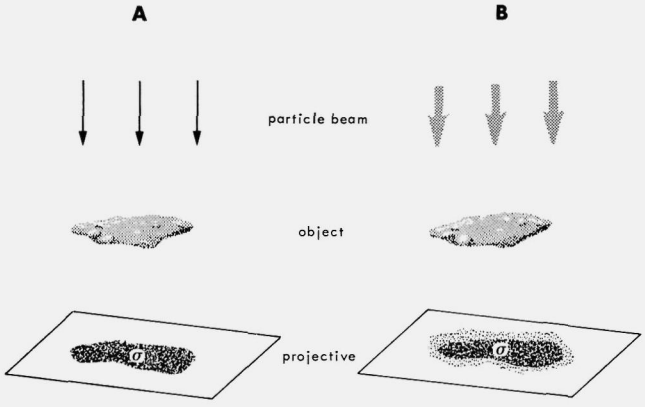

Fig. VI-10. Schematic representation of the effective cross-section, σ, as derived from an object scanned with:
A. a beam of particles with negligible contributions of δ-rays,
B. as derived for a beam of particles having a track width due to the δ-ray contributions.

elements with a beam of optimally killing particles, each having negligibly small track width, will yield the projective area or cross section of the set. On the other hand, it is evident that a scan with particles of nonneglectable track width will yield a value equal to the cross-section of the set enlarged with a shell having a thickness equal to the track width of the particles used.

VI-6 Derivation of the size of the critical element

The shape of the curve relating the effective cross-section for loss of reproductive capacity to the energy loss per unit path length, as given in figure VI-9, is analogous to the general type of dosage-mortality curves. These curves can be derived from a convolution of a step function representing an inactivation process and a distribution function which expresses the variation in onset of the inactivation process. Based on similar ideas, the effective cross-section curve can explained as resulting from the folding of the inactivation function (VI-2) describing the biological inactivation process for

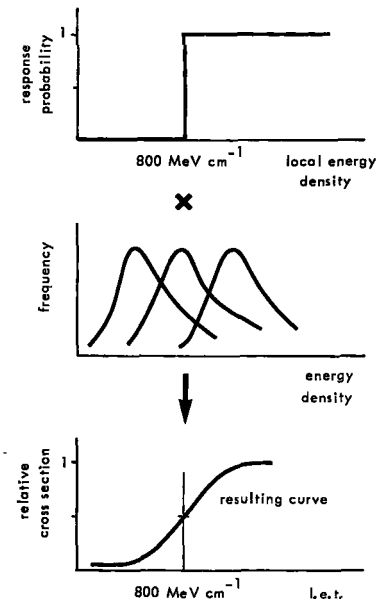

Fig. VI-11. Schematic representation of the "monotopic" action hypothesis. The relative cross-section for mammalian cells, as derived from irradiations with heavy charged particles, is supposed to be the result of a convolution of the step function for the inactivation probability with the local energy distributions of particles of the different energies.

reproductive death, with the distribution functions for the energy loss being the determinant physical quantity for this inactivation process. This idea is schematically illustrated in figure VI-11.

The curve of figure VI-11 indicates that, for particles passing through the sensitive elements with an energy loss per unit path length of 800 MeV cm^{-1}, only half of the particles passing through the critical volume is effective. On the basis of the hypothesis mentioned, this is a consequence of the fact that in 50 percent of the passages insufficient energy is deposited along the particle track within the elementary critical volume to cause the transition required for inactivation.

From the effective cross-section curve for alpha particles in figure VI-9, it is possible to further deduce that about 15 percent of the passages of particles with l.e.t. of 1100 MeV cm^{-1} are still ineffective in producing the biological effect. According to the assumptions of the hypothesis, this is due to the fact that an insufficient amount of energy is deposited within the critical element in 15 percent of the particle traversals. From the energy distributions for various track lengths, presented in figures VI-1 and VI-2, it can be further deduced that this 15 percent of ineffective traversals cannot be explained on the basis of the distribution functions for critical track lengths in the range of 5.6 to 0.15 μm. The energy distributions in this range show that ε/d_s is larger than 800 MeV cm^{-1} in more than 99 percent of the alpha traversals and consequently only about 1 percent of the passages would be expected to be ineffective. These distributions show that, even for a critical length of 0.075 μm, only about 6 percent of the traversals can be expected to be ineffective, as is shown in figure VI-12. This value of 6 percent ineffectiveness in comparison to the required 15 percent indicates that the size of the critical element is smaller than 0.075 μm.

The biological effective cross-section curve extends to l.e.t. values of less than 1100 MeV cm^{-1}, a range for which it was not possible to determine adequate experimental energy loss distributions. Since it was demonstrated in section 3 that the Vavilov distributions are good approximations for the energy loss distributions, calculations of the effective cross-section using these theoretical distributions at $d_s = 0.075$ μm were performed for dE/dx values less than 1100 MeV cm^{-1}. These results are presented in figure VI-12. The calculated curve for $d_s = 0.075$ μm is clearly much steeper than the curve derived from the biological data, supporting the conclusion that the size of the critical elements is smaller than this value of d_s. It is furthermore of interest that the points derived from the measured energy deposition distributions are in good agreement with the calculated spectra.

Further calculations were performed on the theoretical distributions for a critical distance of 0.02 μm and a lower threshold, E_0 of 1300 eV. These results, also presented in figure VI-12, show a very close approximation to the biological curve. It can be concluded from this agreement that the critical elements must have sizes of the order of 20 nm.

The preceeding analysis of relative effectiveness per particle for reproductive death was based on experimental results from irradiations performed in equilibrium with air. Similar experiments have been reported for irradiations under anoxic conditions [Barendsen and Walter, 1964; Barendsen et al., 1966]. The derived curve for the relative effectiveness shows a similar shape as those for aerated conditions, with a translation towards higher values of the energy loss per unit path length. Identical calculations as per-

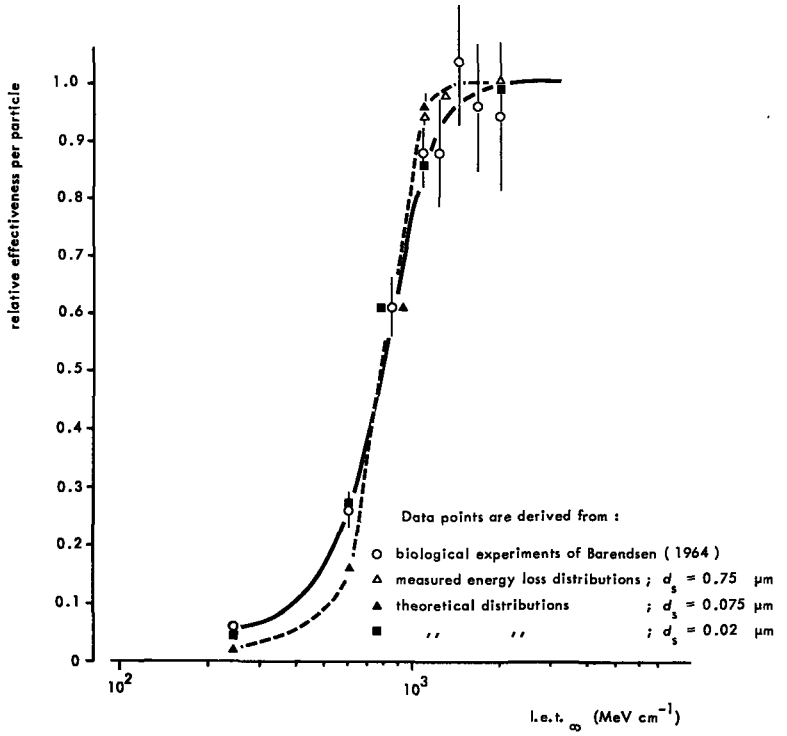

Fig. VI-12. Relative effectiveness per particle for inhibition of clone formation of cultured human kidney (T-1) cells in equilibrium with air for irradiations with particles of different l.e.t. The data points are derived from results of biological experiments [Barendsen, 1964] and from measured and theoretical energy loss distributions for different simulated diameters, d_s.

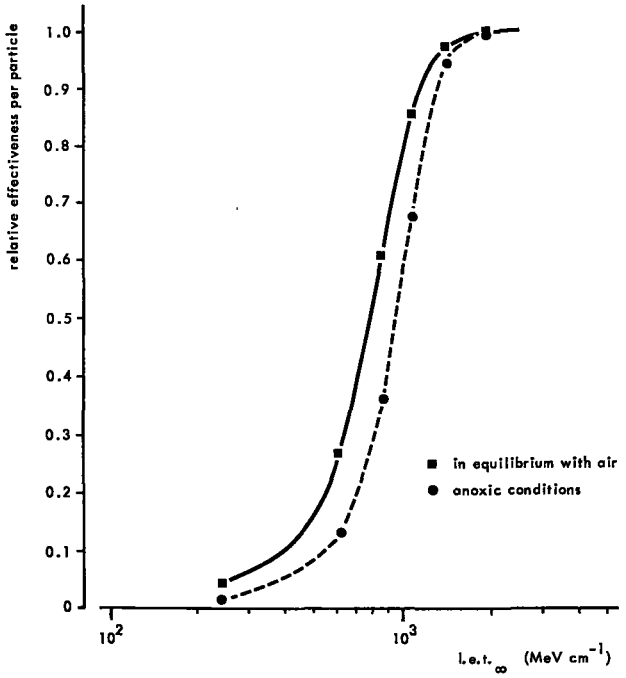

Fig. VI-13. Relative effectiveness per particle for inhibition of clone formation by cultured human kidney cells (T-1) for alpha particle irradiations in equilibrium with air and irradiations under anoxic conditions. Solid and dotted curves represent data from biological experiments [Barendsen, 1964 and 1966]. The data points represent values, calculated on the basis of the hypothesis of "monotopic" action, for a critical distance of 0.02 μm for cells under equilibrium with air and anoxic conditions.

formed for the conditions of air equilibrium have been carried out for these results obtained under anoxic conditions. The shift of the value of 50 percent effectiveness from 800 MeV cm^{-1} valid for aerated conditions to a value of 960 MeV cm^{-1} for the anoxic situation was accounted for by changing the value of the energy threshold from 1300 to 1600 eV. The results of these calculations for the anoxic situation together with the preceding results for the equilibrium conditions in comparison to the biological curves are presented in figure VI-13. This figure shows that both calculated curves fit very well to the biological data, supporting the conclusion that the value for the critical size is of the order of 20 nm.

VI-7 Discussion of the results

The value of about 20 nm derived for the dimension of the critical elements is in strong contrast to values ranging from 0.15 to 3 μm derived on the basis of their hypothesis of dual radiation action by Rossi and Kellerer [1972] for a number of biological systems. The biological systems and endpoints taken from various authors and employed in their analysis were rather complex, such as, for instance, opacification of the murine lens, mammary neoplasma and skin damage. The discrepancy in size is understandable on the basis of the fact that their results were derived from the slopes of the dose-r.b.e. functions for neutrons for these various systems. As mentioned in the introduction of this chapter, neutrons as well as the usually employed x-rays as "standard" radiation have restrictions, because of their spatially scattered interaction sites and the large variation in types of secondary particles and in amounts of

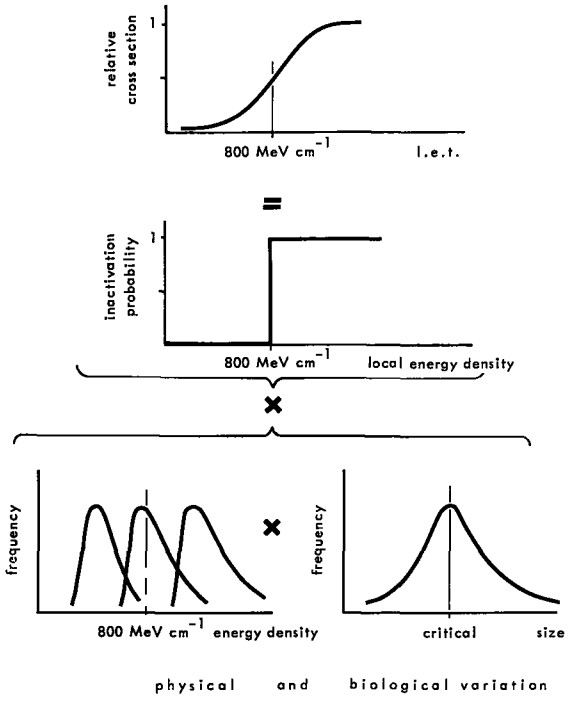

Fig. VI-14. Schematic representation of the "monotopic" action with contributions from biological as well as physical variations. The deconvoluted function, from relative cross-section and inactivation probability, is assumed to result from both variations.

energy imparted. Apart from these complicating physical factors, cellular survival as measured for these radiations is complicated by accumulation and repair of sublethal effects, as demonstrated in fractionated and low dose rate studies [Kal, 1974, 1975; Barendsen, 1975]. The picture is even more complicated for the complex biological systems which were also involved in the studies of Kellerer and Rossi, since measured endpoints are dependent on interaction of various intercellular processes. Consequently, the values for the critical size derived by Kellerer and Rossi are probably to be related to distances over which sublethally damaged critical elements can interact and provide identical endpoints as obtained with heavy particle irradiation.

As discussed in chapter II-4, and as demonstrated by figure VI-5, the actual energy deposition distributions are somewhat wider than the theoretical Vavilov distributions. Due to this difference, a best fit between a convolution of inactivation function (VI-2) with actual energy deposition distributions and the biological data will be derived for somewhat larger diameters than derived with the theoretical distributions used. It should also be recognized that the stepwise inactivation function introduced in the hypothesis neglects any biological variation such as, for instance, the variation in sensitivity of the cells, while additional variations in the energy loss distribution functions due to variations in site dimensions are also neglected. These additional variations are expressed in an extended model to be part of the total distribution function, which is then composed of a biological and physical part, as schematically illustrated by figure VI-14.

Variation and other characteristic parameters of this total distribution function are identical to those of the distribution function for the uncorrected model, since the net result of the convolution, namely, the inactivation cross-section curve remains unaltered.

Due to the fact that the physical part represented by the energy deposition distribution is size dependent, the total distribution function can be separated into two size-dependent components. It should be made clear that this latter method does not imply that the biological variations are dependent on physical distributions. Using the sum rule for the variations of composite distributions, separate contributions of biological and physical components were calculated for various site diameters. The results are presented in figure VI-15. This figure shows that the value of 20 nm for the critical size has to be considered as a lower limit value and that the actual dimensions are probably somewhat larger. Because of the lack of biological data concerning these variations, an estimate for the maximum value has to be derived indirectly. In this derivation, the following aspects must be discussed.

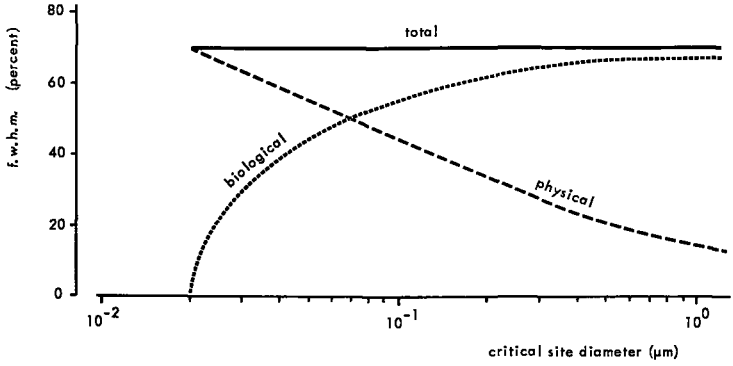

Fig. VI-15. Separation of the total distribution as required in the "monotopic" action model into a biological and a physical part.

In the reproductive process of the cell, the DNA plays an important role and ionizing radiation is known to produce a variety of lesions in this molecule, such as single-strand breaks, double-strand breaks and nucleotide damage. Furthermore, evidence is accumulating that the chromosomal part of the DNA, which is attached to the nuclear membrane, contains a large fraction of the radiosensitive sites responsible for reproductive death [Datta et al., 1976; Hagen, 1973; Dean, 1970]. From their experiments with alpha particle track-end irradiations of CHO cells, Datta et al. [1976] concluded that the sensitive sites are located at a distance of less than 0.2 μm from the nuclear membrane. This sensitive region presumably consists of two or more layers; this results in an upper limit for the size of the critical structure of about 0.1 μm.

With regard to the lesions in the DNA, the double-strand breaks occur at a much lower frequency than do the others. They are nevertheless widely accepted to be more likely identical with the lethal lesions. The energy required for double-strand breakage in dry DNA irradiated with high l.e.t. charged heavy particles is, as reported by Neary et al. [1972], of the order of 450 eV per break. From this value in combination with the derived threshold energy of 1300 eV and the foregoing discussion, it may be concluded that at least 3 breaks are required for the onset of reproductive death and that this lower limit value will increase with increasing size of the critical elements.

The increase in threshold energy from 1300 eV for the equilibrium situation to 1600 eV for the anoxic conditions suggest a "protective" effect in this latter condition. An extensive discussion of this protective phenomenon

has been given by Barendsen [1967]. He suggested, in principle, three possibilities which can explain this effect, namely, an increase in energy required, an increase in critical distance or a combination of both. The calculated results based on Vavilov distributions in combination with the hypothesis of monotopic action slightly favours the first possibility, because an increase in critical distance will increase the slope of the curve. This conclusion is supported by findings of an increase in energy required per break produced under anoxic conditions compared to oxygenated conditions [Palcic and Skarsgard, 1972; Bonura et al., 1975].

Very recently, Barendsen has developed an alternative hypothesis (as yet unpublished) for the induction of radiation damage. He assumes that two types of damage can be distinguished: one due to monotopic action and one to ditopic action [Gray, 1951] of the ionizing radiation. For this latter mode of action, an interaction between two localized regions over a distance of the order of 1 μm is assumed to be possible. On the basis of the hypothesis and data on cellular survival and induction of chromosomal damage published for different types of ionizing radiation, he demonstrates that the localized regions have dimensions of a few nanometers. This value derived for the size of the critical elements is somewhat smaller than the lower limit value of 20 nm as determined on the basis of the energy loss distributions.

The understanding of this discrepancy requires a further analysis of the hypothesis using microdosimetric data; however, this will not be discussed in this thesis.

Although, as discussed earlier in chapter V, energy loss distributions in the region of 20–100 nm required for the interpretation of cellular damage cannot be measured with the proportional counters, valuable information is provided by the measured spectra. Information for practical applications, particularly of indirectly ionizing neutrons, can be derived from lineal energy distributions measured at larger simulated volume sizes. These applications will be discussed in the next chapter.

CHAPTER VII

PRACTICAL APPLICATIONS OF ENERGY DEPOSITION SPECTRA

VII-1 Introduction

As concluded in the discussion of chapter VI, measurements of energy deposition spectra with TE proportional counters cannot be performed for simulated sizes equivalent to dimensions of the critical elements responsible for reproductive death of the cell. This restriction does not imply that data obtained with the TE proportional counter should be considered as of no value for the prediction of radiobiological effects. The contrary is true, since even from data for larger simulated volumes, valuable information on lineal energy and changes in the lineal energy distributions can be obtained. In addition, comparisons between computer generated and measured spectra for sizes above the lower limit of 0.3 μm diameter will provide information which makes extrapolation to the required smaller dimensions more meaningful [Coppola et al., 1974].

The proportional counters generally used have the advantage that they are relatively small in comparison to other types of detectors. This permits the measurement of changes in the energy deposition distribution of particles in much smaller volumes and over much shorter distances than with other detectors. A complicating factor in the translation of the measured lineal energy distributions into energy distributions is that the energy of a particle is not a single-valued function of its energy loss per unit path length (see figure II-2).

A first possible application of the proportional counter as a detector of variations in lineal energy distributions is provided by the study of collimated beams of fast neutrons such as employed for the clinical applications of neutrons in cancer therapy. Changes in energy spectra are of interest for this application, especially with regard to consequential variations in relative biological effectiveness. Lineal energy distributions can also be used to obtain information for health physics applications related to the determination of quality factors for the radiation in and around shieled areas of radiation facilities. Applications of both types will be discussed in the following sections. Because it is useful to refer to and to discuss the data of these studies in relation to the energy deposition distributions for the "free-in-air" situa-

tion, the distributions for this latter situation and the method of presentation will be discussed first.

VII-2 Lineal energy distributions of 3 and 15 MeV neutrons measured "free-in-air"

As mentioned in chapter II, neutrons interact with tissue and tissue-equivalent media by the generation of charged particles varying widely in mass and energy. Consequently, energy distributions, when given as number of events, $N(y)$, per lineal energy interval as a function of lineal energy, y, will cover several decades in magnitude. This is demonstrated in figure VII-1 for the distributions of energy deposition for 3 and 15 MeV neutrons measured at a simulated diameter of 1.2 μm. The method of presentation is, therefore, not very susceptible to variations in the energy spectra of the incident neutrons. A much more suitable method for presentation of the distributions was suggested by Heinz et al. [1971]. They proposed that the product quantity $y^2N(y)$ be plotted as a function of ln y. The distributions presented on a linear scale in figure VII-1, are both presented according to the suggested method in figure VII-2. It is evident that this method of presentation has the advantage of the reduced ordinate range, but a more interesting

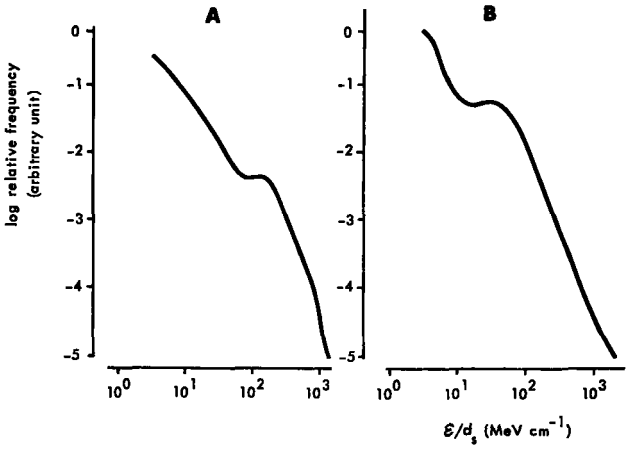

Fig. VII-1. Event size spectra, $N(y)$, of 3 and 15 MeV neutrons "free-in-air", measured with a cylindrical TE proportional counter at a simulated diameter of 1.2 μm.
A. Spectrum for 3 MeV neutrons.
B. Spectrum for 15 MeV neutrons.

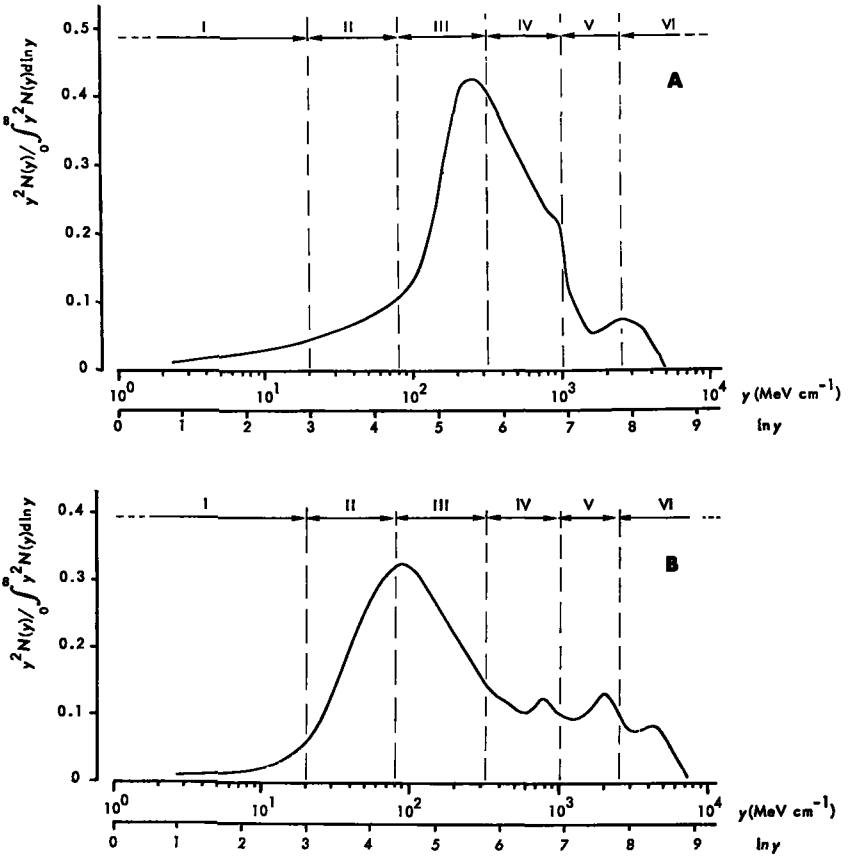

Fig. VII-2. Fractional dose distributions, $y^2N(y)/\int_0^\infty y^2N(y)\,\mathrm{d}\ln y$, of 3 and 15 MeV neutrons derived from spectra presented in figure VII-1.
A. Dose distribution for 3 MeV neutrons "free-in-air".
B. Dose distribution for 15 MeV neutrons "free-in-air".

feature is that the area under the curve is proportional to the dose. This latter property follows from the condition that:

$$\int_a^b y^2N(y)\,\mathrm{d}(\ln y) = \int_a^b yN(y)\,\mathrm{d}y \qquad \text{(VII-1)}$$

Since $yN(y)\mathrm{d}y$ is equal to the energy imparted in the lineal energy range between y and $y+\mathrm{d}y$, the second integral is proportional to the dose deposited by events with lineal energies between the two limits a and b. Applying this

property, the lineal energy distributions for the various conditions are plotted hereafter as $y^2N(y)$ curves as a function of ln y. The curves are all normalised to equal doses in order to better demonstrate variations in the contributions of dose in different regions of lineal energy between the various conditions.

Although the latter method of presentation will be used, a brief discussion of interesting characteristics of the curves given in figure VII-1 is in order. The local maxima in the curves at lineal energy values of 1.2 and 0.3 MeV cm^{-1} for the 3 and 15 MeV neutrons, respectively, are correlated with lineal energy values of the recoil protons resulting from head-on collisions of the neutrons with hydrogen nuclei. These protons are mainly produced in the foreward direction and, consequently, the position of the maxima depend on the angle of incidence of the neutrons with regard to the counter axis [Hogeweg, 1976]. Furthermore, it can be seen that both curves show a sharp decrease at a lineal energy value of about 1000 MeV cm^{-1}. This value corresponds to the maximum value of the stopping power for protons in TE gas. Therefore, the decrease in the curve is generally known as the proton edge. This proton edge is more significant in the distribution for 3 MeV than for 15 MeV neutrons, due to the fact that, for the 15 MeV neutrons, the proton contribution in this region is masked by the contributions of alpha particles and heavy recoils. Analogous edges are present in the distributions for 15 MeV neutrons at lineal energies of 2500 and 5000 MeV cm^{-1}, corresponding to the maximum values of the stopping power of the secondary alpha particles and berylium nuclei produced in neutron reactions.

Similarly as for the event size distributions, general characteristic regions can be recognized in the fractional dose, $y^2N(y)$, curves; these regions are indicated in figure VII-2. Six regions are used, in contrast to the five suggested by Heintz et al. [1971], in order to define the fast neutrons more specifically. The ranges of the various regions are adapted to the simulated diameter of 1.2 μm used in most of our experiments and therefore differ slightly from the values used by those authors. In region I with lineal energy values, y, less than 20 MeV cm^{-1}, the transfer of energy is mainly due to photon interactions. Regions II and III are defined by the conditions 20 MeV $cm^{-1} < y <$ 80 MeV cm^{-1} and 80 MeV $cm^{-1} < y <$ 320 MeV cm^{-1}. The deposition of energy in these regions is due to high energy protons with energies between 15 and 5 MeV and between 5 and 0.8 MeV, respectively, originating from interactions of fast neutrons with hydrogen nuclei. Region IV, represented by the interval 320 MeV $cm^{-1} < y <$ 1000 MeV cm^{-1}, corresponds to protons with energies in the range of about 0.8 to 0.07 MeV. There are also contri-

butions in all of these regions from electrons and protons which do not have energies large enough to cross the sensitive volume and are stopped within this volume. Regions V and VI, defined by lineal energy intervals of $1000 < y < 2500$ MeV cm^{-1} and $y > 2500$ MeV cm^{-1}, are related to energy deposition by alpha particles and heavy recoils, respectively.

The maxima in these fractional dose curves are not related, as were the maxima in the event size distributions presented in figure VII-1, to lineal energy values of protons produced in head-on collisions but depend in a complex way on the secondary proton spectra and the size and shape of the sensitive volume. The positions of the maxima in the curves for the 3 and 15 MeV neutrons are in good agreement with values calculated by Lawson and Watt [1967] and by Caswell and Coyne [1974]. In an identical manner as for the event size distributions, the steep decreases in the fractional dose curves at the different regions correspond to the Bragg peaks in the stopping power curves of the various particles. With respect to the distributions of dose for both neutron energies, it can be seen that the 3 MeV neutrons deposit a much larger fraction of their energy in tissue by proton events of sizes between 500 and 1000 MeV cm^{-1} than do the 15 MeV neutrons. This explains the much higher biological effectiveness of the 3 MeV neutrons in comparison to that of the 15 MeV neutrons [Broerse, 1966].

The selection of the simulated diameter of 1.2 μm for these and subsequent

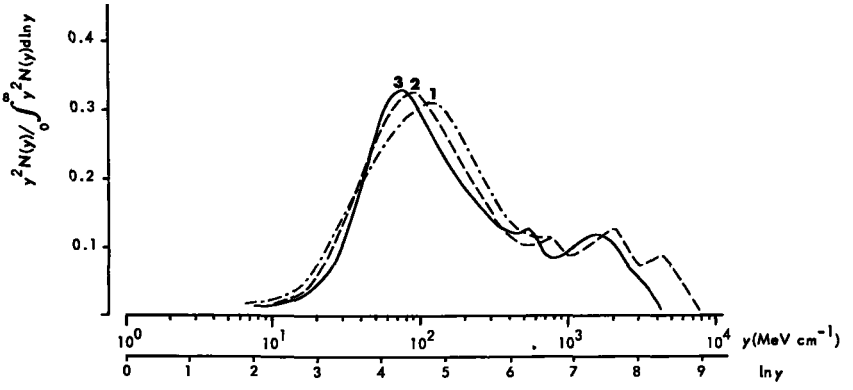

Fig. VII-3. Fractional dose distributions, $y^2N(y)/\int_0^\infty y^2N(y)\,\mathrm{d}\ln y$, measured "free-in-air" for 15 MeV neutrons with simulated diameters of 0.3, 0.6, 1.2 and 5.6 μm, respectively.
Curve 1: for a simulated diameter of 0.3 μm.
Curve 2: for a simulated diameter of 0.6 and 1.2 μm.
Curve 3: for a simulated diameter of 5.6 μm.

measurements was based on the results of energy deposition spectra of 15 MeV neutrons at simulated diameters of 0.3, 0.6, 1.2 and 5.6 μm of unit density tissue. These results are presented in figure VII-3. As can be concluded from the proton edge, the curve measured at a diameter of 0.3 μm shows a substantial loss of resolution. It can also be seen that the distribution curves for diameters of 0.6 and 1.2 μm are identical and that the proton edge in the distribution curve for 5.6 μm is distorted. This latter effect is the consequence of the limited range of these protons, which is shorter than 5.6 μm. In order to permit comparison with reported distributions, the value of 1.2 μm was selected, since measurements of the energy deposition spectra reported in the literature are mainly for simulated diameters in the range of 1 to 2 μm [Paretzke et al., 1972; Coppola et al., 1976; Lindborg, 1976; Menzel et al., 1976].

VII-3 Lineal energy distributions for collimated neutron beams

In the application of ionizing radiation from external sources such as x-rays and neutrons for cancer therapy, the amount of irradiated tissue must generally be restricted as much as possible to the tumor area and adjacent tissue. This requires narrow beams of radiations, which can be obtained by proper combinations of collimators and shields around the source. Due to scattering and absorption interactions of the radiation with the materials of these beam restricting devices, the output spectrum of this collimated radiation will not be identical to an undisturbed "free-in-air" spectrum of the source. Likewise, changes in the particle spectrum will occur with penetration depth of the radiation in the patient as a result of interactions with tissue. For x and gamma rays, the variations in the spectrum with depth are of relatively little interest. This is particularly true with regard to variations in biological effectiveness, because this changes only slowly with photon energy. However, with neutrons, the mean energy value of the spectrum will be reduced and the contribution of gamma radiations will increase due to these interactions. Since these alterations in the energy spectrum of neutrons may result in significant variations in biological effectiveness with depth, study of these spectrum variations is of great interest for the application of neutrons in radiotherapy. With regard to the shielding of normal tissue outside the beam, it can be stated that, in principle, there is no limitation on the level to which the undesired radiation behind the shield can be reduced. However, for the neutrons which are clinically applicable, high energies and associated long interaction distances are required in order to obtain good

depth dose characteristics [Broerse, 1966]. Shields required to reduce the dose to the normal tissue outside the beam region to acceptable levels are therefore rather thick. This thickness of the shield determines not only the level of stray radiation but also the minimum target-to-skin distance. The presently available monoenergetic neutron generators and target constructions provide only limited yields of neutrons. Therefore, the target-to-skin distance cannot be selected to be as long as demanded by extreme shielding requirements, since this would reduce the dose rate to impractically low values. Even for the restricted thickness of shielding material, the number of interactions is such that the original fast neutron spectrum is considerably altered towards lower energies for positions behind the shield. These neutrons of lower energy are biologically more effective than the fast neutrons initially produced. On the other hand, the increase in effectiveness from the neutrons contributing to the dose behind the shield is partly compensated for by the increasing contribution of gamma rays having a low biological effectiveness.

In order to study these modifying effects of collimators, energy deposition spectra for collimated beams of 15, 3, 0.9 and 0.5 MeV neutrons were determined. The production method for the various neutron energies and the collimators employed have been described in chapter IV.

Initial measurements of energy deposition distributions were performed

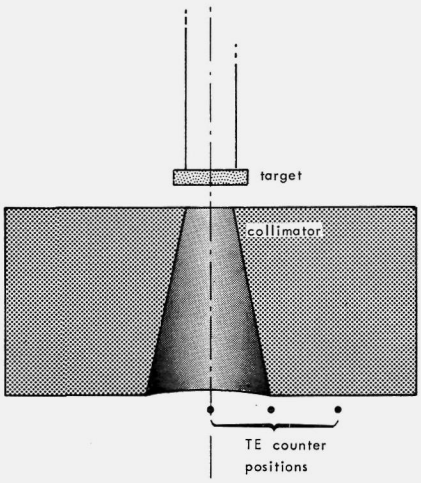

Fig. VII-4. Diagram of the collimator with the three positions (•) at which measurements were performed.

for 15 and 3 MeV neutrons for the conical collimator at three different positions behind the shield, in and outside the main beam (see figure VII-4). These positions were, successively, at the axis of the beam, at the boundary of the collimator duct and behind the shielding at a distance of 8.5 cm from the center of the beam. The fractional dose distributions resulting from these measurements are presented in figure VII-5. A comparison with the cor-

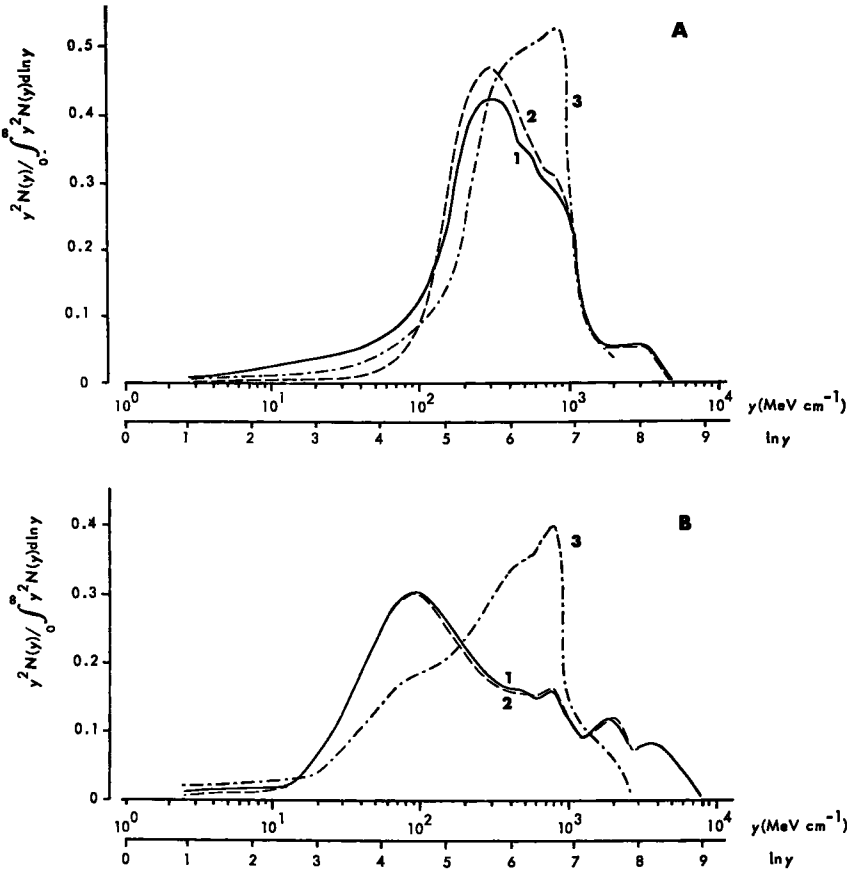

Fig. VII-5. Fractional dose distributions, $y^2N(y)/\int_0^\infty y^2N(y)\,\mathrm{d}\ln y$, of 3 and 15 MeV neutrons behind the conical collimator.
A. Fractional dose distributions for 3 MeV neutrons.
B. Fractional dose distributions for 15 MeV neutrons.
Curves denoted 1 refer to distributions derived at the center of the beam, 2 to distributions of the geometrical beam edge and 3 to distributions derived at the position behind the shielding at 8.5 cm from the center of the beam.

responding "free-in-air" spectra shows that the shapes of the spectra in the collimated beam are almost identical to those for "free-in-air". The maxima in the curves for lineal energy values in region II are shifted to slightly higher lineal energy values, which can be attributed to the shifts of the mean neutron energies to lower values. The comparison further shows that the contribution of events with lineal energies around 1000 MeV cm^{-1} is somewhat increased, in particular for the situation at the boundary of the beam. These increases are related to the increasing contributions of low energy scattered neutrons originating from the inside wall of the collimator duct.

Apart from this increase in the relative contribution of low energy neutrons, the scattering of neutrons also gives rise to an increase in the absolute value of integral $y^2N(y)$ (i.e., to the total dose) in comparison to the "free-in-air" situation for otherwise identical conditions. This increase can be attributed to an increase in the fluence of fast neutrons originating from neutrons scattered over small angles on the inner surface of the collimator duct. The ratio of the integrals of the distributions derived for the center position of the collimated beam and for the uncollimated "free-in-air" position is 1.12 and 1.04 for the 3 and 15 MeV neutrons, respectively. Similar increases in the dose for positions in collimated beams in comparison to "free-in-air" positions have been reported by Broerse [1967] and Attix [1976]. The reported values differ considerably from the above-mentioned values. This is most probably due to differences in collimator design.

The shapes of the lineal energy spectra as derived for the position behind the collimator outside the main beam are distinctly different in comparison to the shapes of the corresponding "free-in-air" spectra. They both demonstrate a large increase in events with lineal energies in the region between 400 and 1000 MeV cm^{-1}, due to the increasing contribution of scattered neutrons and of neutrons degraded in energy. As can be deduced from the small peak at about 100 MeV cm^{-1} in the curve for 15 MeV neutrons, a substantial component of the original spectrum is still present behind the shield. For the 3 MeV neutrons, this contribution of the original spectrum can be neglected. This is in agreement with the higher neutron attenuation coefficient at this energy.

In order to study modifications in the distributions with penetration depth in tissue, spectrum measurements were performed in a cubical paraffin phantom with 25 cm side lengths along the beam axis at 0 and 7 cm depth. The derived fractional dose distributions are presented in figure VII-6. These results show that there are no large variations in the spectra with depth.

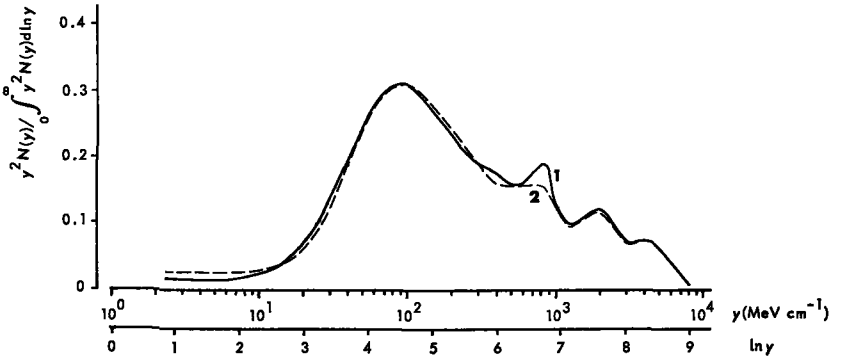

Fig. VII-6. Fractional dose distributions, $y^2N(y)/\int_0^\infty y^2N(y)$ dln y, of 15 MeV collimated neutrons in a paraffin phantom. The counter was positioned in the center of the beam.
Curve 1: at the surface of the phantom.
Curve 2: at 7 cm depth in the phantom.

This finding is in accordance with that derived from the neutron energy spectra determined at different depths with the proton-recoil spectrometer [Hogeweg et al., 1976].

To investigate collimator characteristics for a more practical situation corresponding to conditions of therapeutical applications, the spectral changes in lineal energy distributions were determined for the multilayered collimator which has been used for preclinical studies at the Radiobiological Institute. The lineal energy spectra were measured at the center of the beam, at the boundary and behind the shielding at 4 cm distance from the longest boundary side (equivalent to 7 cm from the center of the beam) for two collimator inserts. The two tapered collimator inserts were constructed of steel and polythene and each defined an exit field size of 6×8 cm^2. The results of the measurements are presented in figures VII-7 and VII-8. The distributions for positions at the center of the beam and at the boundary have the shape as generally reported for 15 MeV neutrons and are almost identical to the spectra measured for the conical collimator. A comparison of the spectra for the positions behind the collimator with that presented in figure VII-6 for the conical collimator shows that the contribution of the original spectrum for this steel insert is somewhat larger. The spectrum for the steel insert shows four local peaks, two of which can be attributed to the original beam. Similar additional peaks have been reported by Coppola [1975]. The phenomenon of the peaks must be attributed to build-up effects in the energy spectrum [Shani, 1976]. The comparison further shows that,

for the polythene insert, the spectrum behind the shielding is nearly identical to the spectrum of an unattenuated 15 MeV neutron beam. This can be explained on the basis of the lower attenuation effected by the wall of the polythene insert in comparison to that effected by the same thickness of

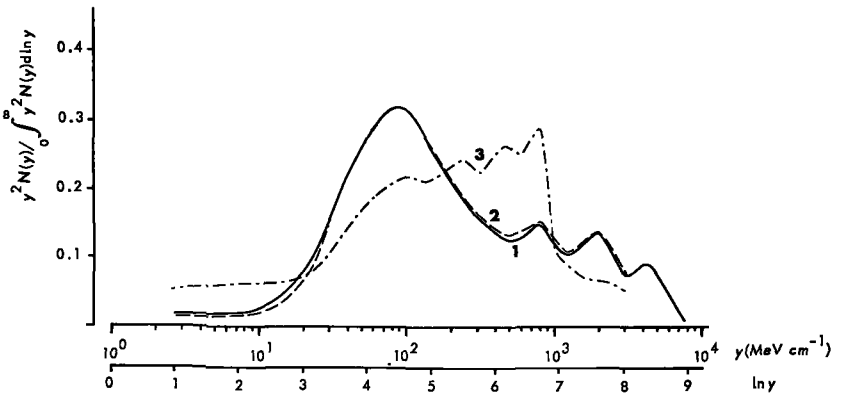

Fig. VII-7. Fractional dose distributions, $y^2N(y)/\int_0^\infty y^2N(y)$ dln y, of 15 MeV neutrons behind the collimator with steel insert as was used in a clinical investigation.
Curve 1: behind the collimator at the beam axis.
Curve 2: behind the collimator at the geometrical edge of the beam.
Curve 3: outside the primary beam behind the shielding at a distance of 7 cm from the center of the beam.

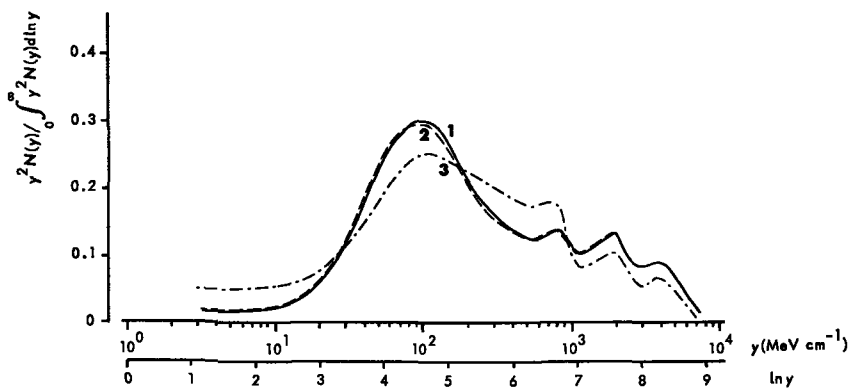

Fig. VII-8. Fractional dose distributions, $y^2N(y)/\int_0^\infty y^2N(y)$ dln y, of 15 MeV neutrons behind the collimator with polythene insert.
Curve 1: behind the collimator at the beam axis.
Curve 2: behind the collimator at the geometrical edge of the beam.
Curve 3: behind the shielding outside the primary beam at a distance of 7 cm from the center of the beam.

steel. From the values of the integral of $y^2N(y)$ for equal beam charges, the relative values of the absorbed dose were calculated at the different positions for both inserts. The values derived for the positions at the center of the beam, at the boundary and behind the shield were 100, 91 and 10 percent, respectively, for the steel insert and 100, 98 and 15 percent, respectively, for the polythene insert. The values derived from depth profile measurements on the same inserts performed by Broers-Challis et al. [1973] were 80 percent at the boundary for both inserts and 10 and 18 percent behind the shield. The differences between the values derived for the boundary position from the lineal energy spectra and the reported values of Broers-Challis et al. can be explained on the basis of small differences in positioning of the counter. Due to the steep decrease in the curve of relative dose with distance from the center in the penumbral region, small deviations in position can produce large differences in relative dose. On the other hand, similar variations in positioning beyond the penumbral region do not have such large effects; consequently, these results behind the shielding are in a better agreement with the data reported by these authors.

Since the fractional dose distributions for the 15 MeV neutrons are nearly identical at the various positions in the beams of the various collimators and inserts, it can be expected that no significant variations in relative biological effects will be detected across the beam region for those neutrons. Effects outside the beam region are much more difficult to predict from these spectra, since the increase in events with high lineal energy values (having a high biological effectiveness) is compensated for in part by an increase in the contribution of low lineal energy events. The contribution of these latter events can be mainly assigned to the gamma ray component of the mixed field and this gamma radiation is less effective in producing biological effects.

The predictions with respect to changes in radiobiological effectiveness with position in and outside the beam were verified in a study on the variation in the r.b.e. for impairment of the clonogenic capacity of cultured cells [Hogeweg et al., 1977]. For this study,cells in culture flasks and in tubes were irradiated with collimated 15 MeV neutrons at different positions in a cubical phantom. Within the beam region, no significant variations in the r.b.e. with penetration depth and with axial distance could be deduced from the results. There were also no significant differences at a position at 4 cm from the boundary behind the shield. As mentioned earlier, this latter finding can be explained on the basis of the compensating effect of the various contributions of scattered neutrons and gamma rays. Similar results were reported by Menzel et al. [1976] for the beam region of d–D neutrons produced by

bombarding a deuterium gas target with 10.6 MeV deutrons accelerated in a cyclotron. The energy distribution of these neutrons is bimodal with peaks in the distribution at about 4 and 12 MeV [Schraube et al., 1975]. The lineal energy distributions are, consequently, markedly different from those produced by 15 MeV monoenergetic neutrons [Menzel et al., 1977]. The greater increase in the gamma contribution outside this beam collimated by a steel-paraffin collimator [Burger et al., 1975], in comparison to that for 15 MeV neutrons, may explain the reduced effectiveness of these d–D neutrons outside the beam [Menzel et al., 1977]. For a collimated beam of d–Be neutrons with a mean energy of about 8.5 MeV, Geraci et al. [1975] reported a slight increase in the r.b.e. across the beam and a substantial increase in the penumbra and outside the beam. The possible cause of this reported increase in the r.b.e. in the penumbral region will be discussed later.

With the aim of determining the energy dependence of the contribution of scattered neutrons from the inner surface of the collimator ducts to the dose, lineal energy distributions were measured for collimated beams of 0.5 and 0.89 MeV neutrons. The method of production of these neutrons is described in chapter III. The distributions were measured for the collimator with steel insert used in the preclinical trial at positions identical to those

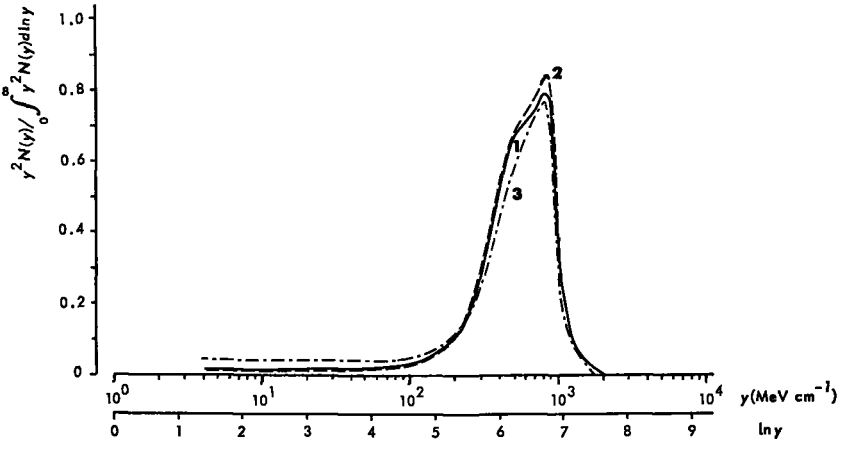

Fig. VII-9. Fractional dose distributions, $y^2N(y)/\int_0^\infty y^2N(y)$ dln y, of 0.89 MeV neutrons behind the collimator with steel insert as was used in a clinical investigation.
Curve 1: behind the collimator at the beam axis.
Curve 2: behind the collimator at the geometrical edge of the beam.
Curve 3: behind the shielding outside the primary beam at a distance of 7 cm from the center of the beam.

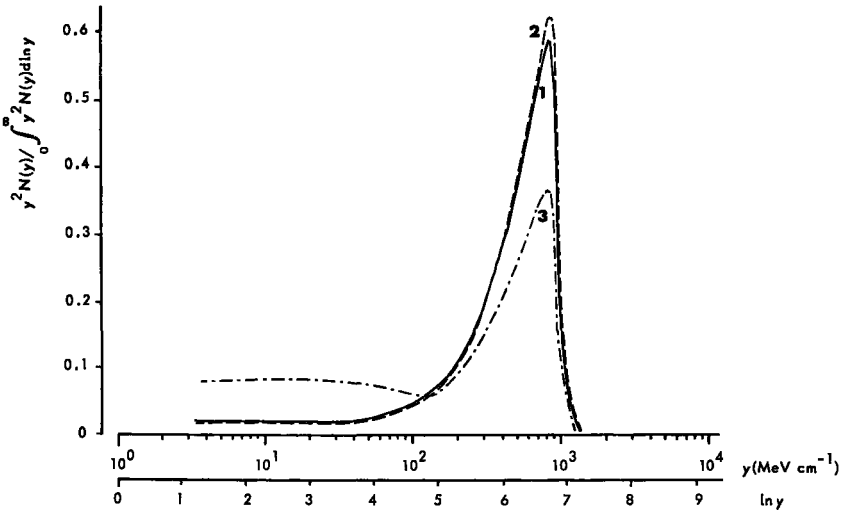

Fig. VII-10. Fractional dose distributions, $y^2N(y)/\int_0^\infty y^2N(y)$ dln y, of 0.5 MeV neutrons behind the collimator with steel insert used in a clinical investigation.
Curve 1: behind the collimator at the beam axes.
Curve 2: behind the collimator at the geometrical edge of the beam.
Curve 3: behind the shielding outside the primary beam at a distance of 7 cm from the center of the beam.

employed in the previous measurements. The derived results for the 0.89 and 0.5 MeV neutrons are presented in figures VII-9 and VII-10, respectively.

As a result of the wider range of possible energies for secondary protons induced by 0.89 MeV neutrons as compared to 0.5 MeV neutrons, the distribution of lineal energy is distinctly wider for 0.89 MeV neutrons. As can be deduced from the inflection of the curves, the influence of protons produced in head-on-collisions is still present in both distributions. It can be further noted that the expected increase in the relative contribution of events with lineal energy values of about 1000 MeV cm^{-1} due to scattered neutrons is clearly present in the distribution at the boundary. From the increase in the absolute value of the integral of the $y^2N(y)$ distribution at the boundary with respect to that at the center for the condition of equal total beam charges of accelerated ions, it follows that the reflected neutrons not only modify the lineal energy distributions but also give rise to an increase in the dose at the boundary. The ratio derived from the integrals between the dose at the boundary and the dose at the center is 1.1 and 1.2 for the 0.89 and 0.5 MeV neutrons, respectively. These values, together with

the value of 0.9 which was derived for the 15 MeV neutrons, obviously demonstrate that the ratio of doses at the boundary and at the center is an increasing function with decreasing energy.

It can be concluded, therefore, that the increase in r.b.e. at the boundary as reported by Geraci et al., and described by them as edge effect, can be explained by this increase. The d–Be neutrons used by these investigators have a wide energy spectrum with a large contribution of low and medium energy neutrons and these components will be markedly increased at the boundary due to the reflections mentioned. Since these lower energy neutrons are biologically more effective, the shift in the distribution toward lower energies will result in a higher r.b.e. value for the scattered neutron spectrum.

The foregoing discussion on the lineal energy distributions for the various situations of collimated neutron beams is illustrative of the valuable information that can be obtained from these spectra. Consequently, it is recommended that, for intercomparisons of biological results which are derived with various neutron beams, not only the dose and the mean neutron energy but also lineal energy distributions be considered as a determining physical parameter.

Apart from this application of the TE counter for the detection of quality variations across and along collimated beams of neutrons, the lineal energy distributions can also be applied in health physics dosimetry. This will be discussed in the following section.

VII-4 Applications of measurements of lineal energy distributions with respect to quality factor

Scatter of neutrons and resulting energy reduction will occur not only in collimated beams but can also arise from interactions with the walls of a generator hall or a treatment room. These scatter effects have two interesting aspects. Firstly, the scatter is of interest with regard to the total body dose given to a patient, which will be increased due to a fraction of these scattered neutrons which can be more effective biologically due to their reduced energy. For large distances between patient and surrounding walls, this contribution can certainly be neglected. The second interesting aspect of the scattering of neutrons on the walls concerns the construction of the protective shielding of neutron generator facilities required to reduce the doses for personnel to prescribed levels. In contrast to the large number of recommendations and guidelines published for the design of x-ray treatment

rooms, only scarce data are available with respect to the construction of neutron irradiation facilities [NCRP, 1971].

To evaluate the attenuation and scatter characteristics on an existing construction, the relative contributions from neutrons and photons to the total dose were determined for various positions in the neutron generator hall of the Repgo Institutes at Rijswijk. A number of different detection techniques were employed for these measurements.

At this facility, energy deposition distributions have been measured as one of the parameters, because the distribution of energy deposition is related to the quality of the radiation.

The radiation quality, Q, is a dose weighting factor introduced by the International Commission on Radiological Protection [ICRP, 1966] for radiation protection purposes, in order to account for the differences in biological effectiveness which will be derived with directly ionizing radiation of different types. The weighted dose, known as dose equivalent, is defined according to ICRU supplement to report 19 [1973] as outlined below.

The dose equivalent, H, is the product of D, Q and N at the point of interest in tissue; where D is the absorbed dose, Q is the quality factor and N is the product of any other modifying factors.

In the mathematical formulation:

$$H = QND \tag{VII-2}$$

The special unit of dose equivalent is the rem, which is defined in such manner that 1 rem is equivalent to 10^{-2} J kg^{-1}.

For all irradiations from external sources, the product factor N is presently assigned a value of 1. The dependence of the quality factor on the type of directly ionizing radiation, represented by its l.e.t. value, L_∞, is formulated in current ICRP publications [ICRP, 1969; ICRP, 1971] as a continuous function for which selected numerical values are provided. These recommended selected values are given in Table VII-1.

Table VII-1. $L_\infty - Q$ Relationship

L_∞ in water (MeV cm^{-1})	Q
35 and less	1
70	2
230	5
530	10
1750 and above	20

When the dose is delivered by indirectly ionizing radiations having wide distributions of secondary charged particles, then, according to the supplement of ICRU report 19 [1973], the equivalent dose can be obtained from the relation:

$$H = \overline{QN}D \tag{VII-3}$$

where $\overline{QN}$ is the mean of QN averaged over the absorbed dose. With $N = 1$ and Q based on the L_∞ relationship, the mean value of Q can be derived from:

$$\bar{Q} = \frac{1}{D}\int_0^\infty Q D_{L_\infty}\, \mathrm{d}L_\infty \tag{VII-4}$$

where D_{L_∞} denotes the differential distribution of D in L_∞.

By definition, for x-radiation or gamma rays, the mean quality factor of the electrons generated within the body is assumed to be 1.

As mentioned in chapter III-4, the lineal energy distributions measured with the long TE proportional counter are nearly identical to l.e.t. distributions. This is due to the fact that the track length distribution for the long TE proportional counter is strongly peaked at a value equivalent to the diameter. Therefore, the integral (formulated by VII-4) of the product of the fractional dose distributions and the specified quality function of table VII-1 will yield the mean quality factor of the radiation for which this fractional dose distribution was determined. In the supplement to ICRP publication 15 [1969], values of Q are presented for intermediate values of L_∞ in a curve. For the calculations based on fractional dose distributions, the values of the quality factor have been approximated by the analytical function given as:

$$Q(L_\infty) = \begin{cases} 1 & \text{for } L_\infty < 35 \text{ MeV cm}^{-1} \\ \exp\left[\sum_{i=1}^{4} a_i (\ln L_\infty - \ln 35)^i\right] & \text{for } 35 \leqslant L_\infty \leqslant 1750 \text{ MeV cm}^{-1} \\ 20 & \text{for } L_\infty > 1750 \text{ MeV cm}^{-1} \end{cases} \tag{VII-5}$$

where the parameters are:

$$a_1 = 1.24 \qquad a_3 = 0.188$$

$$a_2 = -0.467 \qquad a_4 = -0.025$$

Because the fractional dose distributions for x and gamma rays are larger than zero for l.e.t. values in excess of 35 MeV cm^{-1}, the quality factor derived for these radiations by this method will be larger than the postulated value of 1. Consequently, quality factors derived for sources which have large contributions of gamma rays also tend to be too high. A correction can be applied to those distributions for which the contribution of gamma rays can be discriminated from the other contributions. The correct value for the mean quality can be derived for these situations by applying an L_∞ independent quality factor of 1 for the gamma contribution and applying the defined quality dependent factor for the other contribution.

In order to test the described calculation method, mean quality factors were determined for 3 and 15 MeV neutrons in the "free-in-air" situation, for 15 MeV neutrons in the phantom and for the collimated 0.5 and 0.9 MeV neutrons at the center of the beam using their fractional dose distribu-

Table VII-2. Mean quality factors, $\bar{Q}$, derived from lineal energy distributions of neutrons with different energy, E_n, for various situations, in comparison to reported data.

E_n	$\bar{Q}$ (from spectra)	$\bar{Q}$ (from literature)	
15 MeV "free-in-air"	7.5±0.4	7.3±0.4	[Krüger, 1970]
		7.0	[Maier, undated]
		7.5	[ICRP, 1969]
15 MeV in phantom, at 0 cm depth	7.7±0.4	7.3	[Krüger, 1970]
		7.8	[NCRP, 1971]
15 MeV in phantom, at 7 cm depth	7.5±0.4	7.1	[Krüger, 1970]
		7.2	[NCRP, 1971]
3 MeV "free-in-air"	8.1±0.4	8.2±0.4	[Krüger, 1970]
0.89 MeV	11 ±0.5	10.1	[Maier, undated]*
		10.6	[ICRP, 1969]
0.5 MeV	10.1±0.5	10.8	[Maier, undated]
		11.0	[ICRP, 1969]
Am-Be spectrum	3.8±0.2 (uncorrected)	7.4	[Nachtigall, 1967]
	3.3±0.3 (gamma corrected)	3.9	[Maier, undated)
Pu-Be spectrum	7.6±0.4	7.5	[Nachtigall, 1967]

* Both quoted values are for 1 MeV

tion reported earlier in this chapter. The values obtained are presented in table VII-2, in comparison to values reported by various authors [Nachtigall, 1967; ICRP, 1969; Krüger, 1970; NCRP, 1971; Maier, undated]. A comparison of the values in the table shows that there is good agreement between the data calculated from our experimental results and reported data; only the value for the 15 MeV neutrons is somewhat higher but not significantly different from those reported. The values derived for the 15 MeV neutrons in the phantom demonstrate an identical variation with depth as that reported earlier [Krüger, 1970] and adopted by the NCRP [1971].

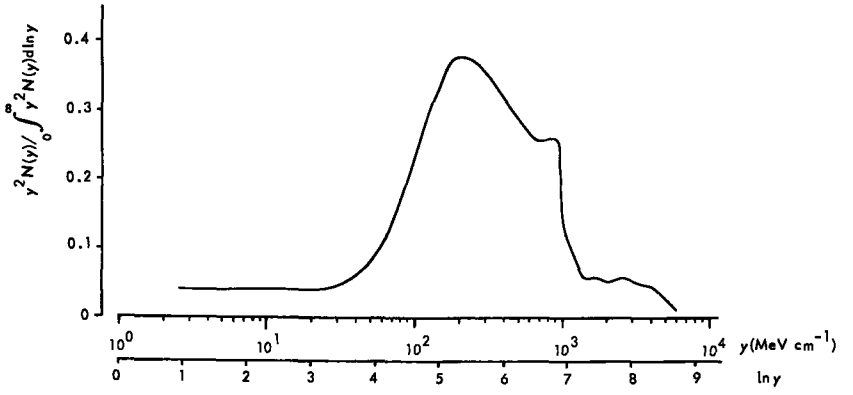

Fig. VII-11. Fractional dose distributions, $y^2N(y)/\int_0^\infty y^2N(y)\,\mathrm{d}\ln y$, of a spectrum of neutrons from a Pu-Be source.

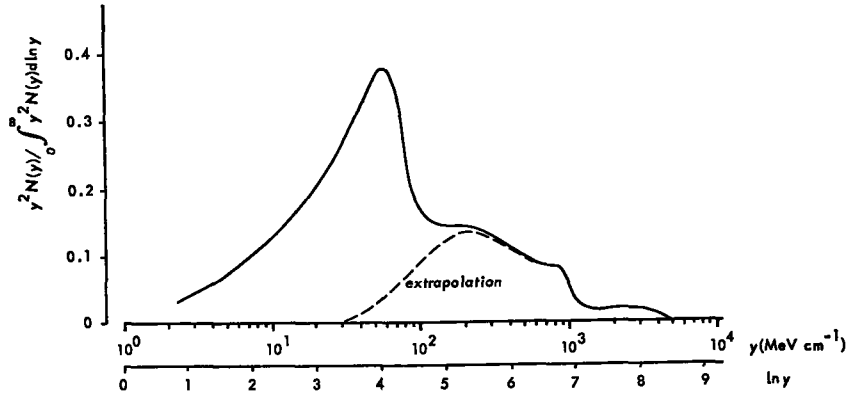

Fig. VII-12. Fractional dose distributions, $y^2N(y)/\int_0^\infty y^2N(y)\,\mathrm{d}\ln y$, of a spectrum of neutrons from an Am-Be source.
The extrapolated curve is derived from the Pu-Be spectrum.

The method of determination of the quality factor from the lineal energy distributions therefore seems to yield reliable results and has been applied to further measurements.

In the scope of the program to evaluate scatter and attenuation characteristics of the shielding construction, a Pu–Be and an Am–Be source were used for the calibration of the various instruments. The characteristics of these sources were briefly described in chapter IV. Lineal energy distributions were measured with the TE proportional counter for both sources. The fractional dose distributions derived from these measurements are presented in figures VII-11 and VII-12 for the Pu–Be and the Am–Be source, respectively. As was to be expected on the basis of the source characteristics, the fractional dose distribution of the americium source shows a large contribution of low lineal energy values due to the high contribution of gamma rays. In addition, the curves of both sources show an identical shape for that part of the spectrum which can be attributed to neutrons.

Quality factors derived from these spectra employing formulas (VII-4) and (VII-5) are 3.8 ± 0.2 for the americium source and 7.6 ± 0.4 for the plutonium source. As demonstrated in table VII-2, the value for the plutonium source is in good agreement with reported values. For the americium source, there is good agreement with the value reported by Maier which was derived in a similar manner from an uncorrected lineal energy spectrum. The great difference as compared with the mean value reported by Nachtigall can be explained on the basis of the fact that his value was determined for the neutrons only and ignored the gamma ray contribution. As discussed earlier, quality factors determined on the basis of lineal energy spectra from sources with a high contribution of gamma radiation will yield values which overestimate the quality factor. Employing the similarity of the shapes of the fractional dose curves for the americium and plutonium sources in the range of high l.e.t. values and further assuming that the similarity will also apply to the neutron component in the low l.e.t. region, the neutron and gamma components of the americium source can be estimated from an extrapolation to this lower l.e.t. region. The corrected mean quality factor derived in this manner has a value of 3.3 ± 0.3 for both radiation components together and a value of 8.0 ± 0.6 for the neutron component only. The relative contribution of gamma rays determined from the various distribution integrals is about 67 percent of the total dose. Consequently, it can be concluded from the difference between corrected and uncorrected quality factor for the americium source that, even for neutron sources with a high gamma contribution, the overestimation of the quality factor is relatively small.

In the study of shielding characteristics, measurements of lineal energy distributions were also performed in the generator hall for direct and scattered 15 MeV neutrons produced with the Van de Graaff K2N-3750 accelerator. The various positions of the measurements were: at 30 cm distance from the target assembly in the foreward direction, at a distance of 6 m in the 45° direction and in the maze entrance. These positions are indicated in figure VII-13 by **a**, **b** and **c**, respectively.

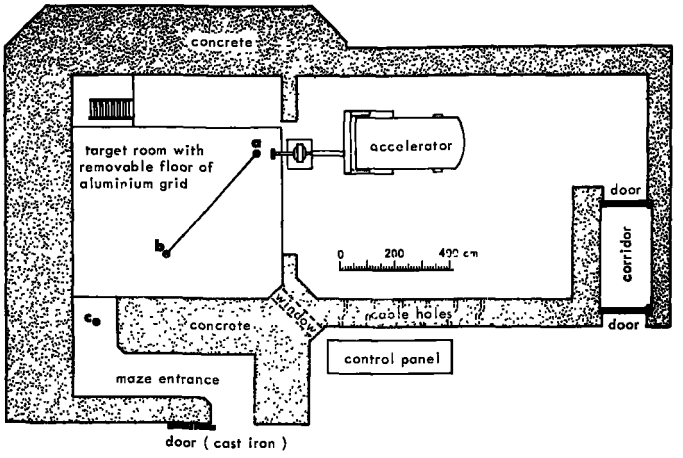

Fig. VII-13. Ground-plan of the generator hall. Positions of the measurements are indicated by **a**, **b** and **c**.

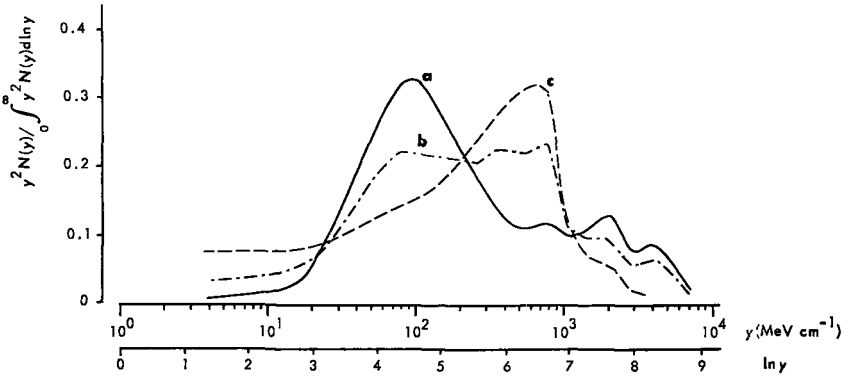

Fig. VII-14. Fractional dose distributions, $y^2N(y)/\int_0^\infty y^2N(y)\,\mathrm{d}\ln y$, for direct and scattered 15 MeV neutrons, measured in the generator hall.
Curve **a**: distributions for the direct beam at position **a** of figure 13.
Curves **b** and **c**: distributions derived for the scattered beam at positions **b** and **c**, respectively.

The resulting fractional dose distributions derived for the various positions are presented in figure VII-14. This figure demonstrates that there is a clear increase in the contribution of event sizes in the range between 300 and 1000 MeV cm^{-1} of unit density tissue for the distributions derived at **b** and **c** in comparison to that of the original beam measured at **a**. The spectrum in **b** can be recognized as a composition of the original spectrum with a scattered contribution. The relative contributions of these components in dose can be approximated from a subtraction method to be about 50 percent. Even more pronounced is the contribution of scattered and attenuated neutrons having event sizes of about 1000 MeV cm^{-1} in unit density tissue for the distribution derived at the maze entrance. It can also be deduced from figure VII-14 that the contribution of gamma radiation is significantly increased for positions **b** and **c**.

The mean quality factors determined from these spectra are 7.9 and 7.5 for positions **b** and **c**, respectively; the mean quality factor derived for position **a** is not significantly different from the value given in table VII-2 for 15 MeV neutrons "free-in-air". These values show that the quality factor does not change markedly for the different positions in the shielded area. On the basis of this finding, it may be predicted that the biological effect resulting from a possible increase in the total body dose from scattered radiation originating from the walls of a treatment room is identical to that of the primary radiation.

The examples described for the application of the proportional counter clearly demonstrate the valuable information which can be derived from lineal energy distributions in the submacrodosimetry range. A further application in this area might be the measurement of energy deposition in boundary regions of materials of different atomic compositions, a situation which may occur in bone marrow where soft tissue is surrounded by bone. Modifications in the energy distributions can possibly induce a higher biological effectiveness in the marrow than would be expected on the basis of energy deposition distributions in soft tissue.

SUMMARY

As a result of the passage of ionizing radiation through a biological object energy will be transferred in discrete events from charged particles to the atoms or molecules. The magnitude of the energy transferred per event and the spatial distribution of the events depend on the type of radiation and determine the quality characteristics of these radiation. As a consequence of the energy deposition by the ionizing radiation, disturbances in cellular and tissue functions will be induced with an effectiveness dependent on the quality of the radiation.

Based on their primary interaction mechanisms, the ionizing radiations can be classified into the directly ionizing charged particles and the indirectly ionizing radiation (e.g., photons and neutrons). Radiations of the indirectly ionizing type deposit their energy through the production of charged particles, which are of the directly ionizing type. The transfer of energy from the directly ionizing particles to the irradiated matter occurs via the Coulomb forces in discrete events with large variations in the amount of energy deposited per event. It can be demonstrated that the mean value and the variation of these discontinuous energy deposition distributions depend on the type of radiation and on the composition of the irradiated material and the size of the elemental volume studied.

It is generally accepted, that the differences in effectiveness among the various types of ionizing radiations for the production of a certain damage in a biological sample are determined by differences in the energy deposition patterns of the various radiations. In order to relate these physical parameters of energy deposition by the ionizing radiation to its biological effects, physical quantities such as absorbed dose and lineal energy have been defined by the ICRU [1971]. The quantity absorbed dose is used to express the total amount of energy deposited in an elemental volume, whereas the stochastic quantity lineal energy, y, is employed to express the amount of energy deposited per event. The mean value derived from the distribution of this latter quantity can be related to the concept of the quality of the radiation. This terminology must not be confused with the concept of radiation quality as employed for radiation protection [ICRP, 1971].

In the present thesis, a method for the measurement of lineal energy distributions, $N(y)$, in tissue-equivalent (TE) volumes of subcellular sizes,

employing a gas-filled TE proportional counter as detector, is described. The proportional counter has the advantage over other detectors that the inherent gas amplification allows a low detection level, as is required for these measurements of energy deposition distributions. The required smaller equivalent detector sizes can be simulated by reduction of the counter pressure.

Employing this detector, energy deposition distributions have been measured for ^{210}Po alpha particles in tissue-equivalent volumes with simulated diameters in the range of 0.075 to 5.6 μm of unit density tissue. It was found that these measured distributions are in good agreement with corresponding theoretical energy loss distributions derived from the Vavilov theory [1957]. These event size distributions of alpha particles of 2.5 to 5 MeV, crossing the sensitive counter volume over different track lengths and at different positions in the counter volume with respect to the central wire, have also been used to study the gas gain characteristics and to verify the homogeneity of the gas gain over the detector volume. It was demonstrated that the measured gas gain was in fair agreement with the theoretical expression of the gas gain, which formulates the dependence on gas pressure, applied voltage and starting point of the avalanche relative to the anode. From the measured and calculated values of the gas gain, it can be deduced that, below a gas pressure of about 5 kPa, the inhomogeneity of the gain over the detector volume is too large for correct operation of the counter. It must be concluded that the detector can not be applied for the measurement of lineal energy distributions for volumes of equivalent diameters smaller than about 0.3 μm of unit density tissue.

Differences in relative biological effectiveness (r.b.e.) for ionizing radiations characterized by different energy deposition patterns have been reported for the induction of reproductive death in cells [Barendsen, 1960, 1964]. The relative cross section per particle for the induction of reproductive death as a function of l.e.t. derived from these reported data, in combination with calculated and measured event size distributions for alpha particles of different energies, have been employed in an analysis in terms of a biophysical model. For this so-called monotopic action model, it was assumed that impairment of the clonogenic capacity followed from the passage of a particle which has deposited a required minimum amount of energy within a small critical volume. It was demonstrated that, with this model, the dependence of the cross section as a function of lineal energy can be explained on the basis of the variations in the energy deposition as observed for the different radiation energies. In a curve fitting method, based on the depen-

dence of these variations with path length, the size of the critical elements for the biological endpoint of reproductive death was estimated to about 20 nm. For an extended model in which the variations are assumed to be distributed over a physical and a biological component, it can be proved that the derived value for the critical size must be considered as a lower limit.

Based on biological data, the suggestion is made that the most likely value for the upper limit of the critical size is of the order of 100 nm. Since the proportional counter can operate correctly only for sizes larger than 0.3 μm, the distributions of energy deposition for volumes in this interesting range of sizes smaller than 0.3 μm have to be derived from calculations. However, it is demonstrated by practical applications of collimated and scattered neutron beams that the fractional dose distributions, $y^2N(y)$, derived from the measured distributions with the detector operating at a simulated diameter of about 1.2 μm can give valuable information. Due to the relatively small dimension of the detector, variations in energy deposition spectra can be measured over small distances. The fractional distributions measured with this detector, furthermore, offers a convenient method for the determination of the average quality factors of the radiation. Such fractional dose distributions were determined for collimated beams of neutrons with energies of 0.5, 0.9, 3 and 15 MeV. From these distributions, it can be concluded that, due to scatter on the inner surface of the collimator duct (in particular, at the penumbral region), the original neutron spectrum is altered quite considerably. Therefore, as a consequence of this scatter effect, an increased r.b.e. may be expected in the boundary region of the beam for neutron energies below about 3 MeV. From the fractional dose distributions for 15 MeV neutrons determined at 0 and 7 cm depth in a phantom and at the boundary of the beam, it can be deduced that no significant changes of the r.b.e. are to be expected over the irradiated region for the 15 MeV neutrons. This finding was confirmed in a study on the variations in the r.b.e. for collimated 15 MeV neutrons, employing impairment of the clonogenic capacity of cultured cells as biological detector.

SAMENVATTING

Tijdens de bestraling van een biologisch object (b.v. weefsel, cellen of DNA moleculen) wordt energie overgedragen door ioniserende deeltjes aan de atomen of moleculen van het bestraalde materiaal. Deze energie-overdracht geschiedt door geladen deeltjes in een groot aantal afzonderlijke gebeurtenissen, waarbij per interactie een bepaalde hoeveelheid energie wordt overgedragen. De grootte van de hoeveelheid energie die per gebeurtenis wordt overgedragen en de verdeling van interacties over de ruimte, hangen af van het type stralen en bepalen aldus kwaliteitskenmerken van deze stralen. Ten gevolge van de energie-afgifte aan cellen kunnen veranderingen in cel- en weefselfuncties worden geïnduceerd door de stralen met een effectiviteit, die afhangt van genoemde kwaliteitskenmerken. De bestudering van de samenhang tussen de kwaliteitskenmerken en de effectiviteit voor het produceren van schade in zoogdiercellen, is van belang voor de ontwikkeling en het afwegen van de waarde van nieuwe technieken voor de behandeling van kwaadaardige gezwellen.

Op grond van hun primaire wisselwerkingsmechanisme met de materie kunnen ioniserende stralen worden onderverdeeld in direct ioniserende geladen deeltjes en indirect ioniserende stralen (b.v. fotonen en neutronen). Een schematische voorstelling van de verschillende soorten ioniserende stralen en de wisselwerkingen met weefsel is gegeven in figuur (I-1). Indirect ioniserende stralen geven hun energie af op indirecte wijze, namelijk door de vorming van geladen direct ioniserende deeltjes. Overdracht van energie aan de bestraalde materie door deze direct ioniserende deeltjes vindt plaats in afzonderlijke gebeurtenissen via de wisselwerking van de Coulomb krachten. De hoeveelheid energie welke daarbij per gebeurtenis wordt afgegeven, is zeer sterk wisselend. Aangetoond kan worden, dat de verdelingsfunctie van de hoeveelheid energie welke wordt overgedragen per gebeurtenis en de gemiddelde waarde van deze verdeling afhankelijk zijn van het soort stralen, van de samenstelling van het bestraalde materiaal en van de afmetingen van het volume hetgeen beschouwd wordt. Deze invloed van volumegrootte op de verdelingsfunctie wordt duidelijk geïllustreerd door figuur (II-2).

Zoals vermeld, wordt algemeen aangenomen dat de verschillen in effectiviteit tussen de verschillende soorten ioniserende stralen, voor het indu-

ceren van een voorgeschreven biologisch effect, bepaald worden door de verschillen in de energieverdelingspatronen voor de energie-afgifte. Teneinde de kenmerken van deze energieverdelingen in weefsel te kunnen karakteriseren, zijn door de ICRU [1971] grootheden als geabsorbeerde dosis en „lineale energie" gedefinieerd. De grootheid geabsorbeerde dosis wordt gebruikt om de totale hoeveelheid energie, afgegeven in een zeer klein volume-elementje, aan te duiden. Om het wisselende karakter van de energie-afgifte per gebeurtenis te kunnen beschrijven, wordt de grootheid lineale energie, y, gebruikt. De theoretische aspecten van de verdelingsfunctie voor de grootte van deze energie-afgifte met betrekking tot reeds eerder genoemde afhankelijkheden, als volume en aard van de ioniserende stralen, worden behandeld in hoofdstuk II van dit proefschrift.

De gemiddelde waarde van de verdelingsfunctie, $N(y)$, van de lineale energie is een maat voor de kwaliteit en de biologische effectiviteit van de stralen. Deze terminologie moet echter niet verward worden met het begrip stralenkwaliteit zoals toegepast in de stralingsbescherming [Beschikking biologische werkzaamheid geabsorbeerde stralingsdosis, Stcrt, 1969, 234; ICRP, 1971]. In de stralenkwaliteitsfactor, zoals gebruikt voor berekeningen in de stralingsbescherming, zijn behalve de verschillen in biologische effectiviteit nog een aantal extra veiligheidsmarges ingebouwd.

In dit proefschrift wordt in hoofdstuk III een methode beschreven om de verdeling, $N(y)$, van de lineale energie in weefsel-equivalente volumes van subcellulaire grootte te meten. Voor deze metingen wordt een met weefsel-equivalent gas gevulde proportionele telbuis gebruikt. De wand van deze telbuis is eveneens van weefsel-equivalent materiaal gemaakt (zie figuur III-1). De proportionele telbuis heeft boven andere typen van detectoren het voordeel, dat de bijbehorende gasversterking een lage detectiegrens mogelijk maakt. Deze lage detectiegrens is nodig om de meting van geringe energie-afgiftes in kleine volumes mogelijk te maken. Het vereiste kleine detectorvolume van subcellulaire grootte kan worden nagebootst door middel van een verlaging van de gasdruk in de telbuis.

Met behulp van deze detector zijn verdelingen van de lineale energie voor gecollimeerde bundels van ^{210}Po alfadeeltjes (met energieën tussen 2.5 en 5 MeV) in kleine weefsel-equivalente volumes gemeten. De diameters van deze nagebootste volumes voor de verschillende gasdrukken lagen bij deze metingen tussen 0.075 en 5.6 μm weefsel met dichtheid 1. De gemeten verdelingen bleken goed in overeenstemming te zijn met de bijbehorende theoretische verdelingen, welke berekend kunnen worden uit de Vavilov theorie [1957]. De verdeling in energie-afgifte van deze bundels alfadeeltjes, welke

het gevoelige volume van de telbuis langs verschillende banen en in verschillende posities doorlopen, zijn ook gebruikt om de gasversterkingskarakteristieken van de telbuis en de homogeniteit van de gasversterking over het volume te bestuderen. In hoofdstuk V wordt aangetoond dat de gemeten gasversterking als functie van gasdruk, van aangelegde spanning en van het beginpunt van de gasversterkingslawine, zeer goed in overeenstemming is met de theoretische functie (zie figuur V-3). Uit de gemeten en berekende waarden van de gasversterking is af te leiden, dat beneden een druk van ongeveer 5 kPa de inhomogeniteit van de gasversterking te groot is voor een goede werking van de detector. Hieruit wordt geconcludeerd, dat de detector niet geschikt is voor het meten van verdelingen van de lineale energie in volumes met diameters die kleiner zijn dan 0.3 μm weefsel.

De reeds eerder genoemde doeltreffendheid voor de werking van ioniserende stralen wordt gewoonlijk uitgedrukt (zie figuur VI-1) in een relatief biologische effectiviteit (r.b.e.). Verschillen in r.b.e.-waarden voor de inductie van schade aan het reproduktievermogen van zoogdiercellen bij deling, ten gevolge van bestraling met ioniserende stralen van verschillend type (verschillend in energie-afgifteverdeling), zijn oorspronkelijk door Barendsen gemeten [1960, 1964]. Uit deze gegevens kan een relatieve werkzame doorsnede voor de inductie van deze schade aan het delingsvermogen worden afgeleid. De relatieve werkzame doorsnede als functie van de l.e.t. (lineïeke energie-overdracht) te zamen met berekende en gemeten verdelingen van de lineale energie voor alfadeeltjes van verschillende energieën, zijn gebruikt in hoofdstuk VI voor een analyse van de experimentele gegevens in termen van een biofysisch model. Bij dit model wordt uitgegaan van de gedachte dat het induceren van schade een gevolg is van een „monotopische" werking van de stralen. Dat wil zeggen, dat de eerste schade het resultaat is van een bepaalde minimale hoeveelheid aan energie, welke binnen een klein kritisch volume is afgegeven. Met behulp van dit model kan worden aangetoond, dat de afhankelijkheid van de werkzame doorsnede van de lineale energie, zoals gevonden werd door Barendsen, een gevolg is van de variatie in de verdeling der energie-afgifte van de gebruikte soorten stralen (zie figuur VI-2). Voorts is via de analyse uit de afhankelijkheid van de variatie in energie-afgifte met de grootte van het volume af te leiden, dat de diameter van de kritische elementen (kritisch met betrekking tot de inductie van schade aan het reproduktievermogen) ongeveer 20 nm is. In een iets uitgebreider model zijn de, voor de analyse vereiste, variaties in de energie-afgifte verdeeld gedacht over een fysische en een biologische component (figuur VI-14). Uit dit uitgebreide model volgt dat de afgeleide waarde van 20 nm als een

ondergrens moet worden beschouwd. Uit biologische gegevens volgt, dat de meest waarschijnlijke waarde van de bovengrens voor de diameter van het kritische element in de orde van grootte van 100 nm ligt.

Aangetoond is, dat de proportionele telbuis slechts goed kan werken voor afmetingen groter dan 0.3 μm. Daarom moeten voor kleinere volumes de verdelingen van de energie-afgifte uit berekeningen worden verkregen. In hoofdstuk VII wordt aangetoond aan de hand van een aantal praktische toepassingen bij gecollimeerde bundels en gestrooide bundels van neutronen, dat ondanks deze beperkingen waardevolle informatie verkregen kan worden betreffende energieveranderingen in deze bundels uit de z.g. fractionele dosisverdeling, $y^2N(y)$, voor equivalente diameters van 1 μm weefsel. Door de kleine afmetingen van de detectoren zijn deze eventuele veranderingen over kleine afstanden te meten. Voorts zijn uit deze fractionele dosisverdelingen op eenvoudige wijze de gemiddelde kwaliteitsfactoren te bepalen.

Fractionele dosisverdelingen, zoals gemeten voor gecollimeerde bundels van 0,5, 0,9, 3 en 15 MeV neutronen, tonen aan dat, door de verstrooiing van de neutronen aan de binnenzijde van de collimator, het spectrum voor laag energetische neutronen in verschillende posities van de bundel sterk verandert. Ten gevolge hiervan is voor neutronen met een energie beneden 3 MeV een toename in de r.b.e. aan de rand van het veld te verwachten. Voor mono-energetische 15 MeV neutronen afkomstig van de d–T reactie, zoals in Nederland voor tumor-therapie worden toegepast, zijn deze effecten niet te verwachten. Fractionele dosisverdelingen voor 15 MeV neutronen in een fantoom, gemeten op 0 en 7 cm diepte, vertonen slechts geringe verschillen; veranderingen in de r.b.e. met toenemende diepte zijn dientengevolge niet te verwachten. Deze bevindingen, verkregen uit de microdosimetrische metingen, konden worden bevestigd in een onderzoek aan r.b.e.-variaties. Hiertoe werden in flesjes en buisjes gekweekte cellen, als biologische detector, geplaatst op verschillende posities in een fantoom en bestraald met een gecollimeerde bundel van 15 MeV mono-energetische neutronen. Ook voor punten achter de collimator konden in dit onderzoek geen duidelijke veranderingen in r.b.e.-waarden worden aangetoond.

Een mogelijke toepassing van proportionele telbuizen met weefselequivalente wanden ligt voorts in het gebied van de meting van energieafgifteverdelingen aan grensvlakken van biologische materialen met sterk verschillende composities, zoals aanwezig in beenmerg. Op basis van deze compositieverschillen zijn wijzigingen in deze energieverdelingen met daarbij behorende wijzigingen in r.b.e. te verwachten.

LIST OF SYMBOLS

Symbol	Description	Chapter and page
β	speed of a charged particle relative to the velocity of of light	II-20
dE/dx	energy loss per unit path length of a charged particle passing through a material	II-20
d_s	diameter of the tissue-equivalent volume simulated by the proportional counter	III-36
ε	energy imparted by ionizing radiation to matter in a volume element	II-16
$\bar{G}$	mean gas multiplication factor of the proportional counter	III-38
I	mean excitation energy of the atoms of the stopping material	II-20
$\varkappa$	straggling parameter employed in the Landau and Vavilov theory for the energy loss distributions	II-25
L	linear energy transfer (l.e.t.), the nonstochastic quantity of energy locally imparted by a charged particle per path element of that particle	II-18
λ_L	straggling parameter for the Landau energy loss distribution	II-25
λ_V	straggling parameter for the Vavilov energy loss distributions	II-26
μ_0	mobility of the positive ion at a gas pressure of 1Pa	III-39
p	pressure (in pascal) of the gas in the proportional counter	III-36
Q	quality factor, a dose modifying factor used in radiological protection, which accounts for the differences in biological effectiveness of the various types of radiation	VII-118
$\bar{Q}$	mean quality factor	VII-119
W	average energy required for the formation of one ion pair	III-37

W_α	average energy required for the formation of one ion pair by alpha particles	V-68
W_e	average energy required for the formation of one ion pair by electrons	V-68
y	lineal energy, a stochastic quantity of energy locally imparted during an energy deposition event, by a charged particle to a medium in a volume element per mean chord length of that volume	II-18

ACKNOWLEDGEMENTS

The publication of this thesis and the work described has been possible as a result of the cooperation of a large group of persons working at the Radiobiological Institute TNO. The author wishes to express his gratitude to all those, who contributed directly or indirectly and in particular to:

Prof. Dr. G. W. Barendsen for introducing him into the domain of radiation action at the cellular level. His advices, physical as well as radiobiological, and stimulating discussions, especially during the writing of this thesis, are highly appreciated.

Prof. Dr. D. W. van Bekkum for providing the facilities to perform the experiments.

Prof. Dr. F. A. Muller for his willingness to act as co-referent and critically reading of the manuscript.

Dr. J. J. Broerse for his amical cooperation and stimulating discussions on the dosimetric problems.

Dr. M. Chemtob and Dr. V. D. Nguyen for their invaluable cooperation in the deconvolution of the proton spectra.

Dr. M. W. M. Oostenbrug for his expert help with the computer application of the fast Fourier transform used for the calculations of the pulse attenuation.

Dr. J. Zoetelief, Mr. A. C. Engels and Mr. C. J. Bouts for their cooperation in the experiments with fast neutrons during long operating sessions at conditions of extraordinary small beam currents.

Mr. J. E. Nelemans, Mr. F. A. van Calsteren and Mr. H. A. Versteegh for their technical advices and assistance in the realization of the tissue-equivalent counters.

Mr. J. S. Groen and Mr. L. A. Reeder for their assistance in keeping the electronic instrumentation in good working conditions.

Mrs. A. S. M. van Rijsoort, Mr. J. F. Gaiser and Mr. J. Hasper for their contributions, employing tissue culture techniques, in the determination of the r.b.e. variations.

Mr. J. Ph. de Kler for the exact and expert preparation of the figures and cover design.

Dr. A. C. Ford for his careful editing of the english text.

Mrs. H. M. Jense and Mrs. M. C. von Stein for typing and cheerfully retyping of the manuscript.

Mr. P. G. M. van Rossum and co-workers for collecting the literature.

Part of the work has been performed under contract with EURATOM (Commission of the European Communities), Brussels, Belgium, contract number 101-72-1 BIOC.

Finally, but not at least, I wish to express my gratitude to my parents, enabling me to study at the Delft University of Technology.

With great emphasis, but most likely against her own modest wishes, I want to thank Mia for her continuous support in all phases of this work.

REFERENCES

ADAMS Jr., J. H., SILBERBERG, R. and BADHWAR, G. D. Calculation of the Vavilov distribution (A correction). *Nucl. Instr. and Meth.* **124**, 551–556 (1975).

ALKHAZOV, G. D. Statistics of electron avalanches and ultimate resolution of proportional counters. *Nucl. Instr. and Meth.* **89**, 155–165 (1970).

ATTIX, F. H., AUGUST, L. S. and SHAPIRO, P. Scattered radiation from a neutron collimator. pp. 27–33. In: *Monograph on Basic Physical Data for Neutron Dosimetry*. Ed. J. J. Broerse, Commission of the European Communities, Luxembourg (1976).

BACH, R. L. and CASWELL, R. S. Energy transfer to matter by neutrons. *Radiat. Res.* **35**, 1–25 (1968).

BADHWAR, G. D. Calculation of the Vavilov distribution allowing for electron escape from the absorber. *Nucl. Instr. and Meth.* **109**, 119–123 (1973).

BAGLIN, J. E. E. and ZIEGLER, J. F. Test of Bragg rule for energy loss of ^{4}He ions in solid compounds. *J. Appl. Phys.* **45**, 1413–1415 (1974).

BARENDSEN, G. W. Impairment of the proliferative capacity of human cells in culture by alpha-particles with differing linear-energy transfer. *Int. J. Radiat. Biol.* **8**, 453–466 (1964).

BARENDSEN, G. W. Mechanism of action of different ionizing radiations on the proliferative capacity of mammalian cells. pp. 167–231. In: *Advances in Theoretical and Experimental Biophysics. Vol. I.* Ed. A .Cole, Marcel Dekker, New York (1967).

BARENDSEN, G. W. Responses of cultured cells, tumours and normal tissues to radiations of different linear energy transfer. pp. 293–356. In: *Current Topics in Radiation Research. Vol. IV.* Eds. M. Ebert and A. Howard, North-Holland Publishing Co., Amsterdam (1968).

BARENDSEN, G. W. Characteristics of cell survival curves for different radiations in relation to iso-effect curves for fractionated treatments of a rat rhabdomyosarcoma. pp. 270–279. In: *Cell Survival at Low Doses of Radiation: Theoretical and Clinical Implications.* Proc Sixth L. H. Gray Conf., London, 1974. Ed. T. Alper, John Wiley & Sons, London (1975).

BARENDSEN, G. W. and BEUSKER, T. L. J. Effects of different ionizing radiations on human cells in tissue culture. I. Irradiation techniques and dosimetry. *Radiat. Res.* **13**, 832–840 (1960).

BARENDSEN, G. W., BEUSKER, T. L. J., VERGROESEN, A. J. and BUDKE, L. Effects of different ionizing radiations on human cells in tissue culture, II. Biological experiments. *Radiat. Res.* **13**, 841–849 (1960).

BARENDSEN, G. W. and BROERSE, J. J. Experimental radiotherapy of a rat rhabdomyosarcoma with 15 MeV neutrons and 300 kV x-rays. I. Effects of single exposures. *Eur. J. Cancer* **5**, 373–391 (1969).

BARENDSEN, G. W., KOOT, C. J., KERSEN, G. R. VAN, BEWLEY, D. K., FIELD, S. B. and PARNELL, C. J. The effect of oxygen on impairment of proliferative capacity of human cells in culture by ionizing radiations of different LET. *Int. J. Radiat. Biol.* **10**, 317–327 (1966).

BARENDSEN, G. W. and WALTER, H. M. D. Effects of different ionizing radiations on human cells in tissue culture. IV. Modification of radiation damage. *Radiat. Res.* **21**, 314–329 (1964).

BARENDSEN, G. W., WALTER, H. M. D., FOWLER, J. F. and BEWLEY, D. K. Effects of different ionizing radiations on human cells in tissue culture. III. Experiments with cyclotron-accelerated alpha-particles and deuterons. *Radiat. Res.* **18**, 106–119 (1963).

BENEZECH, G. Private communication (1975).

BERGER, M. J. and SELTZER, S. M. Tables of energy-losses and ranges of electrons and positrons. pp. 205–268. In: *Studies in Penetration of Charged Particles in Matter*. NAS-NRC publ. 1133, Washington, D.C. (1964).

BICHSEL, H. Charged-particle interactions. pp. 157–228. In: *Radiation Dosimetry. Vol. I. Fundamentals*. Ed. F. H. Attix and W. C. Roesch, Academic Press, New York (1968).

BIRKHOFF, R. D. The passage of fast electrons through matter. pp. 53–138. In: *Handbuch der Physik. Vol. 34. Korpuskeln und Strahlung in Materie II.* Ed. S. Flügge, Springer Verlag, Berlin (1958).

BIRKHOFF, R. D., TURNER, J. E., ANDERSON, V. E., FEOLA, J. M. and HAMM, R. N. The Determination of LET spectra from energy – proportional pulse-height measurements. I. Track-length distributions in cavities. *Health Phys.* **18**, pp. 1–14 (1970).

BIRKS, J. B. The scintillation process in organic materials II. pp. 185–234. In: *The Theory and Practise of Scintillation Counting*. Pergamon, Oxford (1964).

BLUNCK, O. and LEISEGANG, S. Zum Energieverlust schneller Elektronen in dünnen Schichten. *Z. Physik*, **128**, 500–505 (1950).

BLUNCK, O. and WESTPHAL, K. Zum Energieverlust energiereicher Elektronen in dünnen Schichten. *Z. Physik* **130**, 641–649 (1951).

BOHR, M. On the decrease of velocity of swiftly moving electrified particles in passing through matter. *Phil. Mag.* **30**, 581–612 (1915).

BONURA, T., TOWN, C. D., SMITH, K. C. and KAPLAN, H. S. The influence of oxygen on the yield of DNA double-strand breaks in x-irradiated *Escherichia Coli* K-12. *Radiat. Res.* **63**, 567–577 (1975).

BOOZ, J. The relation between energy absorption and ionization in tissue equivalent gas for gamma quants of low energy. pp. 331–347. In: *Proc. First Symp. Microdosimetry*, Ispra, 1967. Ed. H. G. Ebert, Commission of the European Communities, Brussels (1968).

BOOZ, J. and COPPOLA, M. Energy deposition by fast neutrons to small spheres. pp. 983–998. In: *Proc. Fourth Symp. Microdosimetry*, Verbania, 1973. Eds. J. Booz, H. G. Ebert, R. Eickel and A. Waker, Commission of the European Communities, Luxembourg (1974).

BOOZ, J., SMIT, TH. and WAKER, A. Energy dependence of the differential W-value of alpha particles in tissue-equivalent gas. *Phys. Med. Biol.* **17**, 477–485 (1972).

BÖRSCH-SUPAN, W. On the evaluation of the function

$$\phi(\lambda) = \frac{1}{2\pi i} \int_{\sigma-i\infty}^{\sigma+i\infty} e^{u \ln u + \lambda u} du$$

for real values of λ. *J. Res. Natl. Bur. Stand.* 65B, 245–250 (1961).

BRAGG, W. H. and KLEEMAN, R. On the alpha particles of radium, and their loss of range in passing through various atoms and molecules. *Phil. Mag.* **10**, 318–340 (1905).

BREYER, B. and CIMERMAN, M. Attenuation of proportional counter pulses by pulse shaping networks. *Nucl. Instr. and Meth.* **92**, 19–20 (1971).

BROERS-CHALLIS, J. E., ENGELS, A. C., BOUTS, C. J., and BROERSE, J. J. Depth-dose measurements of d-T neutrons in tissue-equivalent phantoms. pp. 201–210. In: *Proc. Symp. Neutron Monitoring for Radiation Protection Purposes*, Vienna, 1972. International Atomic Energy Agency, Vienna (1973).

BROERSE, J. J. *Effects of Energy Dissipation by Monoenergetic Neutrons in Mammalian Cells and Tissues*. Thesis, University of Amsterdam, The Netherlands (1966).

BROERSE, J. J. Penetration parameters for 15-MeV neutron beams. *Kerntechnik* **9**, 446–451 (1967).

BROERSE, J. J., BROERS-CHALLIS, J. E. and MARUYAMA, T. Dosimetry of D-T neutrons for radiotherapeutic applications. pp. 627–647. In: *Proc. First Symp. Neutron Dosimetry in Biology and Medicine*, Neuherberg, 1972. Eds. G. Burger and H. Schraube, Commission of the European Communities, Luxembourg (1972).

BROLLEY Jr., J. E., and FOWLER, J. L. Monoenergetic neutron sources: Reactions with light nuclei. pp. 73–132. In: *Fast Neutron Physics. Part I. Techniques*. Eds. J. B. Marion and J. L. Fowler, Interscience Publishers, Inc., New York (1960).

BURGER, G., GRÜNAUER, F., MORHART, A. und SCHRAUBE, H. Entwicklung eines Neutronentherapie-Bestrahlungskopfes mit Neutronentarget für das DKFZ-Heidelberg. *GSF bericht S 346*, Gesellschaft Für Strahlen- und Umweltforschung mbH, München (1975).

BURLIN, T. E. Cavity-chamber theory. pp. 331–392. In: *Radiation Dosimetry. Vol. I. Fundamentals*. Eds. F. H. Attix and W. C. Roesch, Academic Press, New York and London (1968).

BURRUS, W. R. and VERBINSKI, V. V. Fast-neutron spectroscopy with thick organic scintillators. *Nucl. Instr. and Meth.* **67**, 181–196 (1969).

CAMPION, P. J. A study of proportional counter mechanisms. *Int. J. appl. Radiat. Isotopes* **19**, 219–234 (1968).

CAMPION, P. J. The operation of proportional counter at low pressures for micro-dosimetry. *Phys. Med. Biol.* **16**, 611–616 (1971).

CAMPION, P. J. Some comments on the operation of proportional counters. pp. 601–617. In: *Proc. Third Symp. Microdosimetry*, Stresa, 1971. Ed. H. G. Ebert, Commission of the European Communities, Luxembourg (1972).

CAMPION, P. J. and KINGHAM, M. W. J. The measurement of the gas multiplication in tissue equivalent gas. *Int. J. appl. Radiat. Isotopes*, **22**, 703–706 (1971).

CASWELL, R. S. and COYNE, J. J. Interaction of neutrons and secondary charged particles with tissue: Secondary particle spectra. *Radiat. Res.* **52**, 448–470 (1972).

CASWELL, R. S. and COYNE, J. J. Neutron energy deposition spectra studies. pp. 967–979. In: *Proc. Fourth Symp. Microdosimetry*, Verbania Pallanza, 1973. Eds. J. Booz, H. G. Ebert, R. Eickel and A. Waker, Commission of the European Communities, Luxembourg (1974).

CHARLES, M. W. Gas gain measurements in proportional counters. *J. Phys. E; Sci Instr.* **5**, 95–100 (1972).

CHARLES, M. W. and COOKE, B. A. Proportional counter resolution. *Nucl. Instr. and Meth.* **61**, 31–36 (1968).

CHECHIN, V. A. and ERMILOVA, V. C. The ionization-loss distribution at very small absorber thickness. *Nucl. Instr. and Meth.* **136**, 551–558 (1976).

COPPOLA, M. Private communication (1975).

COPPOLA, M., EICKEL, R., FITZGERALD, M., PIRRWITZ, D., PORRO, F. and BOOZ, J. Experimental evaluation of the spectral energy deposition in small volumes by low-LET radiations, pp. 377–391. In: *Proc. Fifth Symp. Microdosimetry*, Verbania Pallanza, 1975. Eds. J. Booz, H. G. Ebert and B. G. R. Smith, Commission of the European Communities, Luxembourg (1976).

COPPOLA, M., PIRRWITZ, D. and BOOZ, J. Influence of detector size and thickness on neutron produced energy deposition spectra. pp. 1001–1012. In: *Proc. Fourth Symp. Microdosimetry*, Verbania Pallanza, 1973. Eds. J. Booz, H. G. Ebert, R. Eickel and A. Waker, Commission of the European Communities, Luxembourg (1974).

COULSON, C. A. Electricity. pp. 51–72. In: *Dielectrics*. Oliver and Boyd, Edinburg (1951).

CUTLER, J. M., GREENBERGER, S., and SHALEV, S. Pulse risetime discrimination for ^{3}He counters. *Nucl. Instr. and Meth.* **75**, 309–311 (1969).

DATTA, R., COLE, A. and ROBINSON, S. Use of track-end alpha particles from ^{241}Am to study radiosensitive sites in CHO cells. *Radiat. Res.* **65**, 139–151 (1976).

DEAN, C. Repair mechanisms in DNA. Abstracts of papers of the second IRPA congres, Brighton, 1970. *Health Phys.* **19**, 67–172 (1970).

DERTINGER, H. and JUNG, H. Directe und indirecte Strahlenwirkung. pp. 76–98. In: *Molekulare Strahlenbiologie.* Springer Verlag, Berlin (1969).

ELKIND, M. M. and SUTTON, H. Radiation response of mammalian cells grown in culture. I. Repair of x-ray damage in surviving chinese hamster cells. *Radiat. Res.* **13**, 556–593 (1960).

FAIRSTEIN, E. and HAHN, J. Nuclear pulse amplifiers – Fundamentals and design practice. *Nucleonics* **23**, 56–61 (1965); **23**, 81–88 (1965); **23**, 50–55 (1965) and **24**, 54–60 (1966).

FANO, U. Note on the Bragg-Gray cavity principle for measuring energy dissipation. *Radiat. Res.* **1**, 237–240 (1954).

FANO, U. Penetration of protons, alpha particles, and mesons. pp. 1–66. In: *Annual Review of Nuclear Science. Vol. 13.* Eds. E. Segré, G. Friedlander, and P H. Gand Noyes, Annual Reviews, Inc., Palo Alto, California (1963).

FLAMM, L. Theoretische Untersuchungen über Ursache und Grösze der Reichweiteschwankungen bei den einzeln alpha-Strahlen eines homogenen Bündels. *Akad. Wiss. Wien, Sitzb.d.mathem.-naturw. Kl.* **123**, 1393–1426 (1914).

FOWLER, J. F. Differences in survival shapes for formal multi-target and multi-hit models. *Phys. Med. Biol.* **9**, 177–188 (1964).

GERACI, J. P., JACKSON, K. L., THROWER, P. D. and FOX, M. S. An estimate of the patient risk in cyclotron neutron radiotherapy using mouse testes as a biological test system. *Health. Phys.* **29**, 729–737 (1975).

GILLESPIE, A. B. Signal to noise ratio. pp. 49–78. In: *Signal, Noise and Resolution in Nuclear Counter Amplifiers.* Pergamon Press, London (1953).

GRAY, L. H. Biological actions of ionizing radiations. *Prog. Biophys. Biophys-Chem.* **2**, 240–305 (1951).

GREENE, D. and THOMAS, R. L. The attenuation of 14 MeV neutrons in steel and polyethylene. *Phys. Med. Biol.* **14**, 45–54 (1969).

HAGEN, U. Strahlenwirkung auf Struktur und Funktion der Desoxyribonukleinsäure. *Biophysik* **9**, 279–289 (1973).

HANSON, A. O., TASCHEK, R. F. and WILLIAMS, J. H. Monoergic neutrons from charged particle reactions. *Revs. Modern Phys.* **21**, 635–650 (1949).

HEINTZ, P. H., ROBKIN, M. A., WOOTON, P. and BICHSEL, H. In-phantom microdosimetry with 14.6 MeV neutrons. *Health Phys.* **21**, 598–602 (1971).

HENDRICKS, R. W. A pulse-matching method for estimating the gas amplification factor in proportional counters. *Nucl. Instr. and Meth.* **106**, 579–588 (1973).

HEITLER, W. Bremsstrahlung. pp. 161–177. In: *Quantum Theory of Radiation.* Oxford University Press, Oxford (1944).

HEYLEN, A. E. D. Influence of molecular bonding on the Townsend ionisation coefficients of hydrocarbon gases. *J. Chem. Phys.* **38**, 765–771 (1963).

HOGEWEG, B. Variations in energy deposition distributions in collimated neutron beams. pp. 575–588. In: *Proc. Fifth Symp. Microdosimetry*, Verbania Palanza, 1975. Ed. J. Booz, H. G. Ebert and B. G. R. Smith, Commission of the European Communities, Luxembourg (1976).

HOGEWEG, B. and BARENDSEN, G. W. Local energy distributions for α-particles of different energies in relation to the evaluation of critical sizes and energy requirements involved in the induction of damage in mammalian cells. pp. 857–868. In: *Proc. Third Symp. Microdosimetry*, Stresa, 1971. Ed. H. G. Ebert. Commission of the European Communities, Brussels (1972).

HOGEWEG, B., BARENDSEN, G. W. and BROERSE, J. J. Evaluation of the biological effectiveness of different types of radiation. pp. 28–31. In: *Annual Report 1972, Programme Biology – Health Protection.* Commission of the European Communities, Luxembourg (1973).

HOGEWEG, B., BROERSE, J. J., CHEMTOB, M. and NGUYEN, V. D. Measurements of neutron energy spectra for collimated beams. pp. 12–14. In: *Annual Report 1975 of the REP-institutes*, Rijswijk (1976).

HOGEWEG, B., BROERSE, J. J., CHEMTOB, M. and NGUYEN, V. D. Neutron energy spectra for collimated d-D and d-T neutron beams as employed for ENDIP, pp 49–53. In: *Monograph on Basic Physical Data for Neutron Dosimetry.* Ed. J. J. Broerse, Commission of the European Communities, Luxembourg (1976).

HOGEWEG, B., BROERSE, J. J., GAISER, J. F., RYSOORT, A. S. M. VAN, HASPER, J., MIJNHEER, B. J., DEYS, B. F. and GORTER, H. R.b.e. and energy spectra of d+T neutrons as a function of depth in a human phantom. In: Abstr. Meeting, Progr. Exp. Radiotherapy, Amsterdam, 1977. *Int. J. Radiat. Biol.* **32**, 375–390 (1977).

HURST, G. S. and RITCHIE, R. H. On energy resolution with proportional counters. *Rev. Sci. Instr.* **24**, 664–668 (1953).

HUTCHINSON, F. The molecular basis for radiation effects on cells. *Cancer Res.* **26**, 2045–2052 (1966).

ICRP publication 5. *Handling and Disposal of Radioactive Materials in Hospitals and Medical Research Establishments.* International Commission on Radiological Protection, Pergamon Press, Oxford (1964).

ICRP publication 9. *Recommendations of the International Commission on Radiological Protection.* Pergamon Press, Oxford (1966).

ICRP publication 15. *Protection against Ionizing Radiation from External Sources.* International Commission on Radiological Protection ,Pergamon Press, Oxford (1969).

ICRP publication 21. *Data for Protection against Ionizing Radiation from External Sources: supplement to ICRP publication 15.* International Commission on Radiological Protection. Pergamon Press, Oxford (1971).

ICRU Report 10b. *Physical Aspects of Irradiation.* National Bureau of Standards Handbook 85, Washington ,D.C. (1964).

ICRU Report 16. *Linear Energy Transfer.* International Commission on Radiation Units and Measurements, Washington, D.C. (1970).

ICRU Report 19. *Radiation Quantities and Units.* International Commission on Radiation Units and Measurements, Washington, D.C. (1971).

ICRU supplement to report 19. *Dose Equivalent.* International Commission on Radiation Units and Measurements, Washington, D.C. (1973).

ICRU Report 26. *Neutron Dosimetry for Biology and Medicine.* International Commission on Radiation Units and Measurements, Washington, D.C. (1977).

JAEGER, J. C. Fundamental Theory. p. 1. In: *An Introduction to the Laplace Transformation.* Methuen and Co., Ltd., London (1951).

JESSE, W. P. and SADAUSKIS, J. Alpha-particle ionization in mixtures of the noble gases. *Phys. Rev.* **88**, 417–418 (1952).

JOHNS, H. E., CORMACK, D. V., DENESUK, S. A. and WHITMORE, G. F. Initial distribution of Compton electrons. *Can. J. Phys.* **30**, 556–564 (1952).

JONES, D. W. and TOMS, M. E. A Neutron Spectrometer Using Organic Scintillators. *NRL Report 7324*, Naval Research Laboratory, Washington, D.C. (1971).

KAL, H. B. *Response of a rat rhabdomyosarcoma and rat skin to irradiation with gamma rays and 15 MeV neutrons at low dose rates.* Thesis, University of Amsterdam, The Netherlands (1974).

KAL, H. B. Effects of protracted gamma irradiation on cells from a rat rhabdomyosarcoma treated *in vitro* and *in vivo*. pp. 259–269. In: *Cell Survival after Low Doses of Radiation: Theoretical and Clinical Implications*. Proc. Sixth L. H. Gray Conf., London, 1974. Ed. T. Alper, John Wiley & Sons, London (1975).

KATZ, R., ACKERSON, B., HOMAYOONFAR, M. and SHARMA, S. C. Inactivation of cells by heavy ion bombardment. *Radiat. Res.* **47**, 402–425 (1971).

KASTNER, J., ROSE, J. E. and SHONKA, F. R., Muscle-equivalent environmental radiation meter of extreme sensitivity. *Science* **140**, 1100–1101 (1963).

KELLERER, A. M. Considerations on the random traversals of convex bodies and solutions for general cylinders. *Radiat. Res.* **47**, 359–376 (1971).

KELLERER, A. M. and ROSSI, H. H. RBE and the primary mechanism of radiation action. *Radiat. Res.* **47**, 15–34 (1971).

KELLERER, A. M. and ROSSI, H. H. The theory of dual radiation action. *Current Topics in Rad. Res. Quarterly.* **8**, 85–158 (1972).

KEMMOCHI, M. Measurement of W-values for alpha particles in tissue equivalent gases. *Health Phys.* **30**, 439–446 (1976).

KEMSHALL, C. D., BEAUCHAMP K. G. and BENJAMIN, P. W. The attenuation of proportional counter pulses by RC amplifier time constants. *Nucl. Instr. and Meth.* **68**, 153–156 (1969).

KIM, Y. K. Energy Distribution of secondary electrons. I. Consistency of experimental data. *Radiat. Res.* **61**, 21–35 (1975).

KIM, Y. S. Density effect in dE/dx of fast charged particles traversing various biological materials. *Radiat. Res.* **56**, 21–27 (1973).

KIM, Y. S. Human tissues: Chemical composition and photon dosimetry data. *Radiat. Res.* **57**, 38–45 (1974).

KIM, Y. S. Human tissues: Chemical composition and photon-dosimetry data. A correction. *Radiat. Res.* **60**, 361–362 (1974).

KISER, R. W. Characteristic parameters of gas-tube proportional counters., I. Methane, methane-argon and ethanol-argon counters. *Apl. sci. Res.* B **8**, 183–200 (1960).

KRÜGER, H. *Bestimmung der Energiedosis und der lokalen spezifischen Energie fur schnelle Neutronen und ihre Bedeutung bei strahlenbiologische Experimenten.* Inaugural-Dissertation der Philips-Universität, Marburg/Lahn (1970).

LANDAU, L. On the energy loss of fast particles by ionization. *Journ. Phys. U.S.S.R.* **8**, 201–205 (1944).

LAULAINEN, N. and BICHSEL, H. Energy removed by delta rays from finite volumes in passage of charged particles. *Nucl. Instr. and Meth.* **104**, 531–539 (1972).

LAWSON, R. C. and WATT, D. E. The LET distribution of the recoil proton dose from DD and DT neutrons. *Phys. Med. Biol.* **12**, 217–228 (1967).

LEA, D. E. Physical properties and dosimetry of different radiations. pp. 1–32. In: *Actions of Radiations on Living Cells.* University Press, Cambridge (1962).

LEBLANC, O. H. and DEVINS, J. C. Townsend ionization constant in n-Alkanes. *Nature* **188**, 219–220 (1960).

LEONARD, B. E. and BORING, W. J. The average energy per ion pair, $\overline{W}$, for hydrogen and oxygen ions in a tissue equivalent gas. *Radiat. Res.* **55**, 1–9 (1973).

LIDÉN, K. The new special names of S.I. units in the field of ionizing radiations. *Phys. Med. Biol.* **20**, 1029–1036 (1975).

LINDBORG, L. Microdosimetry measurements in beams of high energy photons and electrons: technique and results. pp. 347–375. In: *Proc. Fifth Symp. Microdosimetry*, Verbania Pallanza, 1975. Eds. J. Booz, H. G. Ebert and B. G. R. Smith, Commission of the European Communities, Luxembourg (1976).

LISKIEN, H. and PAULSEN, A. Neutron production cross sections and energies for the reactions T(p,n) ^{3}He, D(d,n) ^{3}He and T(d,n) ^{4}He. *Nuclear Data Tables* **11**, 569–619 (1973).

MAIER, E. *Untersuchungen zur LET-Spectrometrie.* Diplomarbeit der Techn. Universität, München (undated).

MARUYAMA, T. and BOUTS, C. J. Attenuation of 15 MeV neutrons in multilayer shields composed of steel, polyethylene and borated materials. *Phys. Med. Biol.* **17**, 420–424 (1972).

MATHIESON, E. and CHARLES, M. W. Attenuation of proportional counter pulses by equal integrating and differentiating time constants. *Nucl. Instr. and Meth.* **72**, 155–156 (1969)

MATHIESON, E. and HARRIS, T. J. Pulse shape discrimination in proportional counters – Theory of electronic system. *Nucl. Instr. and Meth.* **88**, 181–192 (1970).

MCBETH, G. W., WINYARD, R. A. and LUTKIN, J. E. *Pulse Shape Discrimination with Organic Scintillators.* Koch-Light Laboratories Ltd., Colnbrook, Bucks, England (1971).

MCGINNIES, R. T. Energy spectrum resulting from electron slowing down. *Circ.* 597, Natl. Bur. Std., (U.S.), Washington, D.C. (1959).

MENZEL, H. G., WAKER, A. J., GRILLMAIER, R., BIHY, L. and HARTMANN, G. Radiation quality studies in mixed neutron-gamma fields. In: *Third Symp. Neutron Dosimetry in Biology and Medicine*, Neuherberg, 1977. Proc. in press.

MENZEL, H. G., WAKER, A. J. and HARTMAN, G. Radiation quality studies of a fast neutron therapy beam. pp. 591–606. In: *Proc. Fifth Symp. Microdosimetry*, Verbania Pallanza, 1975. Eds. J. Booz, H. G. Ebert and B. G. R. Smith, Commission of the European Communities, Luxembourg (1976).

MYERS, I. T. Ionization. pp. 317–330. In: *Radiation Dosimetry. Vol. I. Fundamentals.* Ed. F. H. Attix and W. C. Roesch, Academic Press, New York and London (1968).

MIJNHEER, B. J., BROERS-CHALISS, J. E. and BROERSE, J. J. Measurements of radiation components in a phantom for a collimated d-T neutron beam. pp. 423–439. In: *Proc. Second Symp. Neutron Dosimetry in Biology and Medicine*, Neuherberg, 1974. Ed. G. Burger, Commission of the European Communities, Luxembourg (1975).

NACHTIGALL, D. Average and effective energies, fluence-dose conversion factors and quality factors of the neutrons spectra of some (α, n) sources. *Health Phys.* **13**, 213–219 (1967).

NCRP report 38. *Protection against Neutron Radiation.* National Council on Radiation Protection and Measurements, Washington, D.C. (1971).

NEARY, G. J., HORGAN, V. J., BANCHE, D. A. and STRETCH, A. Further data on DNA strand breakage by various radiation qualities. *Int. J. Radiat. Biol.* **22**, 525–537 (1972).

NEUERT, H. Proportionalzähler. pp. 26–52; Beweglichkeit positiver Ionen in Gasen bei kleinen Feldstärken. p. 507. In: *Kernphysikalische Meszverfahren.* Verlag G. Braun, Karlsruhe (1966).

OKADA, S. DNA as target molecule responsible for cell killing. pp. 103–146. In: *Radiation Biochemistry. Vol. I. Cells.* Eds. K. J. Altman, G. B. Gerber and S. Okada, Academic Press, New York (1970).

OLDENBURG, U. and BOOZ, J. A Monte Carlo analysis of neutron-produced single event spectra. *Biophysik* **8**, 71–80 (1971).

OLDENBURG, U. and BOOZ, J. Calculation and measurement of neutron-produced single-event spectra. RADIAT. RES. **51**, 551–568 (1972).

OLDENBURG, U. and BOOZ, J. *Mass Stopping Power and Pathlength of Neutron Produced Recoils in Tissue and Tissue Equivalent Materials. I. Neutron Energy* $\leqslant$ 6 MeV. Euratom, Brussels (1972).

OOSTENBRUG, M. W. M. Private communication (1976).

PALCIC, B. and SKARSGARD, L. D. The effect of oxygen on DNA single-strand breaks produced by ionizing radiation in mammalian cells. *Int. J. Radiat. Biol.* **21**, 417–433 (1972).

PARETZKE, H. G., GRÜNAUER, F., MAIER, E. and BURGER, G. The change of radiation quality in a neutron irradiated phantom. pp. 73–91. In: *Proc. First Symp. Neutron Dosimetry in Biology and Medicine*, Neuherberg, 1972. Eds. G. Burger, H. Schraube and H. G. Ebert, Commission of the European Communities, Luxembourg (1972).

PAUW, H. *Energy Spectra of Radioactive Neutron Sources*. Thesis, University of Amsterdam, The Netherlands (1970).

PEPERZEEL, H. A. VAN, BREUR, K., BROERSE, J. J. and BARENDSEN, G. W. RBE values of 15 MeV neutrons for responses of pulmonary metastases in patients. *Eur. J. Cancer* **10**, 349–355 (1974).

POLLARD, E. C. and KRAUS, K. All-or-nothing character of DNA degradation in bacteria after ionizing radiation. *Bioph. J.* **13**, 332–339 (1973).

POLLARD, E. C. and TILBURG, A. Action of ionizing radiation on sensitive strains of *Escherichia Coli* B. *Bioph. J.* **12**, 133–156 (1972).

PUCK, T. T., MARCUS, P. J. and CIERCIURA, S. J. Clonal growth of mammalian cells *in vitro*. *J. Exp. Med.* **103**, 273–284 (1956).

ROSSI, H. H. and FAILLA, G. Tissue-equivalent ionization chambers. *Nucleonics* **14**, 32–37 (1956).

ROTONDI, E. Energy loss of alpha particles in tissue. *Radiat. Res.* **33**, 1–9 (1968).

RUTHERFORD, E., CHADWICK, J. and ELLIS, C. D. The scattering of alpha and beta particles. pp. 191–239. In: *Radiations from Radioactive Substances*. Cambridge University Press, London (1951).

SCHRAUBE, H., MORHART, A. and GRÜNAUER, F. Neutron and gamma radiation field of a deuterium gas target at a compact cyclotron. pp. 979–1001. In: *Proc. Second Symp. Neutron Dosimetry in Biology and Medicine*, Neuherberg, 1974. Eds. G. Burger and H. G. Ebert, Commission of the European Communities, Luxembourg (1975).

SELTZER, M. S. and BERGER, M. J. Energy-loss straggling of protons and mesons: Tabulation of the Vavilov distribution. pp. 187–203. In: *Studies in Penetration of Charged Particles in Matter*. NAS-NRC publ. 1133, Washington, D. C. (1964).

SHANI, G. Build-up of 14-MeV neutrons in iron shielding. *Atomkernenergie* **27**, 282–283 (1976).

SHONKA, F. R., ROSE, J. E. and FAILLA, G. Conducting plastic equivalent to tissue, air and polystyrene. pp. 184–187. In: *Proc. Second United Nations Conference on Peaceful Uses of Atomic Energy. Vol* 21. United Nations, New York (1958).

SHULEK, P., GOLOVIN, B. M., KULYUKINA, L. A., MEDVED, S. V. and PAVLOVICH, P. Fluctuactions of ionization loss. *Soviet J. Nucl. Phys.* **4**, 400–401 (1967).

SKARSDARD, L. D., KIHLMAN, B. A., PARKER, L., PUJARA, C. M. and RICHARDSON, S. Survival, chromosome abnormalities, and recovery in heavy-ion and x-irradiated mammalian cells. *Radiat. Res. Suppl.* **7**, 208–221 (1967).

SMATHERS, J. B., OTTE, V. A., SMITH, A. R., ALMOND, P. R., ATTIX, F. H., SPOKAS, J. J., QUAM, W. M. and GOODMAN, L. J. Composition of A-150 tissue-equivalent plastic. *Med. Phys.* **4**, 74–78 (1977).

SPOKAS, J. J. Composition variability and equivalence of Shonka TE plastic. Radiation Research Society, Miami Beach (1975).

SRDOČ, D. Tissue equivalent proportional counter and gas flow system. pp. 42–59. In: *Annual Report on Research Project, NYO*-2740-5, Radiobiological Research Laboratory, New York (1968).

SRDOČ, D. and KELLERER, A. M. Event-frequency in small cylinders exposed to γ-rays. pp. 497–508. In: *Proc. Third Symp. Microdosimetry*, Stresa, 1971. Ed. H. G. Ebert, The Commission of the European Communities, Luxembourg (1972).

SRIVASTAVA, B. K. and MUKHERJI, S. Range and stopping-power equations for heavy ions. *Phys. Rev. A.* **14**, 718–725 (1976).

STARODUBTSEV, S. V. and ROMANOV, A. M. Passage of electrons through matter. pp. 158–206. In: *The Passage of Charged Particles through Matter.* (Translated from Russian). Israel Program for Scientific Translations, Jerusalem (1965).

SWARTZ, C. D. and OWEN, G. E. Recoil detection in scintillators. pp. 211–246. In: *Fast Neutron Physics. Part I. Techniques.* Eds J. B. Marion and J. L. Fowler, Interscience Publishers, Inc., New York (1960).

TENNELEC. *Instruction Manual* 100 *C. Preamplifier.* Tennelec, Oak Ridge (1964).

TENNELEC. *Instruction Manual TC*133 *FET Preamplifier.* Tennelec, Oak Ridge (1967).

TODD,. P. Heavy-ion irradiation of cultured human cells. *Radiat. Res. Suppl.* **7**, 196–207 (1967).

TODD, P. Fractionated heavy ion irradiation of cultured human cells. *Radiat. Res.* **34**, 378–389 (1968).

TOMS, M. E. A computer analysis to obtain neutron spectra from an organic scintillator. *Nucl. Instr. and Meth.* **92**, 61–70 (1971).

TSCHALÄR, C. Straggling distributions of large energy losses. *Nucl. Instr. and Meth.* **61**, 141–156 (1968).

TSCHALÄR, C. Straggling distributions of extremely large energy losses. *Nucl. Instr. and Meth.* **64**, 237–243 (1968).

TURNER, J. E. Values of I and I_{adj} suggested by the subcommittee. pp. 99–101. In: *Studies in Penetration of Charged Particles in Matter.* NAS-NRC publ. 1133, Washington, D.C. (1964).

VAVILOV, P. V. Ionization losses of high-energy heavy particles. *Soviet Phys. JETP* **5**, 749–751 (1957).

VERBINSKI, V. V., BURRUS, W. R., LOVE, T. A., ZOBEL, W., HILL, N. W. and TEXTOR, R. Calibration of an organic scintillator for neutron spectrometry. *Nucl. Instr. and Meth.* **65**, 8–25 (1968).

WAKER, A. J. and BOOZ, J. Measurement of the W-value of low energy electrons. pp. 455–478. In: *Proc. Second Symp. Neutron Dosimetry in Biology and Medicine,* Neuherberg, 1974. Eds. G. Burger and H. G. Ebert, Commission of the European Communities, Luxembourg (1975).

WALSH, P. J. Stopping power and range of alpha particles. *Health Phys.* **19**, 312–316 (1970)

WESTRA, A. *De Invloed van Straling op het Vermogen tot Proliferatie van in vitro Gekweekte Zoogdiercellen.* Thesis, University of Amsterdam, The Netherlands (1971).

WILKINSON, D. H. The electrostatics of pulse formation. pp. 59–104. In: *Ionization Chambers and Counters.* Cambridge University Press, London (1950).

WILLIAMSON, J. and WATT, D. E. The Influence of Molecular binding on the stopping power of alpha particles in hydrocarbons. *Phys. Med. Biol.* **17**, 486–492 (1972).

WILSON, B. J. *The Radiochemical Manual.* 2nd Edition. Ed. B. J. Wilson, The Radiochemical Centre, Amersham (1966).

WOLF, R. S. Measurement of the gas constant for various proportional-counter gas mixtures. *Nucl. Instr. and Meth.* **115**, 461–463 (1974).

ZAIDINS, S. C. A method for energy-loss and range calculations based on empirical approximations. *Nucl. Instr. and Meth.* **120**, 125–129 (1974).

ZIRKLE, R. E. The radiobiological importance of linear energy transfer. pp. 315–350. In: *Radiation Biology. Vol. I. High Energy Radiation.* Ed. A. Hollaender, McGraw-Hill Book Company, Inc. New York (1954).